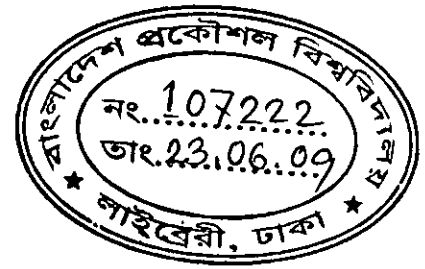# Experimental Investigation of Lift to Drag Ratio between Volumetrically Equivalent Fuselages

By

Mohammad Mainuddin
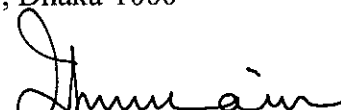
A thesis

Submitted to the

Department of Mechanical Engineering

in partial fulfillment of the requirements for the degree

of

MASTER OF SCIENCE IN MECHANICAL ENGINEERING,

BANGLADESH UNIVERSITY OF ENGINEERING AND TECHNOLOGY
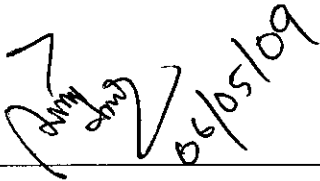
DHAKA

May 2009

The thesis titled "**Experimental Investigation of Lift to Drag Ratio between Volumetrically Equivalent Fuselages**" submitted by **Mohammad Mainuddin,** Roll no. 100610023 P, Session October 2006 has been accepted as satisfactory in partial fulfillment of the requirement for the degree of Master of Science in Mechanical Engineering on 6 May 2009.

BOARD OF EXAMINERS

1. _____   6·5·09

   Dr. M. A. Taher Ali   Chairman
   Professor
   Department of Mechanical Engineering
   BUET, Dhaka-1000

2. _____

   Dr. Abu Rayhan Md. Ali   Member (Ex-Officio)
   Professor and Head
   Department of Mechanical Engineering
   BUET, Dhaka-1000

3. _____

   Dr. Md. Quamrul Islam   Member
   Professor
   Department of Mechanical Engineering
   BUET, Dhaka-1000

4. _____

   Dr. Mohammad Mamun   Member
   Associate Professor
   Department of Mechanical Engineering
   BUET, Dhaka-1000

5. _____

   Dr. A.K.M. Iqbal Hussain   Member (External)
   Professor, MCE Department, IUT
   Former--Director General, BITAC &
   Director, Bangladesh Institute of Technology, Chittagong.

ii

CANDIDATE'S DECLARATION

It is hereby declared that this thesis or any part of it has not been submitted elsewhere for the award of any degree or diploma.

_____

Mohammad Mainuddin

To my Parents

ACKNOWLEDGEMENT

ABSTRACT

To improve the overall lift to drag a new concept on fuselage of an Unmanned Aerial Vehicle (UAV) is investigated where the fuselage also provides some lift. To investigate the improvement of lift to drag two fuselages are considered, one is conventional cylindrical cross-section and the other is aerofoil cross-section. A number of fuselages models with a scale of 1:32 with aerofoil cross-section and with conventional cylindrical cross section are manufactured in such a way that both models have the same volume. Same set of wings is used in both types of models so that the results can be used to show the comparison between the fuselages. To reduce the induced drag winglets are used in aerofoiled fuselage. All the three fuselages i.e., circular cross-sectioned, aerofoil cross-sectioned and aerofoil cross-sectioned with winglets are used for wind tunnel test. Lifts and drags are measured with the help of spring balance system for different angle of attack of the fuselages to find out the best fuselage corresponding to overall lift to drag ratio. From this result it is also found out what should be the best angle of attack of the fuselage at different speed during take off, flying and landing condition. Finally lifts and drags are also measured by pressure tapping around the fuselages at different angles of attack to verify the results found in spring balance system.

TABLE OF CONTENTS

CHAPTER 3

ABOUT THE MODELS

CHAPTER 4

EXPERIMENTAL SETUP

CHAPTER 5

EXPERIMENTAL PROCEDURE

CHAPTER 6

RESULTS AND DISCUSSION

CHAPTER 7

CONCLUSIONS AND RECOMENDATIONS

LIST OF FIGURES

LIST OF TABLES

LIST OF SYMBOLS

Symbols	Meaning	Unit
Re	Reynolds number	--
U	Local velocity	m/s
U_∞	Free stream velocity	m/s
δ	Boundary layer thickness	mm
δ_l	Displacement thickness	mm
V	Relative velocity between the wing and air	km/hr
C_L	Lift coefficient	--
C_D	Drag coefficient	--
C_M	Moment coefficient	--
C_P	Pressure coefficient	--
S_{ref}	Area of the wing when viewed from the overhead	m^2
C	Chord length	mm
b	Span	mm
AR	Aspect ratio	--
ρ	Air density	Kg/m^3
g	Gravitational acceleration	m/s^2
h	Menometric column	mm
x	Stream wise distance from the front of the fuselage	mm
y	Vertical distance	mm
Θf	Fuselage angle of attack in degree	degree
Θw	Relative angle between wing and fuselage	degree
L	Lift force	kg
D	Drag force	kg
L/D	Lift to Drag ratio	--
βi	Angle between cord and pressure taps direction	degree
α	Angle of attack of the pressure taped fuselage	degree
θi	Pressure taps relative angle with air flow	degree
l_i	Corresponding length represent by a single tap	mm
ν	Kinematic viscosity	m^2/s

Chapter 1

INTRODUCTION
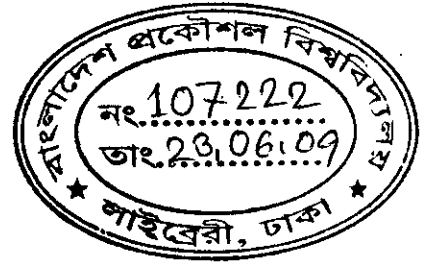
1.1. Preamble

The major thrust in designing of an aircraft is to increase its lift along with the reduction of drag. From the early 20th century research works have continuously been carrying out on these facts at different forms to develop the most efficient aerofoil section which would produce the maximum lift corresponding to relatively small drag. For different airfoil profiles, coefficient of lift (C_L) and that of drag (C_D) have been measured or calculated. The aerofoil section used in conventional airplane wings which basically produce the lift while its fuselage has little or no contribution in it. But the appreciable portion of total drags is contributed by the fuselage. The total drag produced by each exposed parts of the airplane should be minimum such that overall lift to drag ratio is maximum. So the designing of an airplane should also include the reduction of drags of all its exposed parts. On the other hand if it is possible to extract some lift from each exposed parts then that would also maximize the overall lift to drag.

So in order to maximize the efficiency of an aircraft, the basic design premises should be such that all elements/components of the aircraft must contribute to the aircraft lift. In pursuit of this goal and to solve the present challenges and future goals of the air transportation system of increased efficiency, passenger safety and productivity combined with greater personal mobility and expanded transportation capability, the scientific community is now turning there attention to the lifting-body aircraft. The lifting-body aircraft design principle allows the designer both safe and fuel-efficient aircraft for an efficient utilization of the air transportation system for the movement of people and goods. This design would also provide increased payload and a dramatically improved short take-off and landing (STOL) capability, over conventionally designed [1-5] aircraft. In conventional design the aircraft, fuselages are generally circular and the wings are aerofoiled shaped. Although the circular fuselage has less drag but it produces no lift. Instead of circular fuselage if an aerofoiled section fuselage is incorporated in an

airplane then it will produce some lift and will be expected to increase overall lift to drag ratio. The airplane with aerofoiled section fuselage is termed as all body lifting aircraft.

1.2. Background of the Work on Aerofoiled Fuselage

In early 20th century a famous professional aircraft designer Vincent Justus Burnelli [6] developed the concept of all body lifting aircraft where he used fuselages of aerofoil cross section. But this fuselage aerofoil section had to be sufficiently thick such that man could ride on it. So the scientific community had raised a number of technical concerns related to the large fuselage and its impact on aerodynamics. Amongst these primary concerns was the negative aerodynamic drag effects attributed to the lifting-body fuselage due the increased fuselage frontal area and the fuselage wing interference. Picture 1.1 shows the Burnelli's designed first aerofoiled section fuselage bi-plane [6]. The bi-plane was very large, capable of carrying 26 passengers.
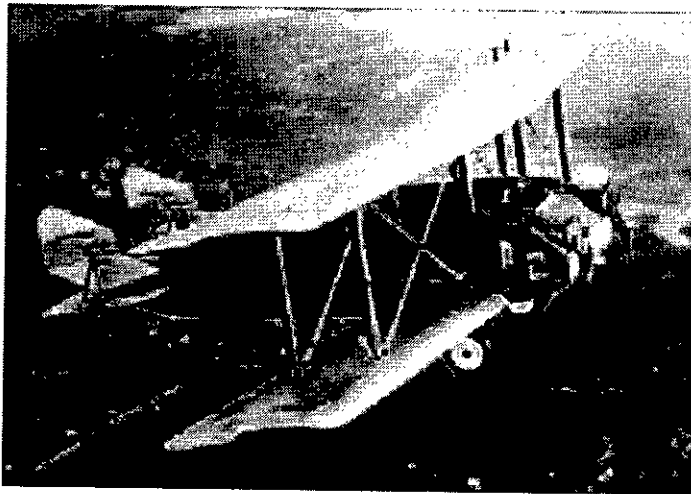
Figure 1.1: Burnelli's all body lifting fuselage bi-plane, RB-1.

An analysis of the concept performed by Wertenson [7, 8] in 1931 showed that the Burnelli's design concept resulted in less frontal area than a conventional twin-engine transport airplane and that the negative fuselage wing interference is more than compensated by the increased lift of the fuselage. Subsequent analysis performed at that time by some researchers [9-12] also supported the findings of Wertenson.

2

The primary focus of Burnelli's research at Lawson Airplane Company of Green Bay and Milwaukee, WI at the end of the First World War was aimed at to build airplanes for peace instead of war. As his research outcome Burnelli built American's first twin engine airplane. This basic element of the Burnelli design principle is just now being considered and utilized by the aeronautical community for a variety of vehicle classes that vary from personal air vehicles (PAVs) to jumbo transports. It is important to note that Burnelli was not alone in the development of all-lifting vehicle technology, there were more than fifty all-lifting aircraft developed during the last century [6, 13]. But all of these aircraft were designed for large carrying capacity. But now-a-days small Unmanned Aerial Vehicle (UAV) concepts are developed and this UAV does not require thicker fuselage besides it uses sophisticated electronic elements that are small in size but heavy. So UAV requires higher lifting force with a smaller size. National Aeronautics Space Administration's (NASA) X-39, X-43B, X-45A and all Unmanned Combat Aerial vehicle (UCAV) also uses all-lifting body fuselage but all of these are designed for high-speed transport under Future Aircraft Technology Enhancements (FATE) program [14,15].

As some of the UAV for area reconnaissance or similar purposes have to operate in the speed of 50km/hr to 100km/hr, the present investigation is carried out in this speed range. On the other hand we should follow the design of nature and the practical aspects of streamline form may be studied from the bodies of fishes and birds, the profiles of which have gradually met the requirements of least resistance for motion through a fluid, water or air, as the case may be [16]. In this context the gliding bird's body shape could be a good natural example for a UAV design and for most of the gliding birds like Harris' hawk (Parabuteo unicinctus) have aerofoil body shape rather than conventional cylindrical shape [17]. Picture 1.2 shows the body shape of a Harris' hawk during flying condition.
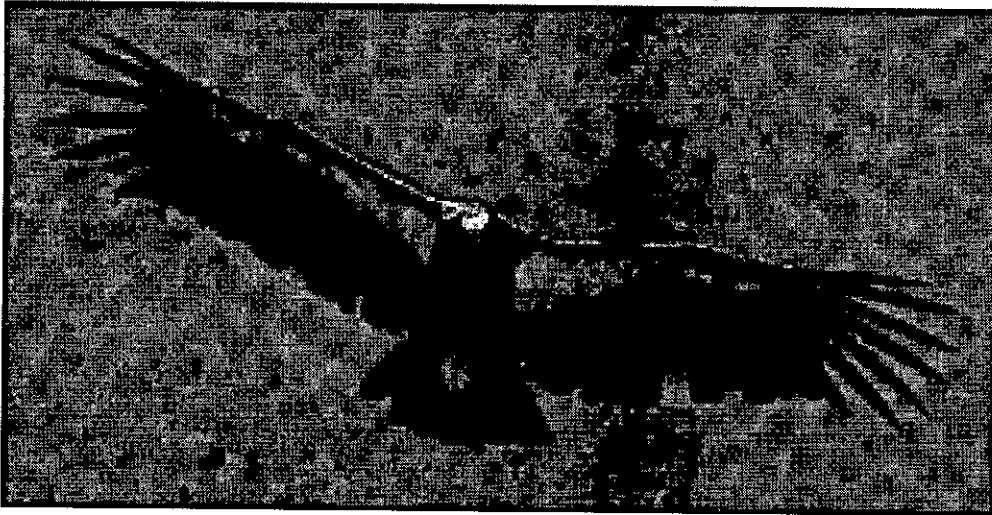
Figure 1.2: All body lifting shape of a Harris' hawk (Parabuteo unicinctus)

Again during their flights, birds continuously change their feathers position to improve their maneuvering capability with minimum energy loss. For example the feathers at the wing tips of most birds that soar over land separate both horizontally and vertically in flight to form slotted tips as shown in picture 1.3 below.
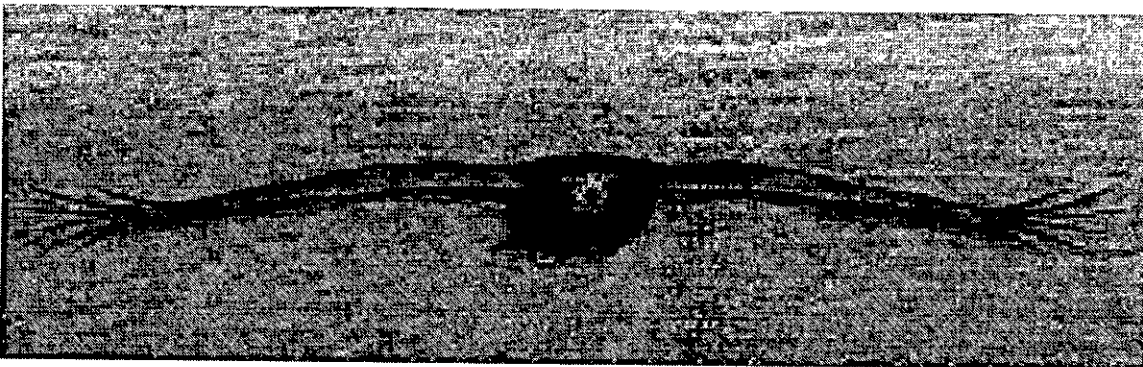
Figure 1.3: The Harris' hawk (Parabuteo unicinctus) is gliding with vertical separation between the feathers in the slotted wing tips.

The individual feathers in the slotted tips resemble the winglets used on the wing tips of some aircraft to reduce induced drag.

V. A. Tuckerm [17] made an extensive research on the lift drag characteristics on wings creating the similar conditions of birds' wings. He found that a wing that produces lift leaves a pair of vortex sheets in its wake which generates the induced drags. The feathers at the wing tips of most birds that soar over land separate both horizontally and vertically in flight to form slotted tips i.e. the winglets and the wing theory shows that winglets can reduce the kinetic energy left in the vortex sheets, and hence the induced drag, by spreading vorticity both horizontally and vertically. He also found that the total drag of the wing with the feathered tip was 12% less than that of a hypothetical wing with the same lift and span, but with tip feathers that did not respond to upwash at the end of the base wing. This value is consistent with wing theory predictions on drag reduction from winglets and the Wings with the tip and the base wing locked together had lift and drag that increased with increasing base wing angle of attack, as expected for conventional wings without winglets. [18, 19, 20, 21, 22, 23, 24]

Eastman N. Jacobs and Albert Sherman [25] tests of wing-fuselage combinations employing an aerofoil-type fuselage were made in the variable-density wind tunnel as a part of the wing-fuselage interference program and the test results showed that the aerofoil-type-fuselage combination should be well faired in such a way as to eliminate the discontinuity at the ends of the fuselage. The results show that the fuselage part of the lifting surface, comprising 33 percent of the total lifting area (exposed wing area plus fuselage area) contributes 26 percent of the total lift.

I. Kroo [26] from Stanford University, USA recently done some research work aiming to increase the commercial aircraft efficiency. His findings shows that the vortex drag of commercial aircraft accounts for a large fraction of airplane cruise drag (typically about 40%) and therefore concepts that result in reduction of vortex drag may have a significant effect on fuel consumption. Vortex drag is even more significant at low speeds where vortex drag typically accounts for 80%-90% of the aircraft's climb drag at critical take-off conditions [26]. Although take-off constitutes a very small portion of the flight, but its influence on the overall aircraft design is profound. Since conditions associated with engine-out climb shortly after take-off are often critical constraints in the aircraft design,

changes in aircraft performance at these conditions influence the overall design and so have an indirect, but powerful, effect on the aircraft cruise performance. While a 1% reduction in drag due to lift might improve the cruise lift-to-drag ratio by 0.4% with a similar effect on range, the improved low speed climb performance may make it possible to achieve acceptable take-off and climb with almost 1% greater take-off weight, leading to an increase in range several times that associated with the simple cruise L/D improvement [26, 27]. Furthermore, lower drag at high lift conditions leads to reduced noise. He also noted that the induced drag may be easily reduced by increasing the span of a planar wing. A 10% increase in wing span leads to a 17% reduction in vortex drag at fixed speed and lift [26]. But the primary reason that wing spans are not increased to reduce drag is that the higher structural weight and cost make such efforts counterproductive. To produce a large change in the vortex drag without a large increase in wetted area, his low aspect ratio endplates were replaced with higher aspect ratio winglets.

To increase the maneuvering capability of the modern fighter plane it's also utilized the all body lifting fuselage concept. For example from Bill Gunston's excellent encyclopedia (page 224), the modern fighter jet MiG-29 has high maneuvering capability as it's design specifics are defined for 40% aerodynamic lift from the central structure component comprising fuselage and inner wing between fins. This type of fighter plane is called Blended Wing Body (BWB) aircraft. For a better understanding of the BWB shape visually and practically a recent visit to Bangladesh Air Force (BAF) has arranged by Mechanical Department, BUET under the guidance of Professor Dr. M. A Taher Ali. The BAF engineers, pilots and the officers extensively describe different parts, body shape and their aerodynamic function by dismantling a BAF owned MIG-29 fighter plane. The visit helps this research works to understand the practical advantage of lifting body fuselage. Picture 1.4 is showing the Blended Wing Body (BWB) outer shape of a MIG-29 fighter plane.

Figure 1.4: Photograph of a MIG-29 showing lifting body fuselage
(Source: http://commons.wikimedia.org/wiki/File:060610-SKP-MIG-29-01-1280x.jpg)

1.3. Overview of the present work

In this research aerofoil fuselage is introduced to produce some lift from the fuselages but this finite width aerofoiled fuselages also generate induced drag due to tip vortices that ultimately reduce the overall lift to drag. So winglets have been incorporated at both sides of the fuselage to reduce the tip vortices and thereby reduce the induced drag. All the three fuselages i.e. circular cross-sectioned, aerofoil cross-sectioned and aerofoil cross-sectioned with winglets are used for wind tunnel test to measure the lifts and drags with the help of spring balance system for different angle of attack of the fuselages and to find out the best fuselage corresponding to overall lift to drag ratio. By comparing the results it is also found out what should be the best angle of attack of the fuselage at different speed during take off, flying and landing condition. Finally lifts and drags are also measured by pressure tapping around the fuselages at different angles of attack to verify the results found in spring balance system.

Chapter 2

THEORETICAL CONSIDERATION

To be successful an aircraft must be capable of doing the job for which it is designed economically and easily. Normally, this entails meeting at least the following requirements:

> ➢ The air craft must have an adequate system for producing lift or sustention.
> ➢ Its structure must be adequate.
> ➢ It must have a satisfactory system
> ➢ It must incorporate design features resulting in adequate stability.
> ➢ It must be provided with a satisfactory means for safety leaving or contacting the ground.
> ➢ It must be capable of completing its mission as economically and as safely.

An aircraft deficient in respect to any one of these requirements cannot be considered satisfactory, regardless of how well it meets all the others. It is difficult in one design to meet perfectly all of the above requirements for a successful airplane. The designer must be satisfied with excellence in as many as characteristics as possible and adequate in the remainder. The designer must exercise his best judgment in deciding what requirements may be considered of secondary importance without jeopardizing the airplane utility.

Aerodynamics is nothing more than the study and application of those natural laws that influence flight. Some of these laws are well defined and well understood, whereas others are obscure and their presence is just beginning to be suspected. Airplane design progress is directly dependent on our advances in understanding the aerodynamics laws. Some of the theoretical consideration and the aerodynamics laws are discussed below.

2.1 Boundary Layer

A boundary layer is a thin region of fluid near a wall where viscous effects are important in determining the flow field. The boundary layer is a buffer region between the wall below and the inviscid free-stream above. The layer of air extending from the surface of the object to the point where no dragging effect is discernible is known as the boundary layer. Mathematically, its main purpose is to allow an inviscid flow solution to satisfy the no-slip condition at the wall.
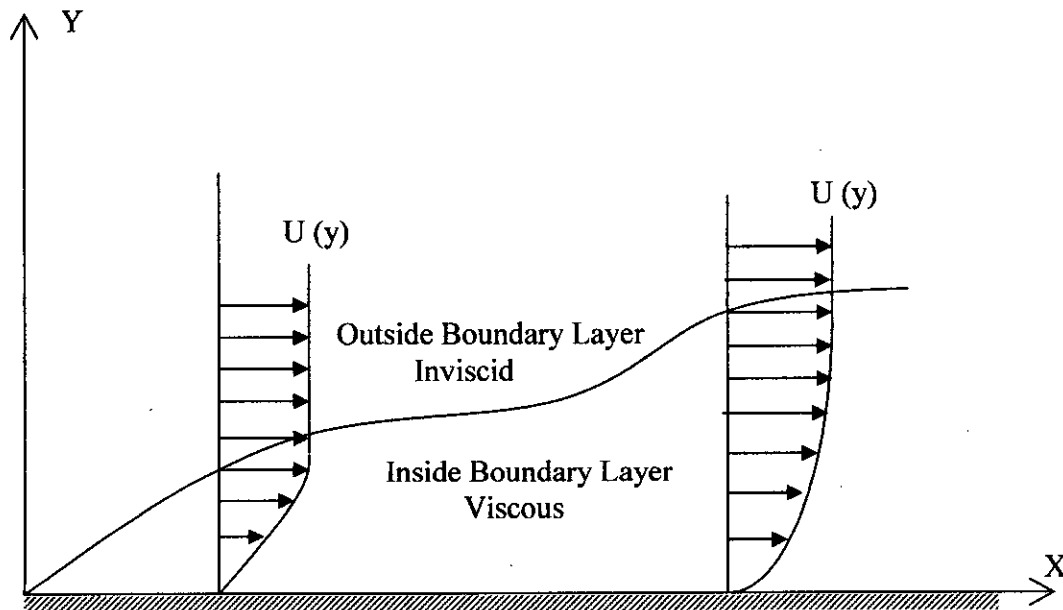
Figure 2.1: Boundary layer formation

Figure 2.1 shows the growth of boundary layer. Conventionally, the X-axis is parallel to the wall, while the Y-axis is perpendicular to the wall and cuts right through the boundary layer. At any given x-coordinate, we can draw the velocity distribution as a function of y. This is the most common way to illustrate a boundary layer. Figure 2.1 also shows velocity cross sections of two points in the boundary layer. The first is the cross section

for a laminar boundary layer; the second one is after the transition and represents a turbulent boundary layer. It should be noted that, in a boundary layer, the velocity is always zero at the wall, and asymptotically approaches the free-steam velocity (denoted by U_∞) at infinity. The boundary layer typically grows in thickness in the stream-wise direction. Turbulent boundary layers grow faster than laminar ones.

The nature of the boundary layer is a controlling factor in the determination of skin-friction drag. More important than this, the nature of the boundary layer determines maximum lift coefficient, stalling characteristics of a wing and, magnitude of the friction and pressure drag and to some extent the high speed characteristics of any object.

Equation for boundary layer thickness and for skin friction drag of a boundary layer may be obtained by dimensional analysis.

2.2 Flow Separation

When the air is unable to follow an object's shape it separates. This is shown in the figure 2.2 for an aerofoil, which while being a streamlined shape, will cause flow separation if it is tilted so that it is more oblique to the flow. This is known as aerofoil *stall*. In order to prevent flow separation it is best to avoid sharp profile changes in flow direction, but making a smooth shape with slow changes in curvature sometimes not possible due to physical limitations. Hence, the design of what we typically call streamlined body shape is actually an attempt at eliminating flow separation. This is usually possible, such as with an aerofoil with a sharp trailing edge, but practical consideration do not always allow us the freedom to build the perfect shape.

Figure 2.2: Flow separation on an aerofoil shape which is at high angle of attack

(Source: http://www.nationmaster.com/encyclopedia/Flow-separation)

There is another way to prevent flow separation though. This relates to boundary layers. Turbulent boundary layers may cause more skin friction drag, but they tend to be thicker and separate later. So for objects in which the pressure drag is dominant, it can be beneficial to artificially trigger a boundary layer to go turbulent to reduce the flow separation effect. This phenomenon is shown in figure 2.3 Laminar boundary layer on smooth ball separate at half way causing a wide wake near pressure drag while the roughness created by and dimples on the surface of a golf ball delays separation past half way around the ball reducing significant pressure drag.

11
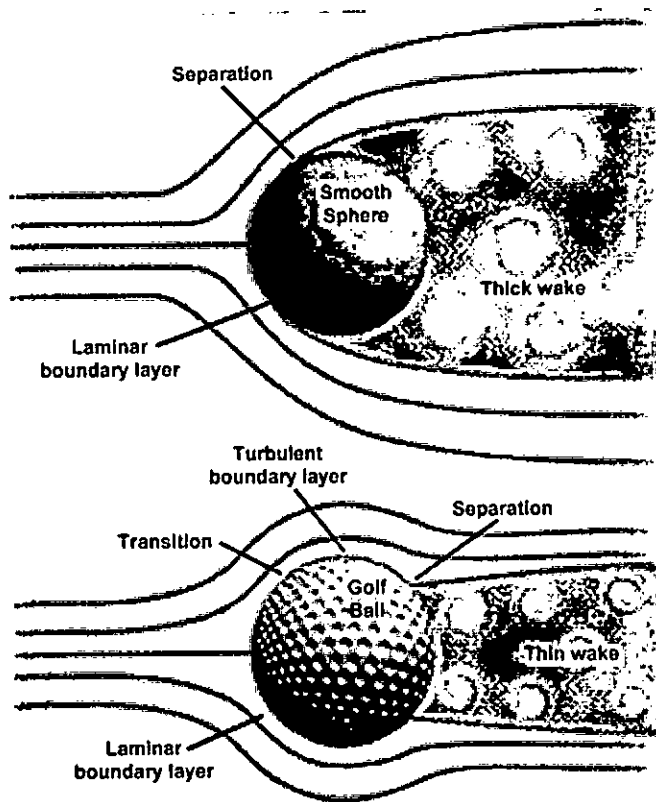
Figure 2.3: Laminar and Turbulent boundary layer on smooth and rough surface
(Source: Aerospace web.org)

2.3 Drag Coefficient

The drag coefficient encompasses the particular drag characteristics on an aerofoil wing. The total drag is the summation of:

- Skin friction drag
- Form, or pressure drag
- Induced drag

The first two are particularly important for any object moving in a fluid including airplane movement in air, while the third (induced drag) is only really important for wings, and hence mainly the aircraft.

2.3.1 Skin Friction Drag

Skin friction drag occurs due to the air having viscosity. Viscosity indicates how thick the air is. Treacle has a high viscosity, water lower, and air lower still. The air all around us tends to stick to objects when it is moving past, or if the object is moving through still air. When air is moving past an object then the air in direct contact with a surface is actually brought to a stop (relative to the surface). Air slightly off the surface moves slightly faster. If we go far enough from the surface then the air is moving at its full (or free-stream) speed. The region just above the surface where the air is not moving at its full speed is known as the boundary layer.

Skin friction drag is not dependent on the particular material that an object is made of, but it is affected by how rough the surface is. As one might expect, smoother surfaces are better than rough surfaces. Also, the amount of surface in contact with the air is a factor, so minimizing this is advantageous in reducing skin friction drag.

2.3.2 Form or Pressure Drag

While skin friction drag is a function of the surface roughness and the cord length of wing in contact with the air, the form, or pressure drag, is dependent on the shape of the wing. It is therefore the main way in which designers can reduce aerodynamic drag. Depending on the shape of a body moving through the air concentrations of high and low pressure can form, relative to the background (usually atmospheric) pressure. These can act to pull the body backwards - i.e. causing drag.

The picture in figure 2.4 shows the flow past a flat plate placed across the flow direction. The diagram shows streamlines, which indicate the path of the air. Ahead of the plate air moves to go around it. Half the flow goes above the plate, and half goes below it. Along the centre of the plate the air actually comes to a stop (at what is known as the stagnation point), and this is known as the separation streamline.

According to Bernoulli's theory, when air is slowed down, its pressure increases and vice-versa. As the air comes to a stop along the centre line, this creates a high pressure region ahead of the plate - pushing it backwards. Behind the plate the air is not able to follow the surface of the plate and so there forms large eddy, swirling around in a

13

random fashion. This is known as separated flow and creates a low pressure region behind the plate. This acts like a vacuum cleaner, literally sucking the plate backwards. It is this high pressure in front of the plate and low pressure behind it that is the pressure drag. Thus we can see that pressure drag is mainly due to the flow separation behind the object in the flow. The flow separation can be reduced by making the body streamlined. The circular cylinder is a streamlined body with slenderness ration 1:1. The flow around a cylinder is shown in the picture in figure 2.5

The high pressure in front of the cylinder and low pressure behind is similar to the flat plate case discussed above. The flow (depicted by streamlines) manages to follow the curve of the cylinder before it starts swirling around. The effect of this is that the low pressure behind the cylinder is not as low as behind the flat plate. The drag is about half that of the flat plate, so a big improvement.
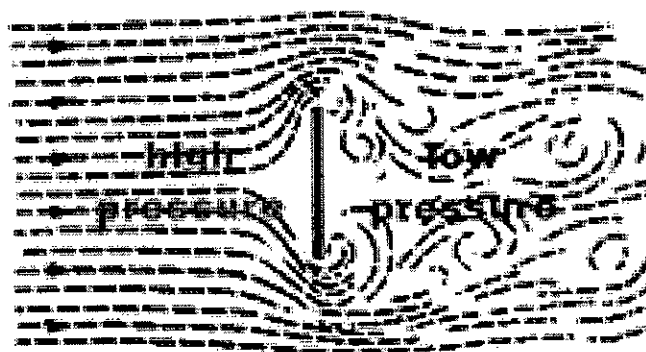
Resistance, 100%

Figure 2.4: Flow around vertical plate (**Source: Mechanics of Flight, Kermode**)
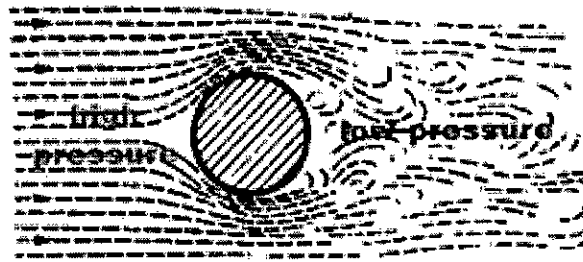
Resistance, 50%

Figure 2.5: Flow around sphere (**Source: Mechanics of Flight, Kermode**)

The streamlines those are able to follow the curve of the upper and lower surfaces and join up towards the trailing edge. In this case there is still a high pressure region at the front, but the low pressure at the rear is much closer to atmospheric pressure. Hence the drag is around 20 times less than the flat plate, and 10 times less than the cylinder. Figure 2.6 shows the comparison of flow separation and drag on blunt and streamlined shape. If the slenderness ratio in the aerofoil increases then the pressure drag decreases. But in that case its length i.e. the contact area increases and the friction drag increases. Also there is physical limitation in practical design to increase the length. The important factor is to make sure that the flow around the body is smooth, and able to follow the shape easily.
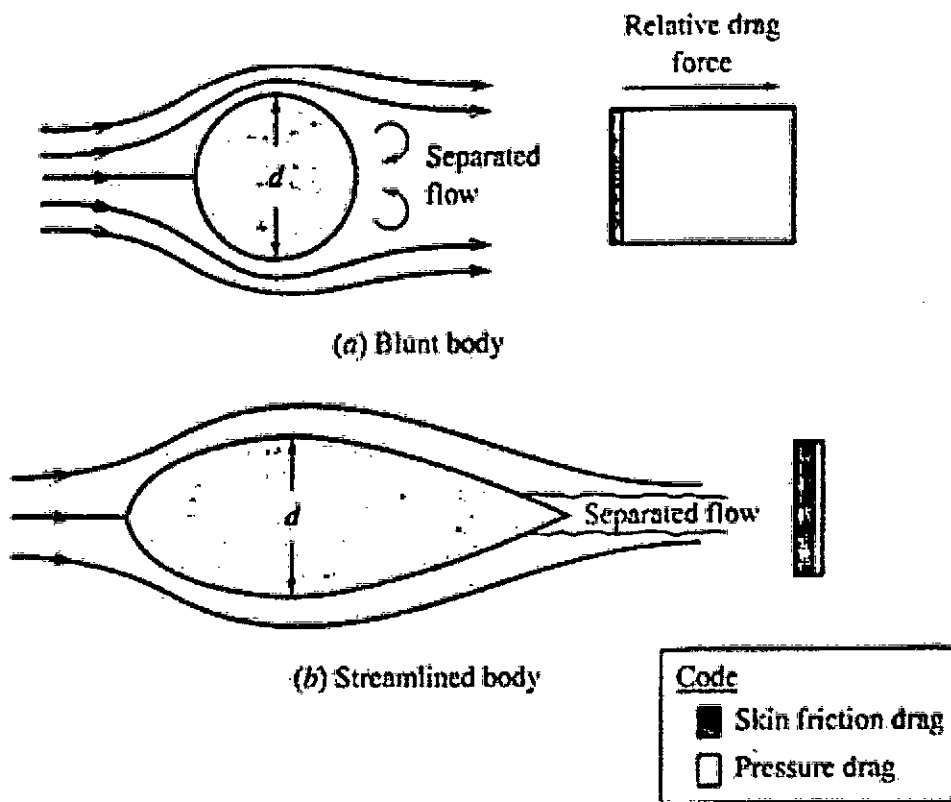
Figure 2.6: Comparison of flow separation and drag on blunt and streamlined shapes

(Source: Aerospace web.org)

2.3.3. Induced drag:

Lift is produced by accelerating airflow over the upper surface of a wing, creating a pressure difference between the air flowing over the wing upper and lower surfaces. On a wing of finite span, some air flows around the wingtip from the lower surface to the upper surface producing wingtip vortices. The vortices change the speed and direction of the airflow behind the trailing edge, deflecting it downwards, and thus inducing downwash behind the wing. This effect cause the induced drag for a finite wing as shown in figure 2.7.

Wingtip vortices also modify the airflow around a wing, compared to a wing of infinite span, reducing the effectiveness of the wing to generate lift, thus requiring a higher angle of attack to compensate, and tilting the total aerodynamic force rearwards. The angular deflection is small and has little effect on the lift. However, there is an increase in the

16

drag equal to the product of the lift force and the angle through which it is deflected. Since the deflection is itself a function of the lift, the additional drag is proportional to the square of the lift. Using the winglets at wing tip the significant amount of induced drag can be checked.
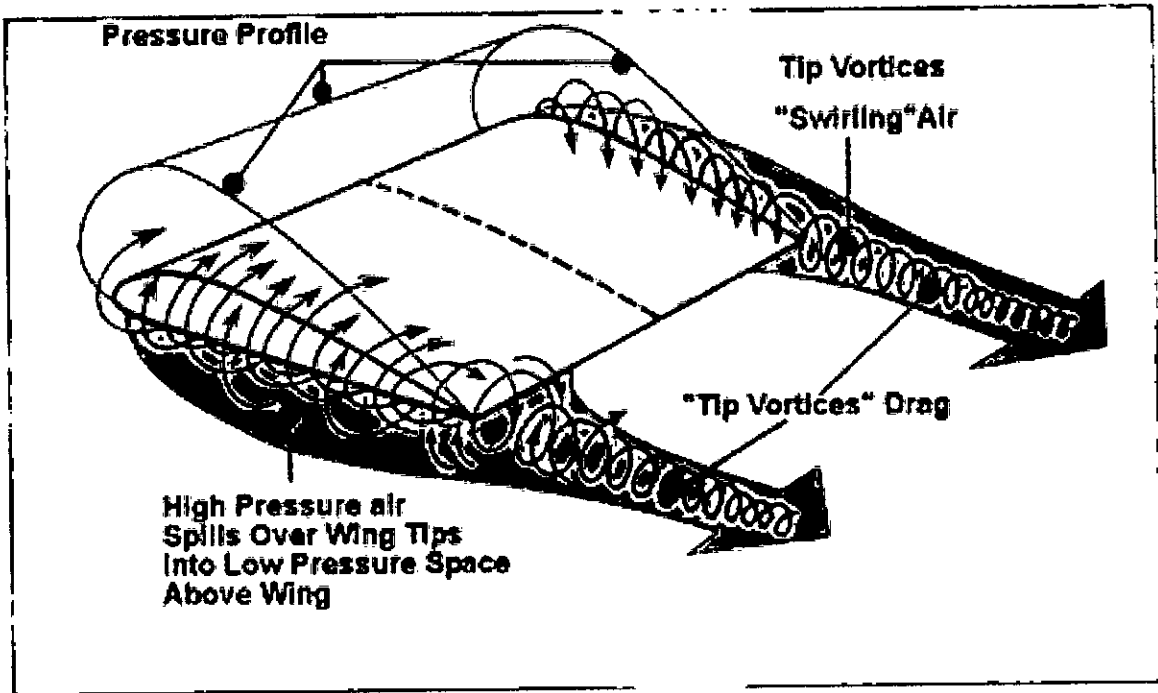
Figure 2.7: Wing tip vortices causes the induced drag
(source: www.centennialofflight.gov/ Theories_of_Flight)

2.3.4. Drag Crisis

The Reynolds number (R_e), for a baseball is calculated using $R_e=vd/\upsilon$. Where the diameter (d) of the baseball is (7.32 cm), v is the velocity relative to air, and υ is the kinematic viscosity of air (about 0.000015 m^2/s at 20° C). So the greater the velocity becomes the greater the Reynolds number. A drag crisis occurs when the laminar flow of air in a boundary layer near the ball begins to separate and becomes turbulent. The effect that the turbulence in the boundary layer causes will actually reduce the size of the turbulent wake behind the ball, and reduce the drag force. The drag crisis produces a regime where the aerodynamic drag force actually decreases as the velocity increases.

From the graph of drag coefficient (C_D) verses Reynolds number (R_e) it can be clearly observe the drag crisis for an immaged body in a flowing fluid.

2.4 Lift Coefficient

Lift is the force that holds an aircraft in the air. Lift is generated by a pressure difference across the wing. Airplanes fly as a result of Bernoulli's principle, which says that if air speeds up the pressure is lowered. When the air separates at the leading edge, the part that goes over the top must converge at the trailing edge with the part that goes under the bottom. This is the so-called "principle of equal transit times". Since the distance over the top of the wing must be longer than under the bottom and thus the airs goes faster over the top creating a region of low pressure. But the principle of equal transit times is not practically true. Practically the air that goes over the top of the wing gets to the trailing edge considerably before the air that goes under the wing. In fact, close inspection shows that the air going under the wing is slowed down from the "free-stream" velocity of the air. The fact is shown in figure 4.8. The pressure difference at the upper and lower surface causes the wing to float in the air and so the wing observes lift force.
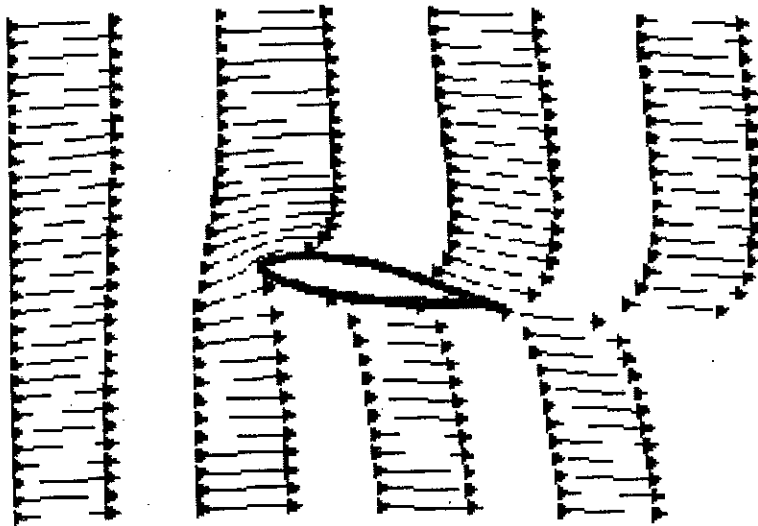
Figure 2.8: Flow over an aerofoil wing shows that the air going under the wing is slowed down from the "free-stream" velocity of the air

Lift coefficient is a non-dimensional value that changes with speed as well as the angle of attack and is dependent on the aircraft aerofoil section. Lift coefficient (C_L) is usually determined from the wind tunnel experiments.

Lift as a function of angle of attack

There are many types of wing: conventional, symmetric, conventional in inverted flight, the early biplane wings that looked like warped boards, and even the proverbial "barn door." In all cases, the wing is forcing the air down, or more accurately pulling air down from above. What all of these wings have in common is an angle of attack with respect to the oncoming air. It is this angle of attack that is the primary parameter in determining lift.

To better understand the role of the angle of attack it is useful to introduce an "effective" angle of attack, defined such that the angle of the wing to the oncoming air that gives zero lift is defined to be zero degrees. If one then changes the angle of attack both up and down one finds that the lift is proportional to the angle. Figure 2.9 shows the coefficient of lift (lift normalized for the size of the wing) for a typical wing as a function of the effective angle of attack. A similar lift versus angle of attack relationship is found for all wings, independent of their design.
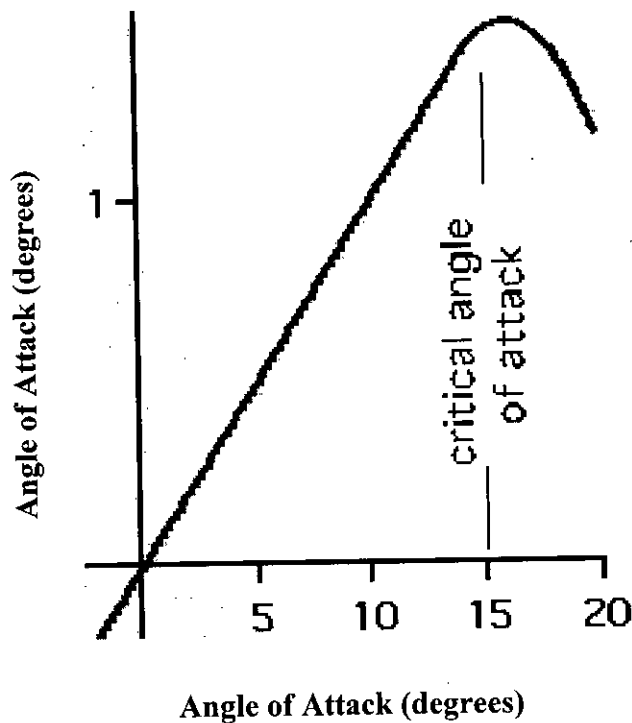
Fig 2.9: Coefficient of lift versus the effective angle of attack.

Typically, the lift begins to decrease at an angle of attack of about 15 degrees. The forces necessary to bend the air to such a steep angle are greater than the viscosity of the air will support, and the air begins to separate from the wing. This separation of the airflow from the top of the wing is a stall.

2.5 Lift and Drag calculation

The equation for lift is:

$$L = 1/2 \, \rho \, V^2 \, S_{ref} \, C_L$$

The equation for drag is:

$$D = 1/2 \, \rho \, V^2 \, S_{ref} \, C_D$$

Where ρ is the density of air, V is the relative velocity between the wing and air, C_L is lift coefficient, C_D is the drag coefficient and S_{ref} is reference area, is the area of the wing when viewed from overhead i,e the reference area is refer to chord length times the wing span.

2.6 Airfoil Geometry

Airfoil geometry can be characterized by the coordinates of the upper and lower surface. It is often summarized by a few parameters such as: maximum thickness, maximum camber, position of max thickness, position of max camber, and nose radius. One can generate a reasonable airfoil section given these parameters. This was done by Eastman Jacobs in the early 1930's to create a family of airfoils known as the NACA Sections. To describe the geometry of airfoil sections, the following terms are used:
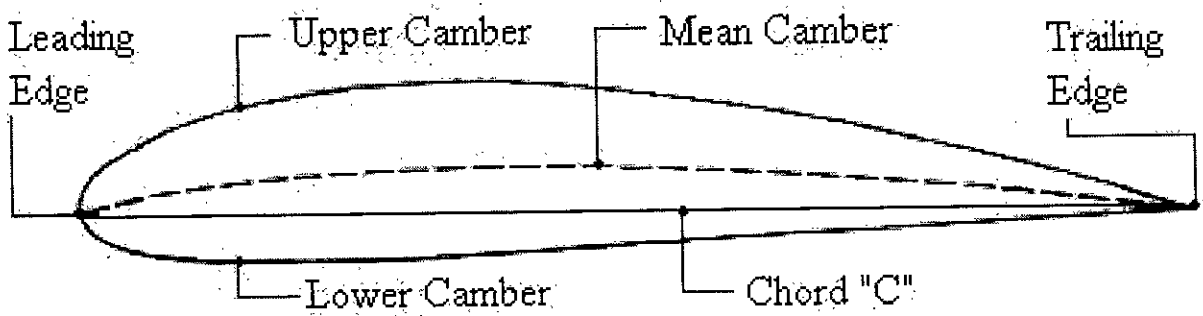
Figure 2.10: Airfoil section showing different geometrical terms.

- Mean line or mean chamber line is the line representing the locus of all points midway between the upper and lower surface of an aerofoil as measured perpendicular to the mean line.
- Chord line is the line joining the ends of the mean camber line.
- Thickness is the height of the profile measured perpendicular to the cord line.
- Camber or the maximum camber is the maximum rise of the mean line from the cord line.

21

- Leading edge radius is the radius of a circle, tangent to the upper and lower surfaces, with its centre located on a tangent to the mean-camber line drawn through the leading edge of this line. The leading edge radius is also given in percent of the chord.

These definitions are illustrated in Figure 2.10.

Chapter 3

ABOUT THE MODELS

A number of fuselages models of 1:32 with aerofoil cross-section and with conventional cylindrical cross section are manufactured in such a way that both the types of models have the same volume.

For pressure measurements static holes are made along the longitudinal axis of the fuselages and the pressure connections are made through small diameter tygon tubes and are connected to the digital pressure transducer through the selector valve.

Wings:

As four digit sections are suitable for low speed aircraft so for both wings and aerofoiled fuselage NACA four digit series aerofoil are considered in the present investigation. Same set of wings are used in both the type of models so that the results would show the comparison between the fuselages.

NACA Four-Digit Series:

The first family of airfoils designed using this approach became known as the NACA Four-Digit Series. The first digit specifies the maximum camber (m) in percentage of the chord (airfoil length), the second indicates the position of the maximum camber (p) in tenths of chord, and the last two numbers provide the maximum thickness (t) of the airfoil in percentage of chord. For example, the NACA 2412 thickness of 12% with a camber of 2% located 40% back from the airfoil leading edge (or 0.4c).

The **NACA 2412** cambered aerofoil wings with a cord 80 mm and a total span of 200 mm are used for both the models. Figure 3.1 shows the cross-section of an **NACA 2412** cambered aerofoil wing section.
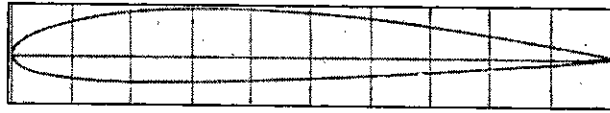
Figure 3.1: The real size cross-section of the model wings

The wings and all the fuselages are manufactured from a single piece of teak wood which has a density of approximately 650 kg/m³

3.1. Model plane with circular fuselage

This model has a total length of 274 mm with 44 mm long nose section, 70 mm long tail section and 160 mm long circular body with a diameter of 50 mm. The detail section is shown below in Figure 3.2.
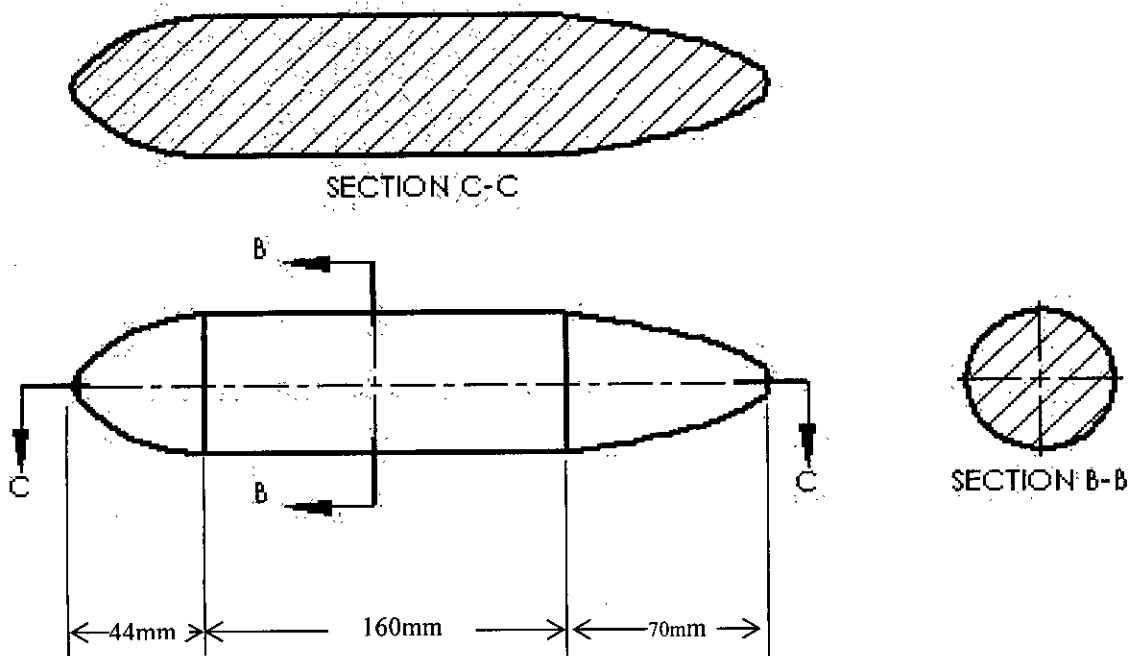
Figure 3.2: Cross section of the circular fuselage

By using SOLID WORKS software it can be found out the total volume of any 3D shape and for this case it is found that total volume of the circular fuselage is 438400 mm^3. Figure 3.3 shows the real model with circular fuselage.
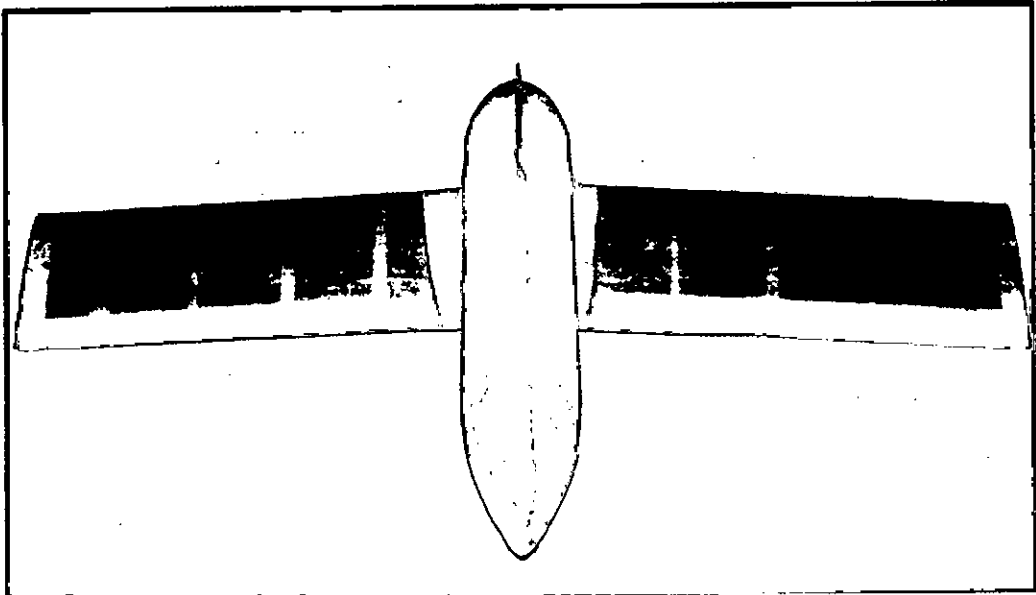
Figure 3.3: Photograph of the model plane with circular fuselage

After wings insertion the ultimate weight of the model plane with circular fuselages was 434 gm.

3.2. Model plane with aerofoil fuselage

In **NACA** aerofoil as 4 digit section are suitable for low speed aircraft so for aerofoiled fuselage it's also used **NACA 2412** cambered aerofoil section with a cord length 238mm and a span of 100mm so that the total volume would be same as circular fuselage i,e 438400 mm^3.

In the next page Figure 3.4 shows the real size cross-section of the model aerofoiled fuselage. Figure 3.5 shows the aerofoiled fuselage model without winglet while Figure 3.6 shows the aerofoiled fuselage model with winglets and both the models fitted with the spring balance to measure lift and drag force.

25
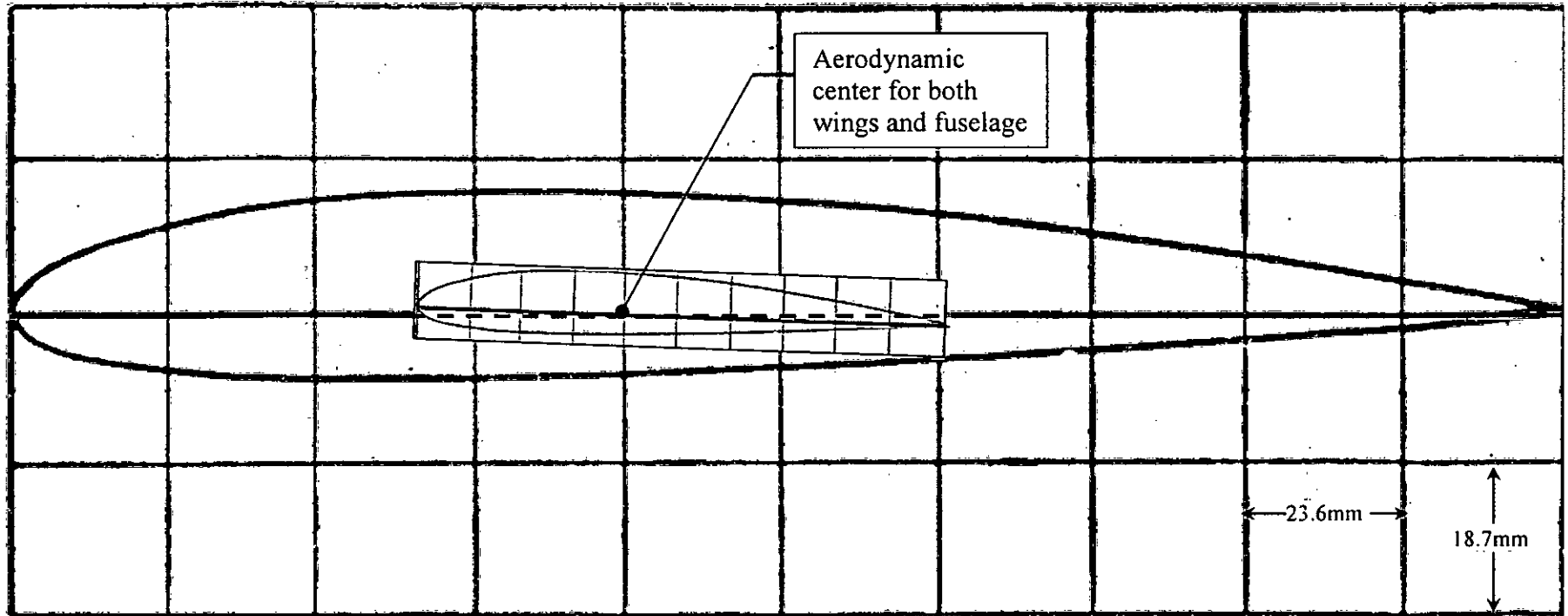
Figure 3.4: The real size cross section of the model aerofoiled fuselage, showing the wing position

26
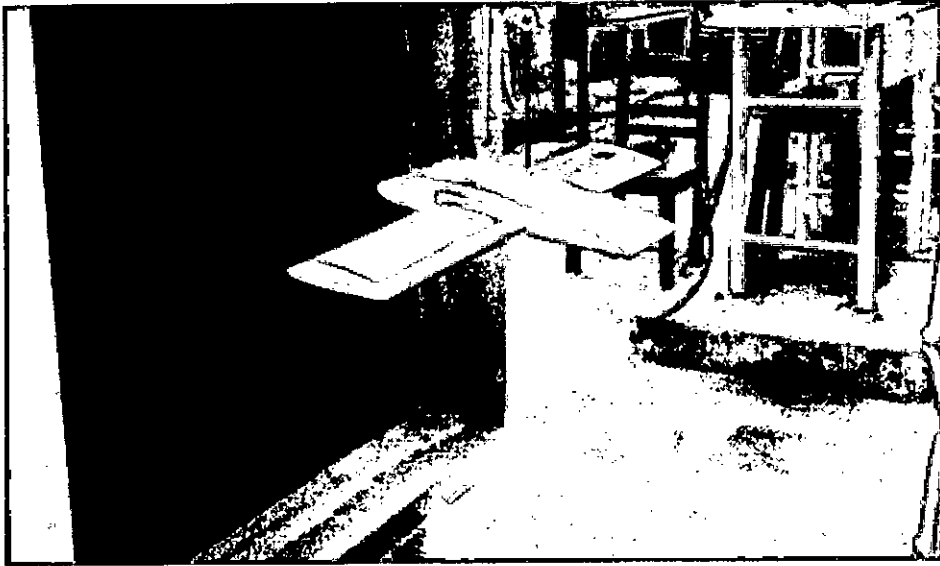
Figure 3.5: Photograph of the model plane with aerofoil fuselage without winglets.

Figure 3.6: Photograph of the model plane with aerofoil fuselage with winglets at the fuselage.

After wings insertion the ultimate weight of the model plane with aerofoil fuselages is 413 gm and after attaching winglets the weight become 509 gm.

27

Chapter 4

EXPERIMENTAL SETUP

A spring balance system specially designed and manufactured for the experiment is inserted in a huge size closed circuit wind tunnel with the models to get the lift and drag forces. So the tunnel section and the spring balance system are the main part of the test setup.

4.1. Wind tunnel:

The experiment is carried out in a 700mm×700mm closed circuit wind tunnel as shown in Figure 4.1. The wind tunnel is powered by the two 700mmD counter rotating Woods (U.K.) aerofoil fans. To minimize transmission of vibration generated in the fans unit, it is mounted in a separated heavy foundation and is connected to the rest of the wind tunnel by two vibration isolators made of heavy canvas cloth at both side of the fan unit. At the discharge of the fans there is a silencer to reduce the sound level. From the silencer air flow passes through the flow controlling butterfly valve, diffuser and the plenum chamber to stabilize the flow to certain level. Air from the plenum chamber passes over the cooling coil and through the air filter before entering the parabolic contraction cone. In the contraction cone the dimension is reduced from 1525mm×1525mm to 700mm×700mm. at the delivery of the contraction cone where there is a honey comb flow strainer to straighten out any flow diversity and break down any large eddy before entering into the 9m long test section. Flow form the test section goes back to the fan unit through the return duct. The fan motors are powered by 400V-3Φ-50Hz power supply through motor speed controller. Thus the wind speed in the tunnel can be varied both by controlling the fan motor speed as well as by controlling the butterfly valve. For better understanding of the Wind Tunnel details of some of its major components are illustrated below:

- **Fan Unit:** The fan unit consists of two counter rotating axial flow fans powered by centrally mounted 22 kw a.c. motors. The blades of the fans are adjustable to minimize the power loss and sound generated in the fan blades; its angles are set

such that the flow enters in both the fan blades tangentially without any shock. By changing the blade angles of both the fans flow velocity range in the wind tunnel can be changed.

- **Air Speed:** In the present setup of fan blade angle setting the maximum air speed is 44.5 m/s (160km/hr) which can be increase to as high as 70m/s (250 km/hr) by changing the blade angles of the fans. The air speed can be varied by two different ways; i) by using an electronically controlled butterfly valve and ii) by controlling the motor speed by an electrical frequency converter. The later one is more convenient to change the air speed smoothly and frequently from zero to any required velocities. In this experiment the frequency converter is used to vary the air speed.

- **Air Temperature Controlling:** In a close circuit wind tunnel as the same air circulates inside the tunnel so the air temperature increases due to adiabatic power transfer from the rotating blades to the flowing air and the friction loss in the tunnel. A 16 ton DX cooling coil is used to control the air temperature to the required level. However it does not require to control the air temperature as in the present investigation test is carried out in the open section and the velocities of air are comparatively low. Although at low speed it produces some heat if the tunnel runs continuously for a long time, so to avoid this, the tunnel was allowed to shutdown for a while after taking each set of data.

4.2. Test sections:

The tunnel has seven 700mm×700mm test sections. To facilitate the present experiment to be carried out in the open air condition the diffuser connected at the end of the last test section is taken out and to avoid the buffer effect of the discharge side of the test section is fitted with a 700mm×700mm discharge duct and to provide a shock less entry a 1000mm×1000mm to 762mm×762mm bell mouth entry is added at the return duct. Thus a 700mm×700mm×406mm open

flow field created between the discharge duct and the bell mouth entry become the experimental space where desire velocity is obtained. Figure 4.1 shows the detail out line of the Wind Tunnel.
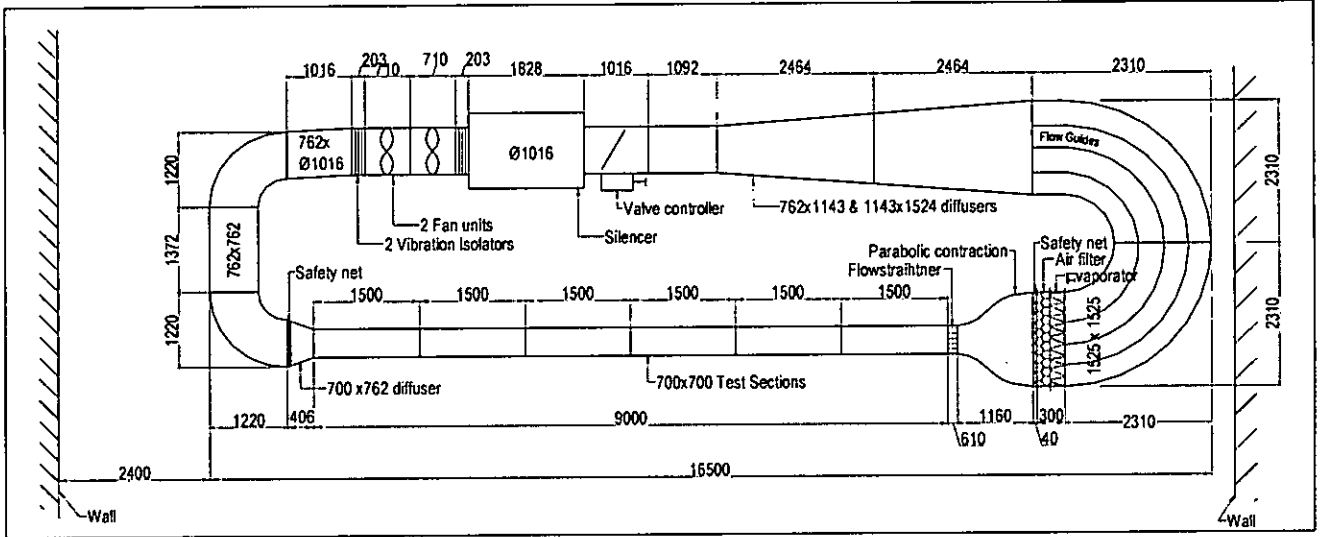
Figure 4.1: 700mm × 700mm closed circuit Wind Tunnel
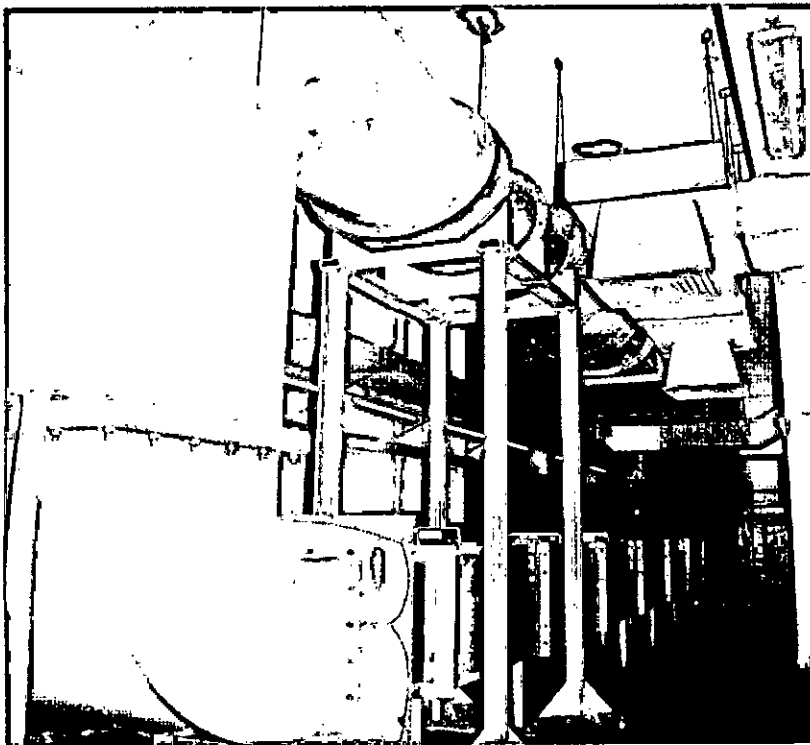
Figure 4.2: Actual photograph of the 700mm × 700mm closed circuit Wind Tunnel
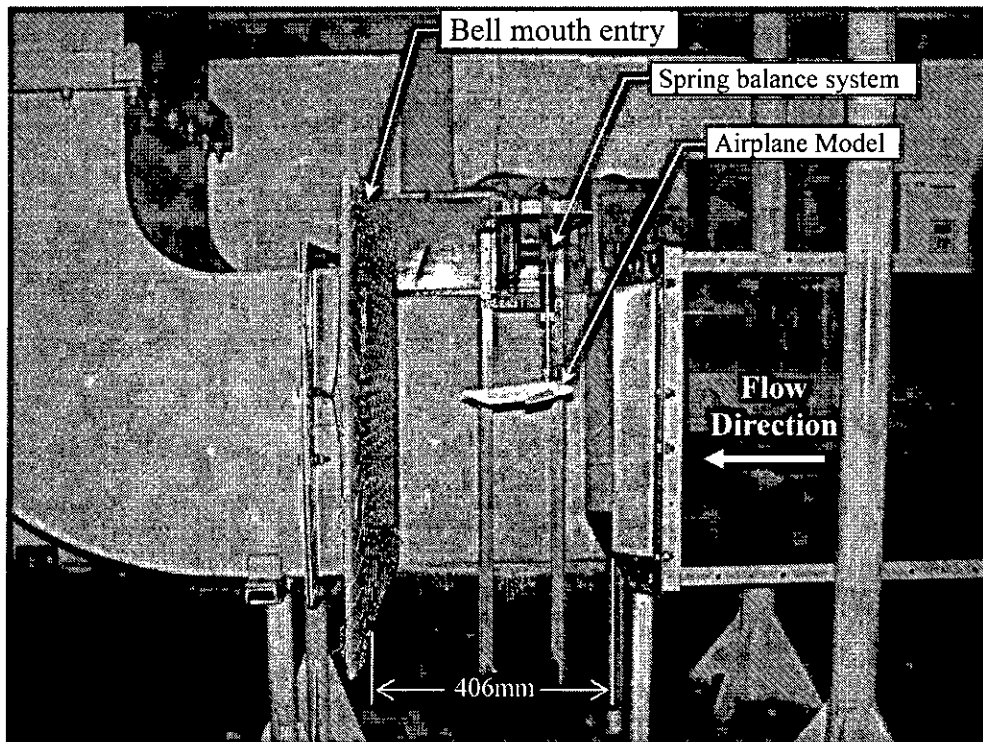
Figure 4.3: Test section photograph of the 700mm × 700mm closed circuit Wind Tunnel

4.3. Spring Balance System:

Two springs in a balance condition are used to determine the lift and drag forces simultaneously. The vertical spring provides the lift forces and the horizontal spring indicates the drag forces.

The two components spring balance system (Figure- 4.4) specially made for the experiment is mounted on the support bar of the mounting frame and is placed in the experimental space. The balance is such that fuselage models can be mounted on the holding bar which is supported by springs and is guided by bearings so that by the action of the lift force it can move up against the spring force with negligible friction. The holding bar is held in the vertical position by a horizontal drag force balancing spring system mounted on the same support bar. When the drag force deviate the holding bar from the vertical position; by adjusting the drag spring the bar can be pushed back to its vertical position and both the drag force and the lift force are found simultaneously from the

31

deflections of the springs. Figure – 4.4 shows the different parts of the spring balance system.
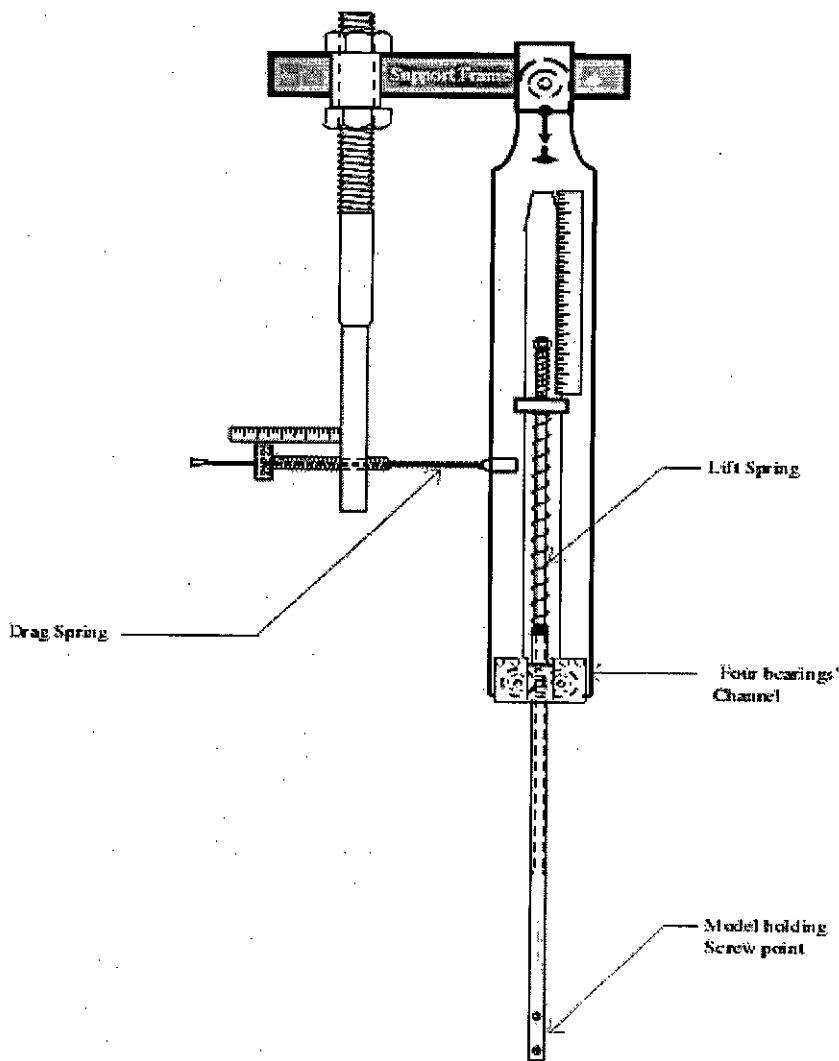
Figure 4.4: Spring balance system to measure the lift and drag simultaneously

Chapter 5

EXPERIMENTAL PROCEDURE

5.1. Working Principle

At first the models with its force balance system were placed in a open space in between the test section elements of a 700mm×700mm wind tunnel. These arrangements were made to get the desired wind speed at atmospheric pressure. Then the tunnel started and the air velocity increased with the help of a simple knob attached to the frequency inverter. The digital velocity transducer showed the air velocity in m/s.

For spring balance system at any air speed the drag spring have to adjust in such a way that the rectangular stem became vertical. This is a balance condition. At this position the deflection of the horizontal spring provides the drag force and the deflection of the vertical spring provides the lift force.

There are two springs in the vertical stem. The small spring provides the lift until the lift overcomes the model self weight. When the smaller spring expands fully the long spring began to compress. Then the long spring force combine with model self weight give the actual lift.

The whole experiments were carried out for different angle of attack of the fuselages and the wings as well as for different air speeds.

For pressure measurements the pressure connections were made through small diameter tygon tubes and were connected to the digital pressure transducer through the selector valve. There were eighteen pressure probes around the fuselages and all were connected to the selector valve which acted like a multiplexer. So, to set 1 in the selector valve means the digital pressure transducer are allowed to show the pressure on the first probe. Before taking any data sufficient time were allowed to make the digital

transducer become stable to a certain value. The corresponding pressures were recorded in the computer and then applying proper equations the lifts and drags were calculated.

5.2. Flow field examination

Before starting the experiment with the models the flow field of the test section is examined with the help of a transverse mechanism. As the whole experiment was carried out for different air velocities so the flow field was also examined for those velocities. The following table shows the grid velocities at different air speeds.

Table 5.1: Flow field analysis (U/U_a at different grid points in test section)

Distance from the surface of the tunnel, mm	Air velocity (km/hr)							
	50	60	70	80	90	100	110	120
2	0.61	0.69	0.67	0.65	0.68	0.68	0.69	0.72
10	0.76	0.84	0.82	0.79	0.78	0.81	0.79	0.8
20	0.83	0.87	0.83	0.86	0.84	0.86	0.85	0.85
30	0.86	0.9	0.87	0.9	0.88	0.88	0.88	0.89
40	0.88	0.95	0.9	0.91	0.9	0.9	0.91	0.9
50	0.9	0.96	0.93	0.92	0.94	0.93	0.92	0.93
60	0.92	0.98	0.94	0.95	0.95	0.94	0.93	0.95
70	0.97	0.99	0.94	0.98	0.96	0.95	0.98	0.96
80	1	1	0.98	0.99	0.97	0.97	0.98	0.97
90	1	1	1	1	0.98	0.99	0.99	0.98
100	1	1	1	1	1	1	1	0.99
110	1	1	1	1	1	1	1	1
120	1	1	1	1	1	1	1	1
210	1	1	1	1	1	1	1	1
300	1	1	1	1	1	1	1	1
350	1	1	1	1	1	1	1	1
400	1	1	1	1	1	1	1	1
490	1	1	1	1	1	1	1	1
580	1	1	1	1	1	1	1	1
590	1	1	1	1	1	1	1	1
600	1	1	1	1	1	1	1	0.99
610	1	1	1	1	0.98	0.99	0.99	0.98
620	1	1	0.98	0.99	0.97	0.97	0.98	0.97
630	0.97	0.99	0.94	0.98	0.96	0.95	0.98	0.96
640	0.92	0.98	0.94	0.95	0.95	0.94	0.93	0.95
650	0.9	0.96	0.93	0.92	0.94	0.93	0.92	0.93
660	0.88	0.95	0.9	0.91	0.9	0.9	0.91	0.9
670	0.86	0.9	0.87	0.9	0.88	0.88	0.88	0.89
680	0.83	0.87	0.83	0.86	0.84	0.86	0.85	0.85
690	0.76	0.84	0.82	0.79	0.78	0.81	0.79	0.8
698	0.61	0.69	0.67	0.65	0.68	0.68	0.69	0.72

Uniform flow regime

1.1

1

0.9

U/Uα 0.8

0.7

0.6

0.5

Circular Fuselage

Wing

|←— 200 —→| 50 |←— 200 —→|

Aerofoiled Fuselage

Wing

|←— 200 —→|← 100 →|←— 200 —→|

2   100   200   300   400   500   600   698

Distance along X axis (mm)
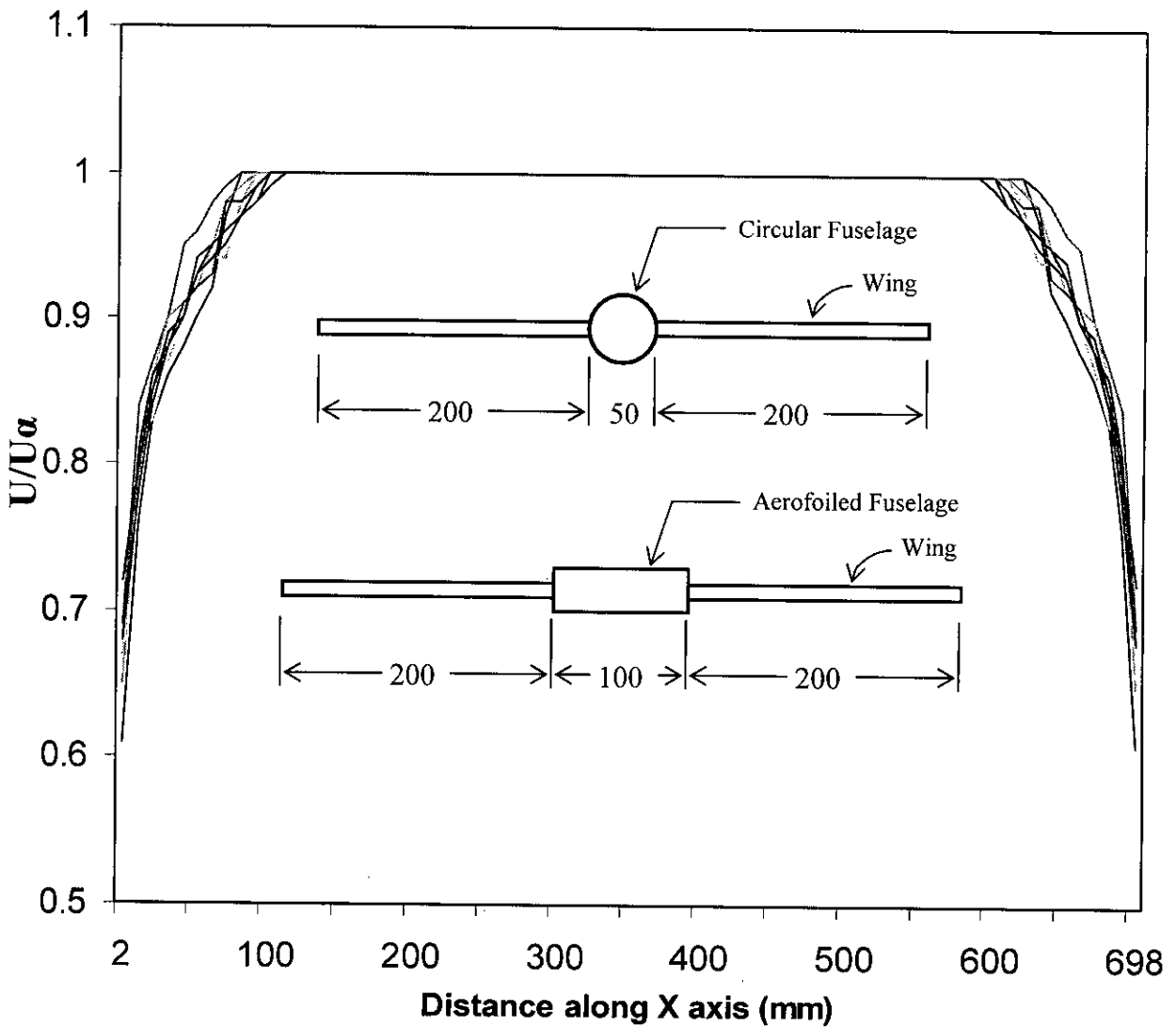
Figure 5.1: Flow field showing all models are in uniform flow regime

So from figure **5.1** it found that the boundary layer increases as flow velocity increase and at maximum air speed the boundary layer consume 100mm at one side i,e 200mm for both side along any axis. Since at test section the tunnel cross section is 700mm×700mm, so considering boundary layer the uniform flow regime become 500mm×500mm. As the maximum width of the models is 500mm and maximum height is 50mm so the model is in uniform flow regime even when the air velocity is maximum, as shown in figure **5.1.**

Chapter 6

RESULTS AND DISCUSSION

6.1 Introduction

The whole investigation is done in two different methods. At first the lifts and drags are measured for different angle of attack of the fuselage and as well as for different angles of attack of the wings with the help of spring balance system specially manufactured for this investigation. For each combination of angle of attack of the fuselage and the wing Lift Coefficient vs. Reynolds No. curves, Drag Coefficient vs. Reynolds No. curves and L/D vs Reynolds No. curves are drawn. For comparison among the models the curves at a particular angle of attack for all the three modes are drawn in a single graph.

After comparison among the models and among the angle of attack the whole investigation is done again where the lifts and drags are measured by pressure taping around the aerofoiled fuselage. So in second investigation the lifts and drags only generated by the fuselages are measured. In second case again the Lift Coefficient vs. Reynolds No. curves, Drag Coefficient vs. Reynolds No. curves and L/D vs Reynolds No. curves are drawn for different angles of attack of the Fuselage. The curves for each case and their findings are discussed in the following segments.

6.2. Lift and Drag measurement with spring balance mechanism

For all the models at first the angle of attack of the fuselage (θf) were fixed at 0° and the relative angle between wings and fuselage (θw) was varied to 2°, 4° and 6° (subsection **6.2.1**). Similarly fixing the fuselage angle (θf) at 4°, 8° and 12° the wing angle was also varied (given in subsections **6.2.2**, **6.2.3** and **6.2.4** respectively). The corresponding spring deflections were recorded in a computer and converted to forces.

For convenience the following symbols are used in all the data tables:

θf => Fuselage angle of attack in degree

θw => Relative angle between wing and fuselage

So, actual wing angle of attack is **(θf +θw)** degree

L => Lift force in kg, C_L => Lift Coefficient

D => Drag force in kg, C_D => Drag Coefficient

L/D => Lift to Drag ratio

6.2.1. Angle of attack of the fuselage, θf = 0°

This section fixed for **θf = 0°** and again subdivided in to three sections i,e **6.2.1.(a)**, **6.2.1.(b)** and **6.2.1.(c)** so that each section represent for **θw = 2°**, **θw =4°** and **θw = 6°** respectively.

6.2.1. (a). θf = 0° and θw = 2°

For different air velocities the lifts, drags and the lift to drag ratios for all the three models are given in the table **6.2.1.(a)**. With the help of the table corresponding graphs are plotted. To compare among the models the variation of lift coefficients for all the models are drawn in a single graph. Similarly the variation of drag coefficients and L/D's are also drawn separately in single graph.

If it's considered the weight of all the models is around 0.4 kg then from the Figure 6.2.1. (a) (i) it can be found that the take of speeds are 75km/hr (Re = 1.54×10^5) for circular fuselage model, 67km/hr (Re = 1.375×10^5) for aerofoil fuselage model and 63 km/hr (Re = 1.29×10^5) for wingleted fuselage model.

From Figure 6.2.1. (a) (ii) it's found that as air speed increases beyond 80 km/hr (Re = 1.64×10^5) the drag suddenly reduces. This drag crisis is due to instability of the flow around the fuselage causes immature separation of the flow. But as the fuselage angle of attack is zero ($\theta f = 0^\circ$) so this immature separation of the flow apparently causes no lift crisis. Beyond this point the flow become turbulent and the velocities beyond 100km/hr (Re = 2.05×10^5) the model become unstable. At this point flattering of the model is clearly observed.

From Figure 6.2.1. (a) (iii) we found the lower values of lift to drag ratio (L/D) for aerofoil fuselage than circular fuselage although aerofoil fuselage produce higher lifts. This is due to tip vortices formed at both side of the finite aerofoil fuselage which generates induced drag and total drag increases to a higher value.

This induced drag can be reduces by using winglet at both sides of the aerofoil fuselage which reduce the tip vortices. So for wingleted aerofoiled fuselages it provides maximum lift to drag ratio.

6.2.1. (b). $\theta f = 0^\circ$ and $\theta w = 4^\circ$

Table 6.2.1. (b). shows the data for $\theta f = 0^\circ$ and $\theta w = 4^\circ$

As wings angle (θw) increases from 2° to 4° similar pattern found in all the curves but take-off speed reduced to 65, 57 and to 55 km/hr for circular, aerofoil and wingleted fuselages respectively as shown in Figure 6.2.1. (b) (i)., Figure 6.2.1. (b) (ii)., Figure 6.2.1. (b) (iii).

Here also drag crisis found after 90 km/hr (Re = 1.85×10^5) but no unstable point found up to 120 km/hr (Re = 1.246×10^5) as total lift increased by the wings.

6.2.1. (c). $\theta f = 0°$ and $\theta w = 6°$

Further increase of the wings angle to $6°$ also provides the similar curves but here take-off speed for all the fuselages are same (from **Figure 6.2.1. (c) (i)**). This is due to the fact that most of the lifts are found from the wings whose are same for all the models. So different fuselage has less effect on overall lift and thereby lift to drag are similar for all the models although from 60 to 90 km/hr speed provide the maximum lift to drag for wingleted fuselage.

At this combination a little drag crisis occur for wingleted fuselage at 70 to 75 km/hr (Re = 1.44×10^5 to 1.538×10^5) air speed as indicates in **Figure 6.2.1. (c) (ii)**.

From the curves in **Figure 6.2.1. (c) (i)**, **Figure 6.2.1. (c) (ii)** and **Figure 6.2.1. (c) (iii)** it can be concludes that $\theta f = 0°$, $\theta w = 6°$ is not a good combination for level flight.

6.2.2. Angle of attack of the fuselage, $\theta f = 4°$

6.2.2. (a). $\theta f = 4°$ and $\theta w = 2°$

Now fuselage angle of attack is increased to $4°$ shows the drag crisis as well as the lift crisis occurs earlier for wingleted fuselage at 60 km/hr (Re = 1.23×10^5). Here the take-off speed reduced to 50 km/hr (Re = 1.03×10^5) for wingleted fuselage (from **Figure 6.2.2. (a) (i)**).

At this combination of angle of attack at lower speed an excellent lift to drag ratio is found as shown in **Figure 6.2.2. (a) (iii)**.

6.2.2. (b). $\theta f = 4°$ and $\theta w = 4°$

For this combination the data are shown in **Table 6.2.2. (b)**.

In this combination high lift to drag ratio found at air speed up to 80 km/hr (Re = 1.64×10^5). But beyond 80 km/hr a sudden reduction in lift i.e., lift crisis found as shown in **Figure 6.2.2. (b) (i) and Figure 6.2.2. (b) (ii)**. This is a very good combination because lift to drag ratio is higher at low speed

(**Figure 6.2.2. (b) (iii)**) and for wingleted fuselage the take-off speed is much lower than 50 km/hr. So this combination requires short runway and low take-off time at operational condition.

6.2.2. (c). $\theta f = 4°$ and $\theta w = 6°$

The data are shown in **Table 6.2.2. (c)**.

Figure 6.2.2. (c) (iii) also shows L/D is best for wingleted fuselage but not as high as the combination of $\theta f = 4°$, $\theta w = 4°$. Between 70 to 80 km/hr (Re = 1.44×10^5 to 1.64×10^5) drag crisis as well as a little lift crisis occur and the take off speed is much lower than 50 km/hr (Re = 1.03×10^5) for both aerofoiled fuselages but for circular fuselage take-off speed is same as $\theta f = 4°$, $\theta w = 4°$ i.e., 53 km/hr (Re = 1.44×10^5). (**Figure 6.2.2. (c) (i) Figure 6.2.2. (c) (ii)**)

Other investigated combinations are:

6.2.3. Angle of attack of the fuselage, $\theta f = 8°$

6.2.3. (a). $\theta f = 8°$ and $\theta w = 2°$
6.2.3. (b). $\theta f = 8°$ and $\theta w = 4°$
6.2.3. (c). $\theta f = 8°$ and $\theta w = 6°$

6.2.4. Angle of attack of the fuselage, $\theta f = 12°$

6.2.4. (a). $\theta f = 12°$ and $\theta w = 2°$
6.2.4. (b). $\theta f = 12°$ and $\theta w = 4°$
6.2.4. (c). $\theta f = 12°$ and $\theta w = 6°$

All of the above combinations shows the similar pattern in the lift coefficient and drag coefficient curves but the lift to drag ratio is not better than the combination $\theta f = 4°$ and $\theta w = 4°$. And for all these curves it's found that circular fuselage model has the same take-off speed (approximately 53 km/hr) but wingleted fuselage has much lower take-off speed than 50 km/hr.

So after analyzing all the graphs we found that aero-foiled fuselages with winglets provided maximum lift with respect to drag. So the wingleted fuselage model is the best model amongst the three models.

6.2.5. Analyzing the graphs for only the wingleted aero-foiled fuselage for different angle of attack of the fuselages (θf) as well as for different wing angle with fuselage (θw).

Now it is analyzed only the graphs for the wingleted aero-foiled fuselage for different angle of attack of the fuselages (θf) as well as for different wing angle with fuselage (θw) to sort out the best angle combination.

To do that it first analyzed different L/D curves for particular θw with different θf. The data for only wingleted aerofoiled fuselage model are shown in **Table 6.2.5. (a), Table 6.2.5. (b)** and **Table 6.2.5. (c).**

So in case of **wingleted aerofoiled fuselage** for any angle between wings and fuselages (i.e. θw = 2°, 4° or 6°) we found that at low speed (below 80 km/hr, i.e. Re = 1.64×10^5) amongst all the angles of attack for θf = 4° provide the maximum lift corresponding to a drag. (From **Figure 6.2.5. (a) (iii), Figure 6.2.5. (b) (iii)** and **Figure 6.2.5. (c) (iii)**)

6.2.6 Analyzing the graphs for the wingleted aero-foiled fuselage for fixing angle of attack of the fuselages (θf =4°) but varying the wing angle (θw).

Now for the same model for a fixed angle of attack of the fuselages at θf = 4° it is found that the curves (**Figure 6.2.6.(i)., Figure 6.2.6.(ii)., Figure 6.2.6.(iii)**) for different wing angles (θw) to sort out best θw. The data for fixed fuselage angle, θf = 4° is shown in **Table 6.2.6.**

Here it is found that for particular angle of attack of the fuselages at $\theta f = 4°$, the relative wing angle $\theta w = 4°$ dominating the lift corresponding to a drag.

So from the whole analysis it can be concluded that $\theta f = 4°$ and $\theta w = 4°$ is the best combination during level flight.

6.3. Lift and Drag measurement by pressure taping

From above data and graphs it is found that during flight of an UAV with wingleted aerofoil fuselages maintaining the fuselages angle at $\theta f = 4°$ provide the maximum lift corresponding to a drag. The all above data were taken by spring balance system. To verify the above data finally lift and drag were measured by pressure taping around the aerofoiled fuselage.

To do that an internally grooved aerofoiled fuselage were manufactured with inserting metallic tubes inside the fuselage along the grove such that the external holes were perpendicular to the local surface. Then tygon tubes connecting the metallic tubes were drawn out from the fuselage through side holes to the selector switch to measure the pressures around the fuselage.

The whole experiments were carried out for different angle of attack of the fuselage and for different air speed and the data were recorded in a computer. From this data necessary lifts and drags were calculated. The pressure taping systems for calculating lifts and drags are shown in the following figures.
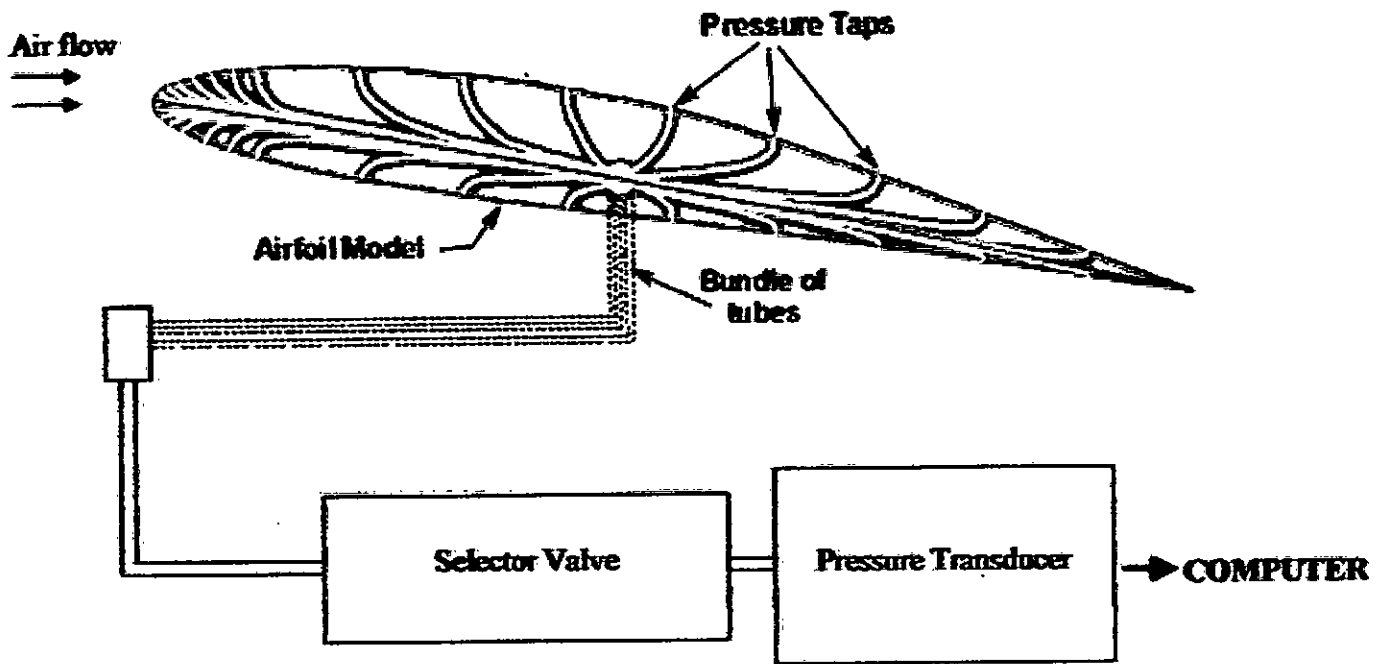
Figure 6.1: Pressure taping system for calculating lifts and drags
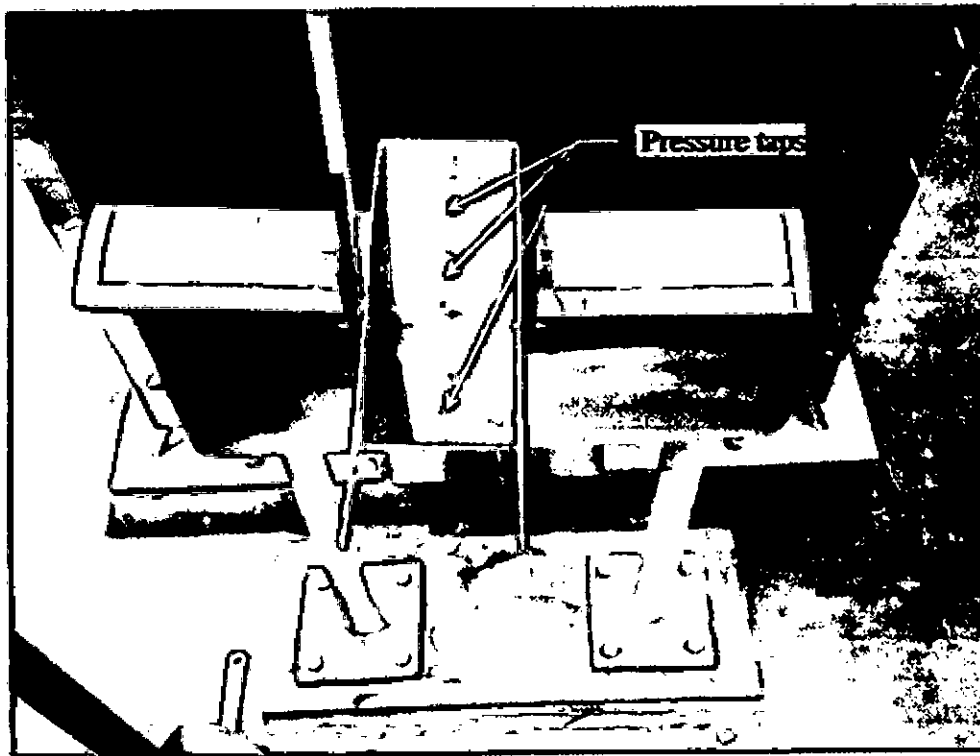
Figure 6.2: Model photograph showing the pressure taps around the aerofoiled fuselage.

The corresponding measuring pressures are given in tables **6.3 (a)**, **6.3 (b)**, **6.3 (c) and 6.3 (d)**. From these tables the lifts and drag can be calculated by the following equation - (i) and equation - (ii).
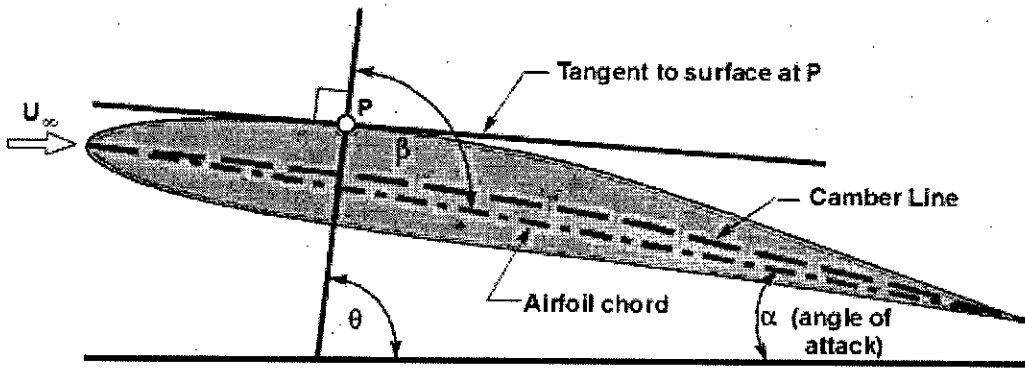
Figure 6.3: Showing angles for calculating lifts and drags by pressure taping.

Here for both upper and lower surface $\theta i = \beta i - \alpha$

$$L = \{\sum Pi \sin \theta i \times li \, (i=11\text{-}18) - \sum Pi \sin \theta i \times li \, (i=1\text{-}10)\} \times 100 \times 10^{-6} \text{ kg} \text{ ----------- (i)}$$

$$D = \{\sum Pi \cos \theta i \times li \, (i=11\text{-}18) - \sum Pi \cos \theta i \times li \, (i=1\text{-}10)\} \times 100 \times 10^{-6} \text{ kg} \text{ --------- (ii)}$$

Where 100 is the width of the fuselage in mm and li is the corresponding length in mm represent by a single pressure tap. So $\sum li \times 100 \times 10^{-6}$ is the total outer surface area of the fuselage in m^2.

Values of βi and li are given in **Table 6.3 (e)** and the calculated lifts and drags are given in table **6.3 (f)**. From this lift and drag forces corresponding lift and drag coefficients are calculated. Then from these calculated data corresponding lift coefficient, drag coefficient and L/D curves are drawn with the change of Reynolds Number. **Figure 6.3 (i), Figure 6.3 (ii)** and **Figure 6.3 (iii)** shows the variation of lift coefficient and drag coefficient on the fuselage with the change of Reynolds Number.

From these curves it's clear that fuselage angle of attack, $\theta f = 4°$ provide the maximum lift to drag ratio (**Figure 6.3 (iii)**) which is also found from spring balance system. So spring balance system is verified by pressure tapping system.

CURVES
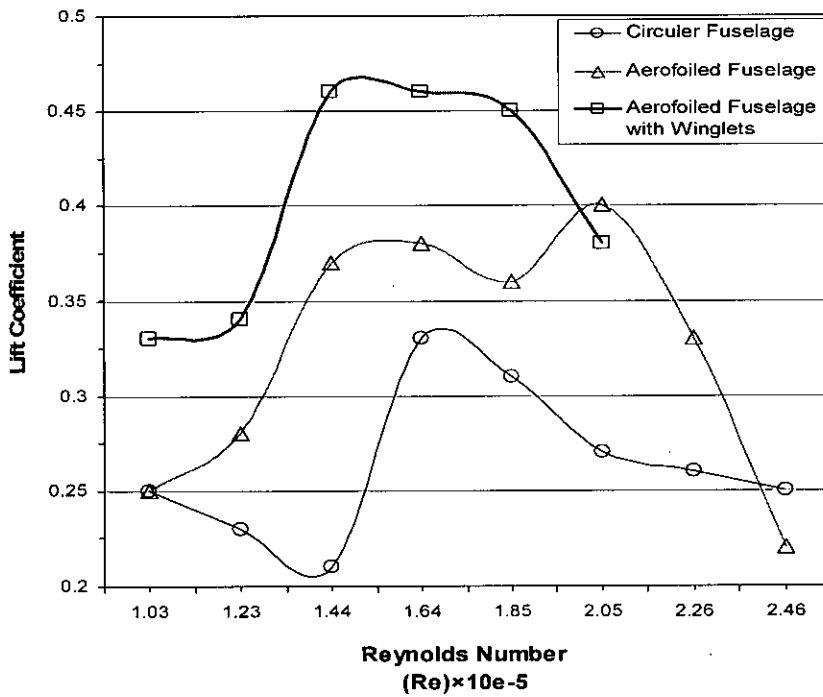
Figure 6.2.1. (a) (i).: Lift Coefficient vs. Reynolds No. curves for θf = 0°, θw = 2°
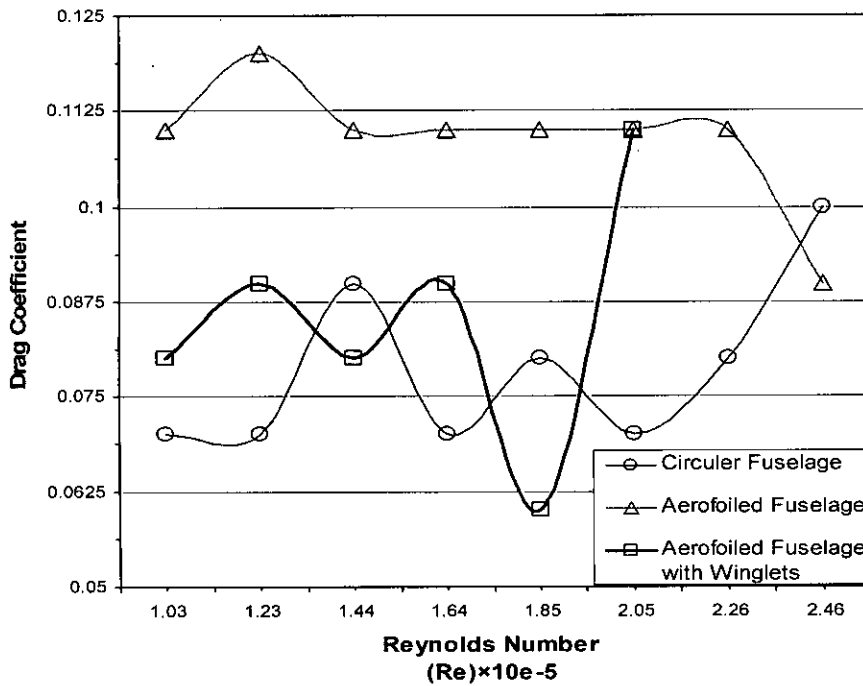
Figure 6.2.1. (a) (ii).: Drag Coefficient vs. Reynolds No. curves for θf = 0°, θw = 2°
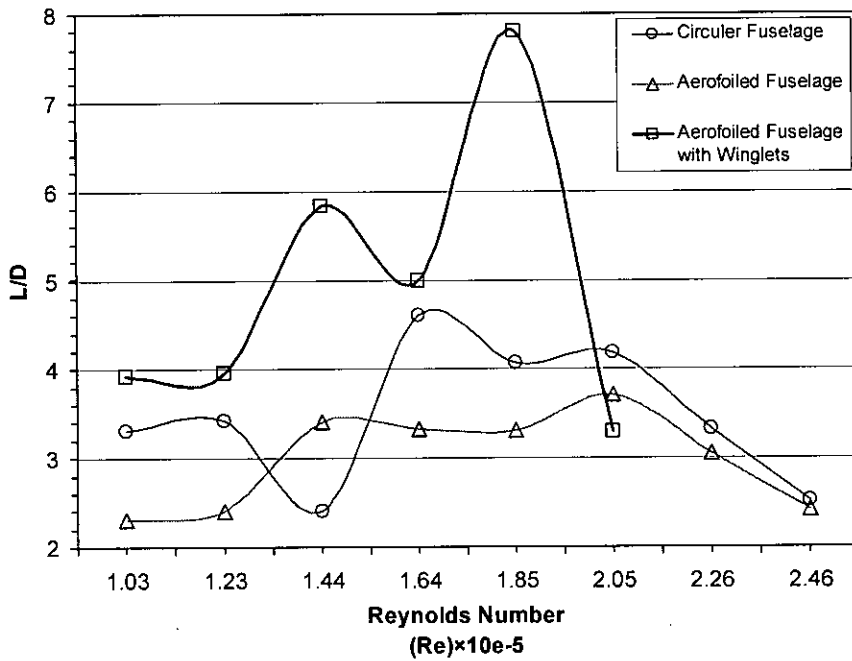
Figure 6.2.1. (a) (iii).: L/D vs. Reynolds No. curves for θf = 0°, θw = 2°
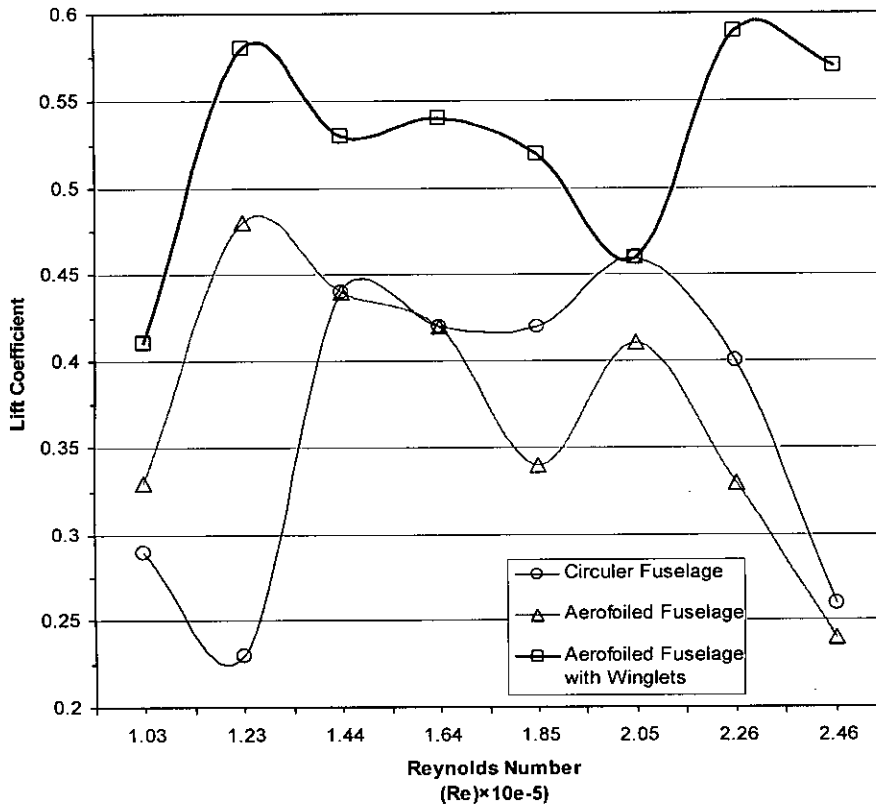
Figure 6.2.1. (b) (i).: Lift Coefficient vs. Reynolds No.curves for θf = 0°, θw = 4°
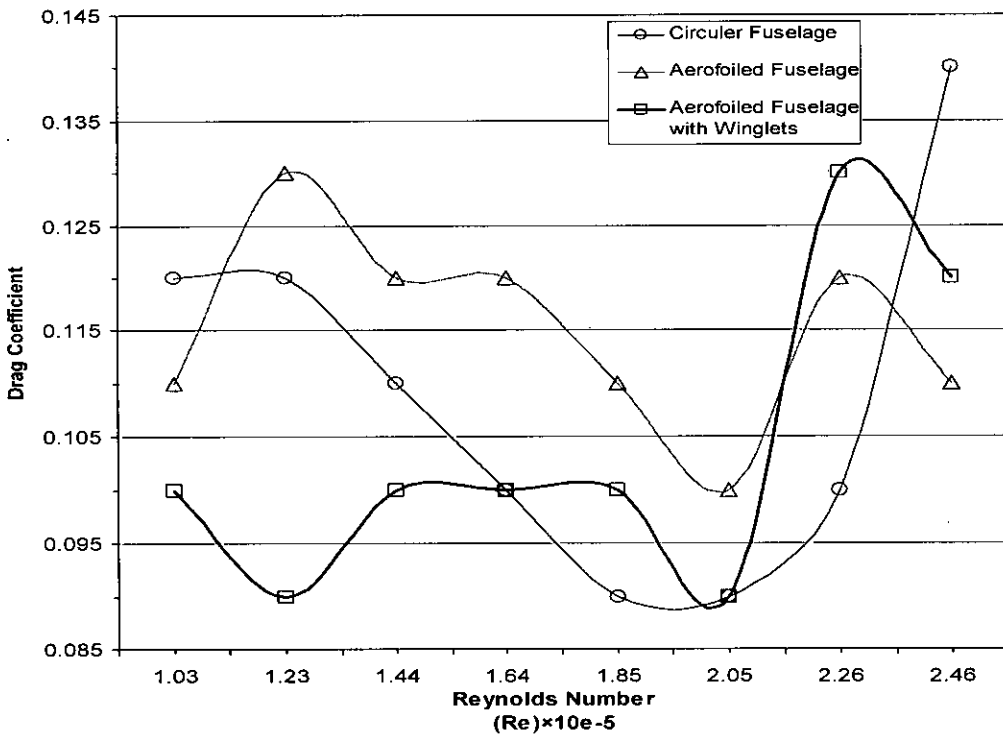
Figure 6.2.1. (b) (ii).: Drag Coefficient vs. Reynolds No. curves for $\theta f = 0°$, $\theta w = 4°$
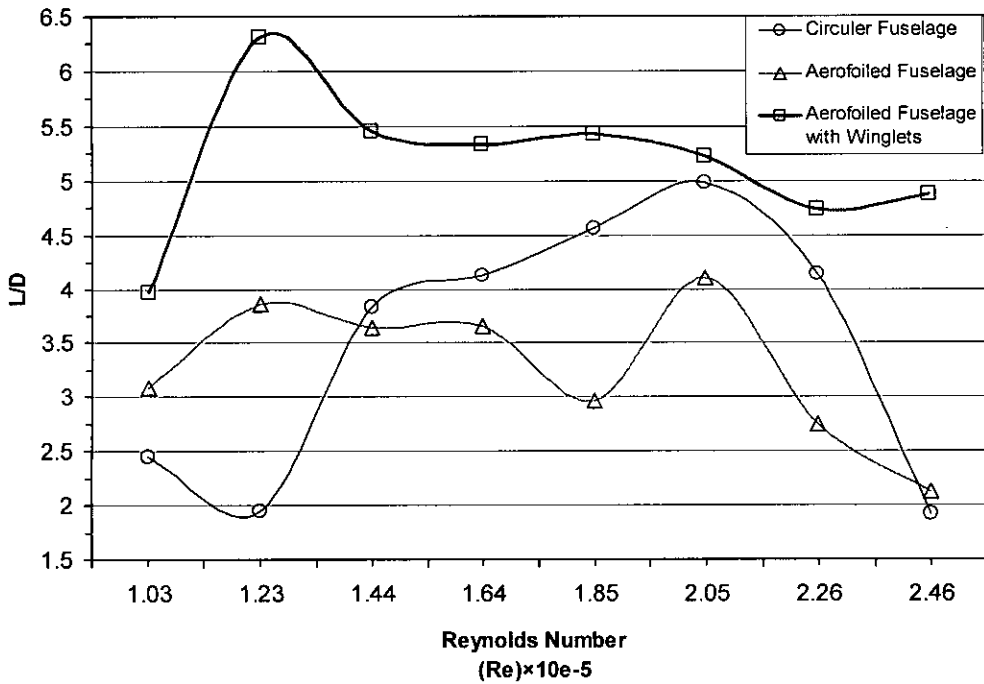
Figure 6.2.1. (b) (iii).:L/D vs. Reynolds No. curves for $\theta f = 0°$, $\theta w = 4°$

49
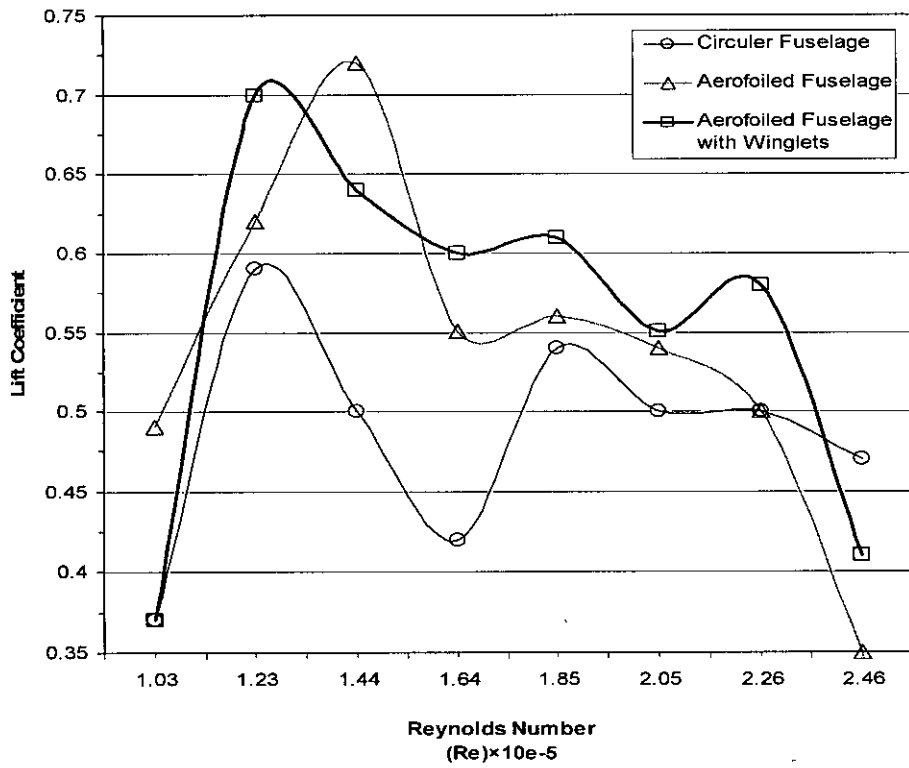
Figure 6.2.1. (c) (i).: Lift Coefficient vs. Reynolds No. curves for θf = 0°, θw = 6°
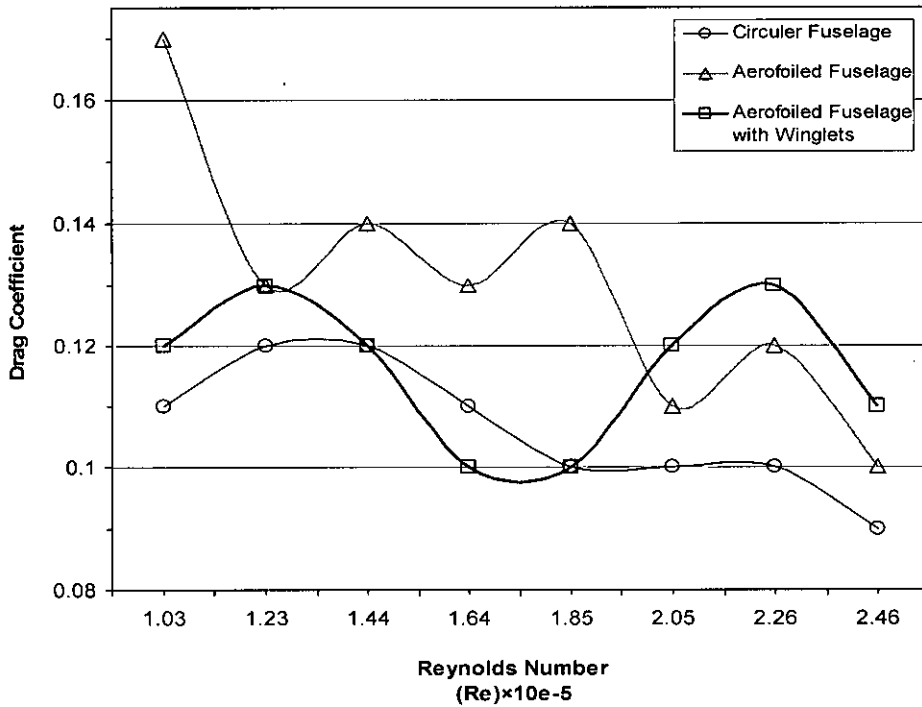
Figure 6.2.1. (c) (ii).: Drag Coefficient vs. Reynolds No. curves for θf = 0°, θw = 6°
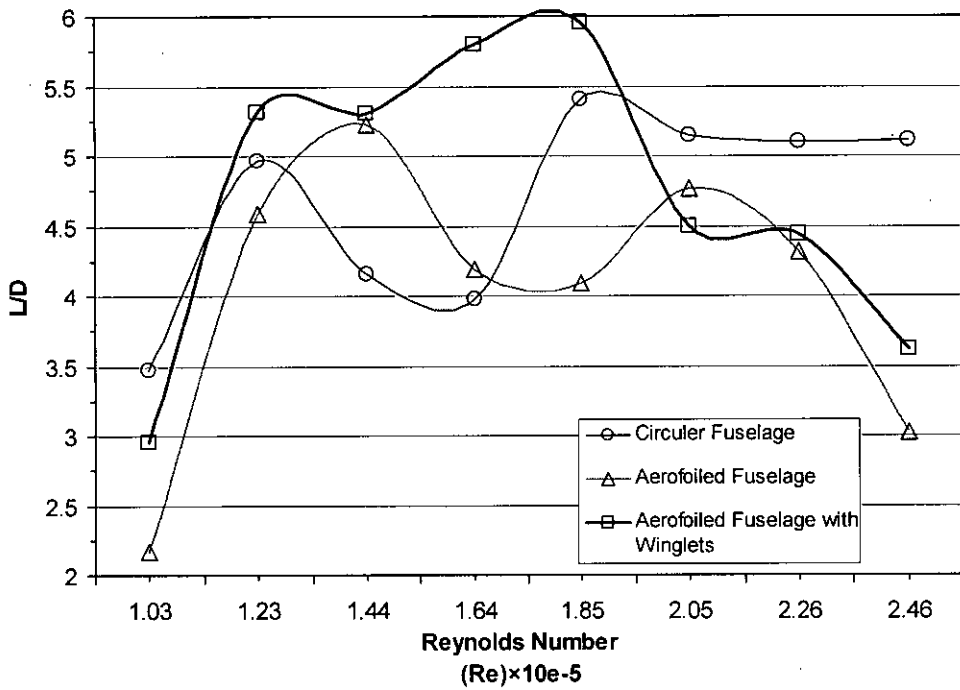
Figure 6.2.1. (c) (iii).:L/D vs. Reynolds No. curves for θf = 0°, θw = 6°
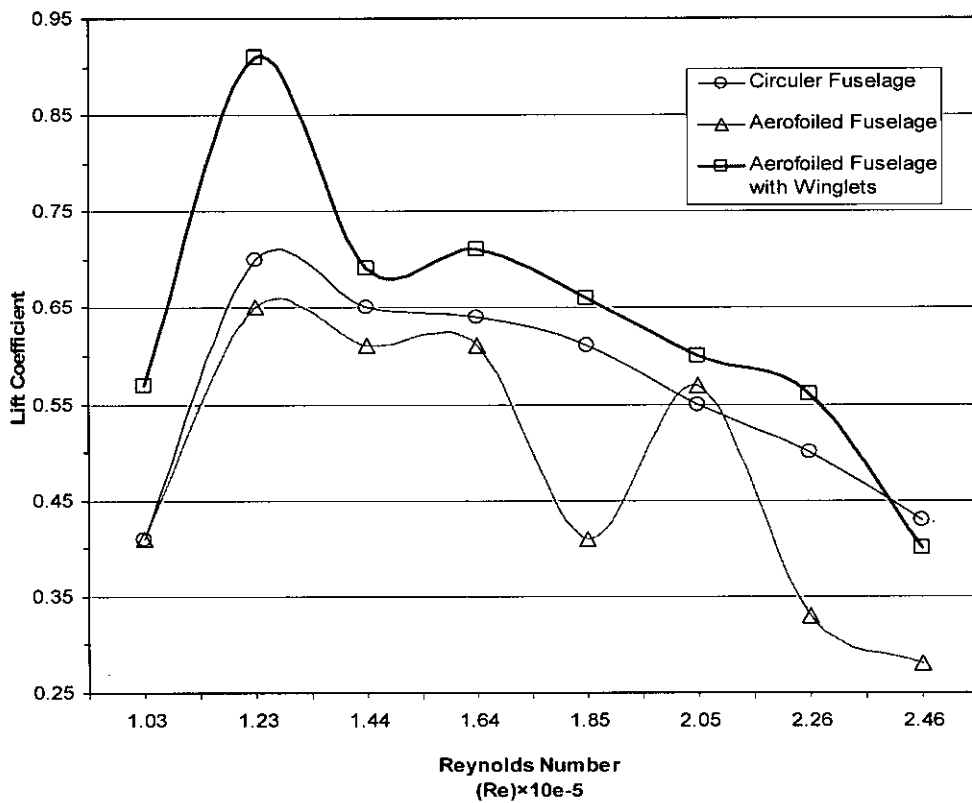
Figure 6.2.2. (a) (i).: Lift Coefficient vs. Reynolds No. curves for θf = 4°, θw = 2°

51
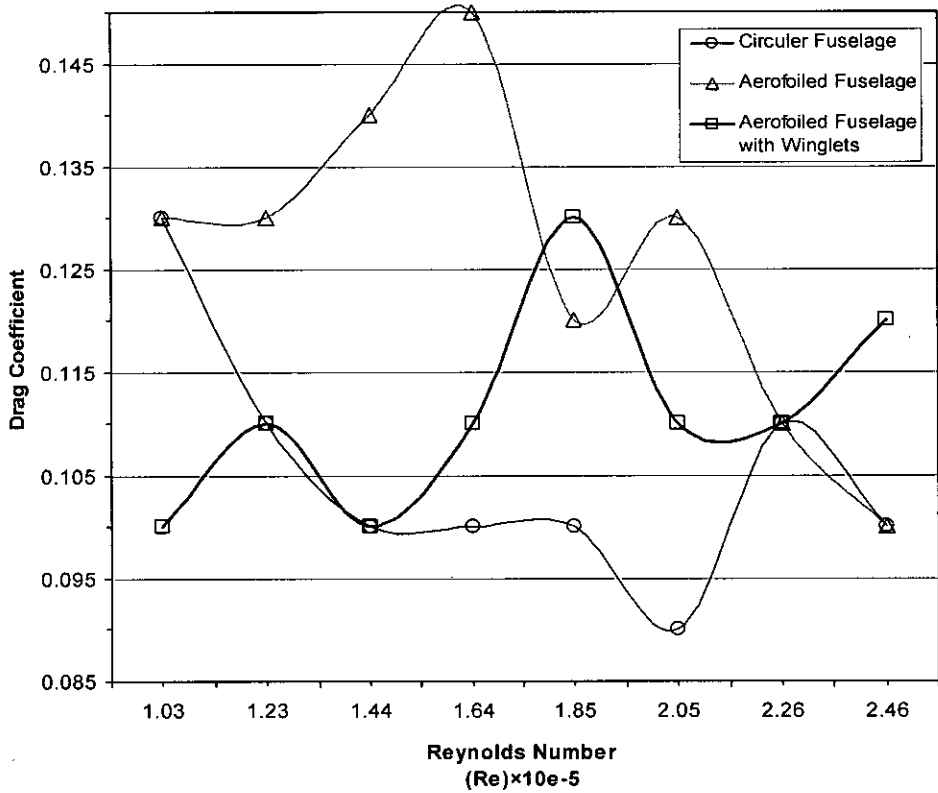
Figure 6.2.2. (a) (ii).: Drag Coefficient vs. Reynolds No. curves for θf = 4°, θw = 2°
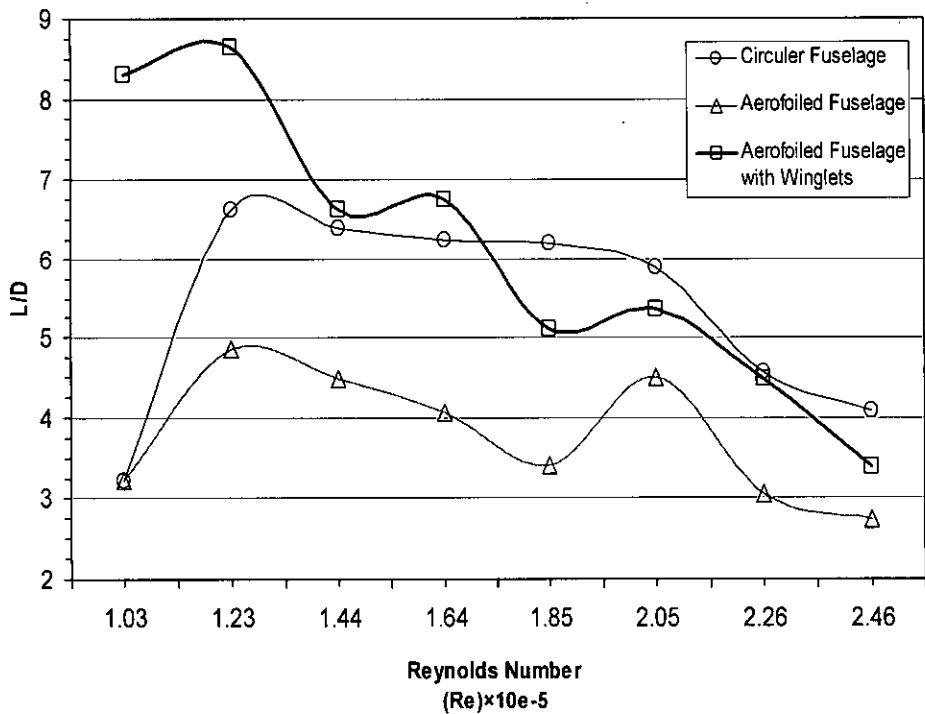
Figure 6.2.2. (a) (iii).:L/D vs. Reynolds No. curves for θf = 4°, θw = 2°
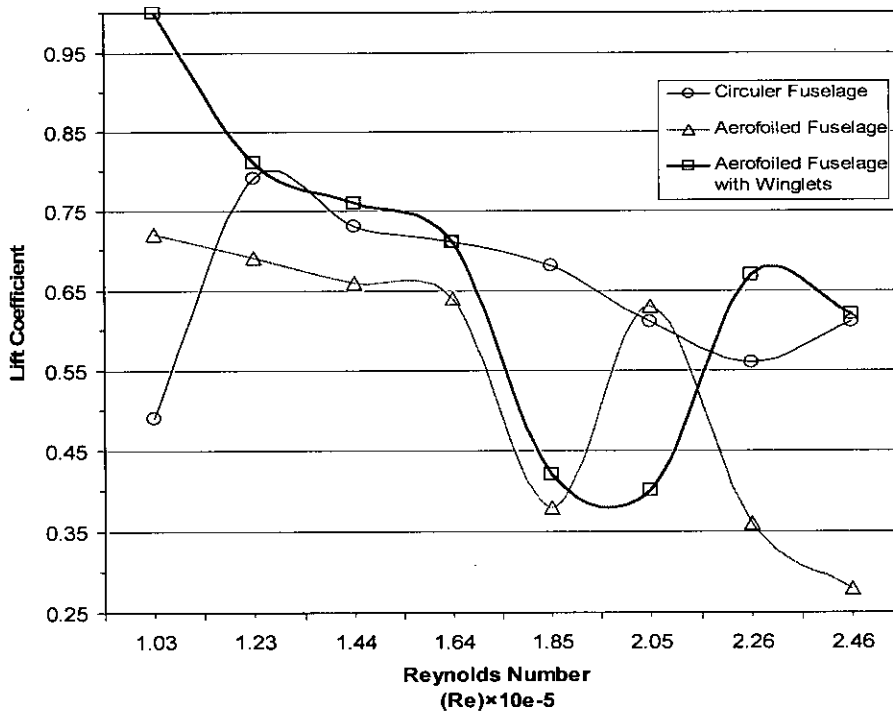
Figure 6.2.2. (b) (i).: Lift Coefficient vs. Reynolds No. curves for $\theta f = 4°$, $\theta w = 4°$
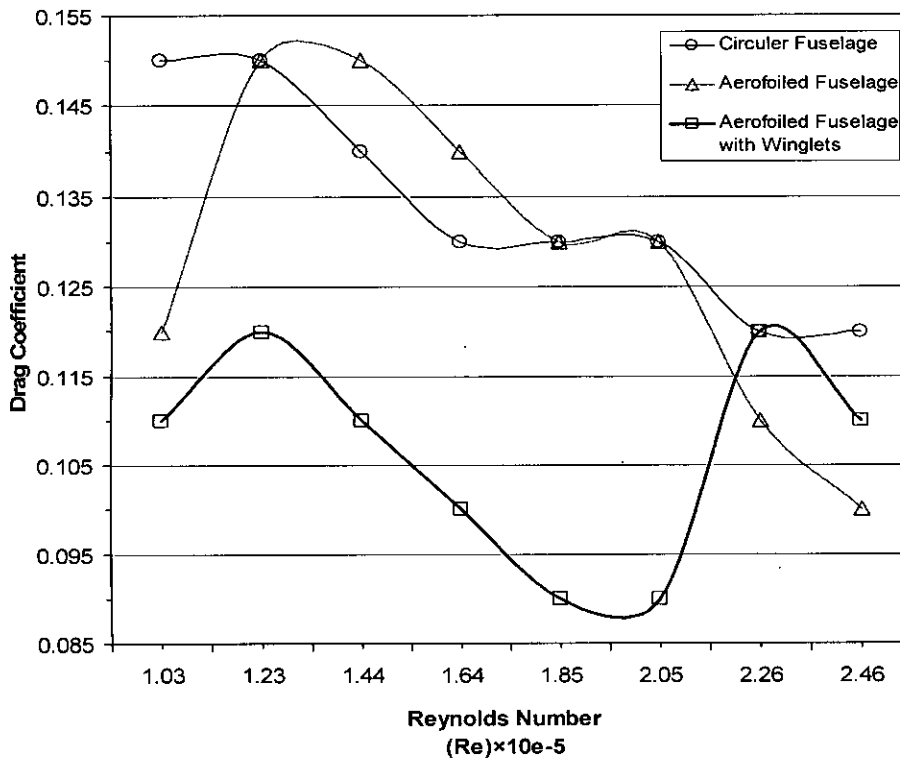
Figure 6.2.2. (b) (ii).: Drag Coefficient vs. Reynolds No. curves for $\theta f = 4°$, $\theta w = 4°$

53
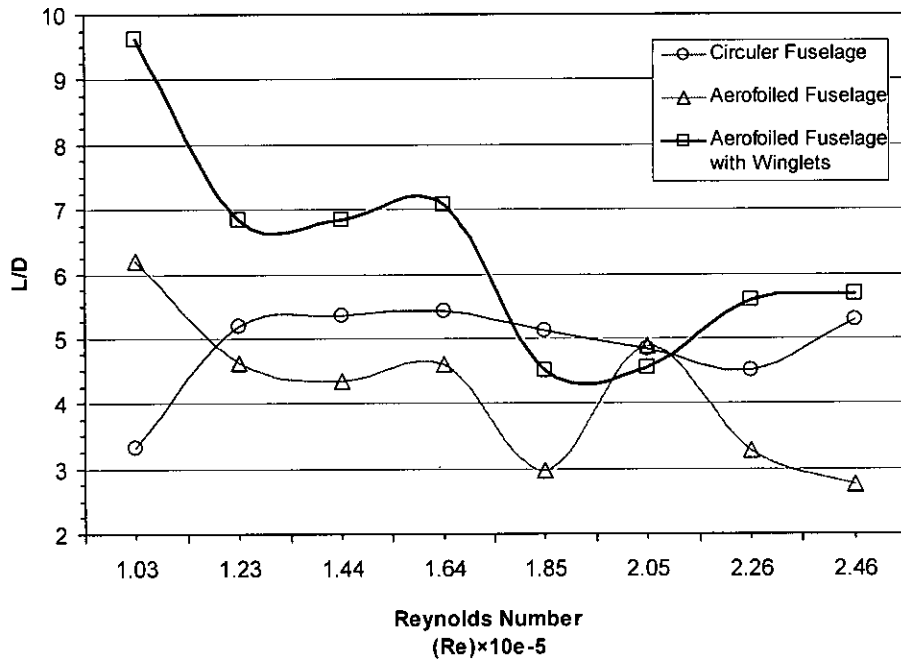
Figure 6.2.2. (b) (iii).: L/D vs. Reynolds No. curves for θf = 4°, θw = 4°
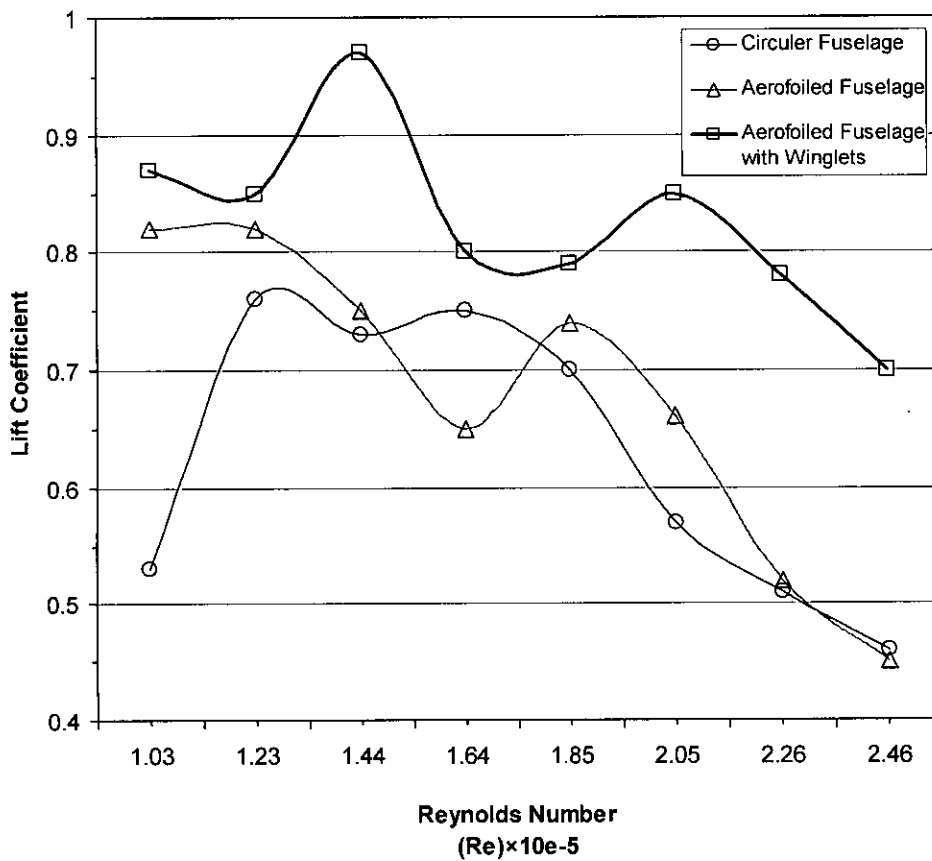
Figure 6.2.2. (c) (i).: Lift Coefficient vs. Reynolds No. curves for θf = 4°, θw = 6°

54
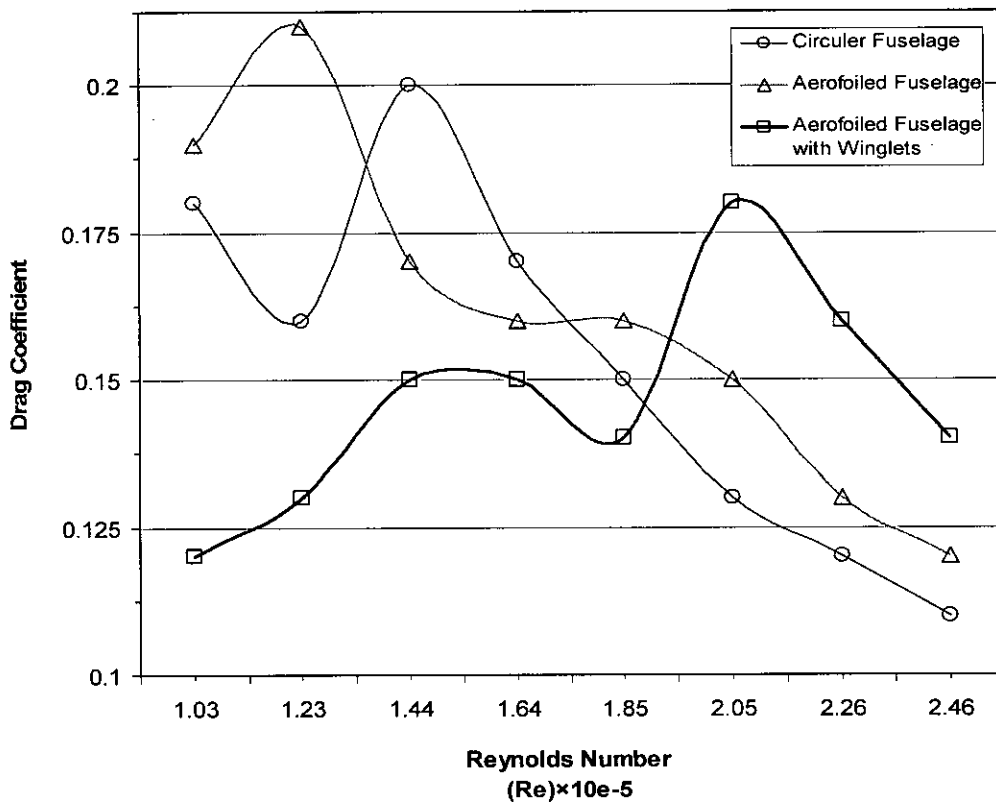
Figure 6.2.2. (c) (ii).: Drag Coefficient vs. Reynolds No. curves for θf = 4°, θw = 6°
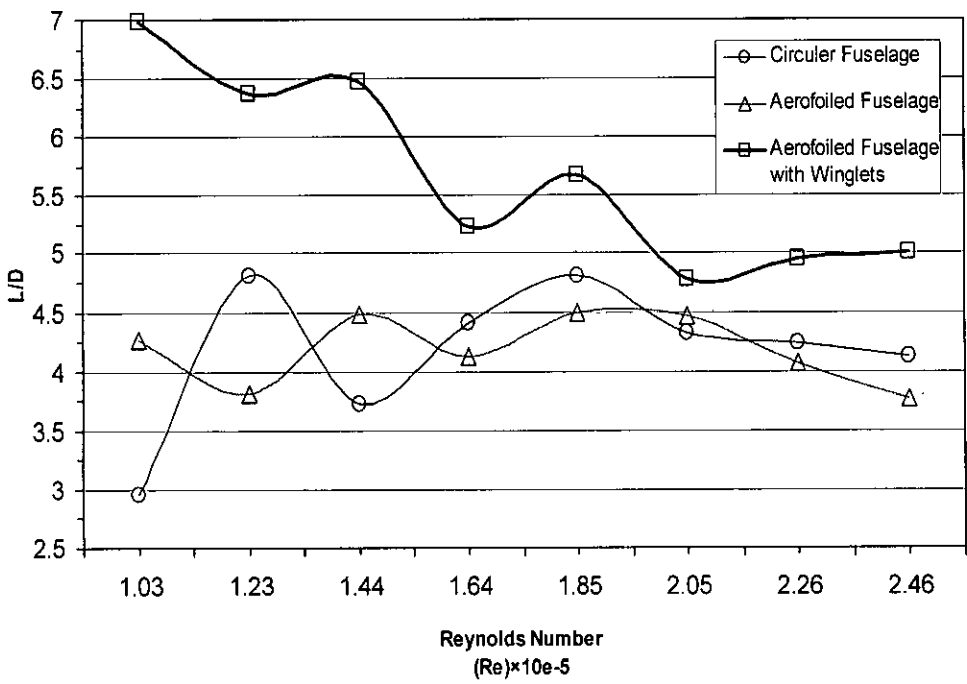
Figure 6.2.2. (c) (iii).: L/D vs. Reynolds No. curves for θf = 4°, θw = 6°
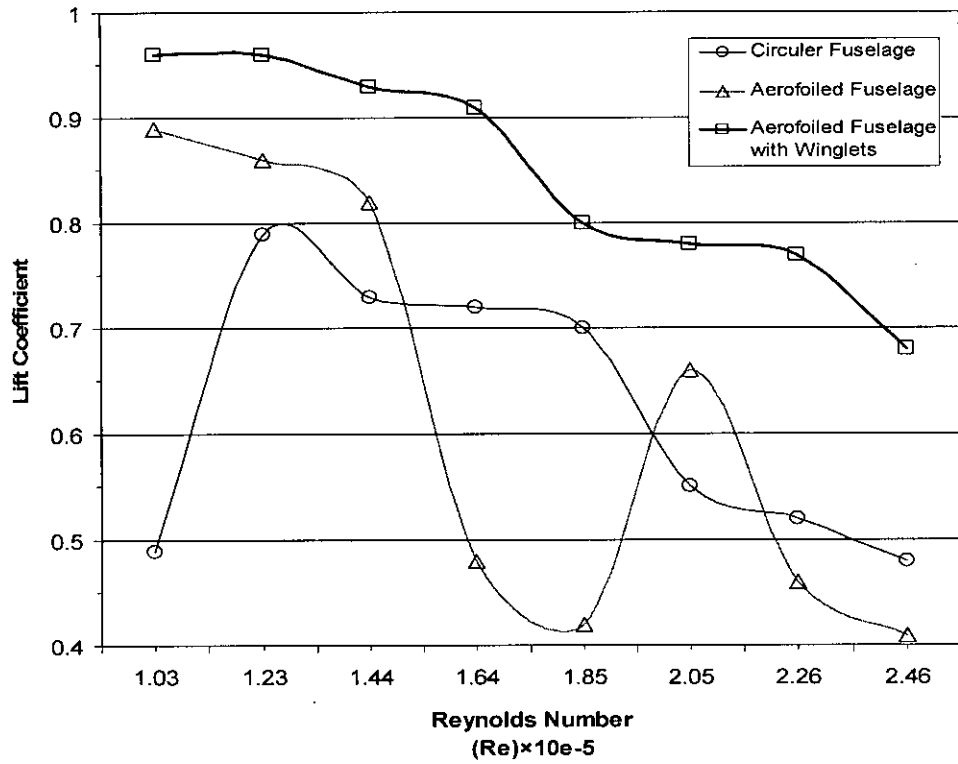
Figure 6.2.3. (a) (i).: Lift Coefficient vs. Reynolds No. curves for $\theta f = 8°$, $\theta w = 2°$
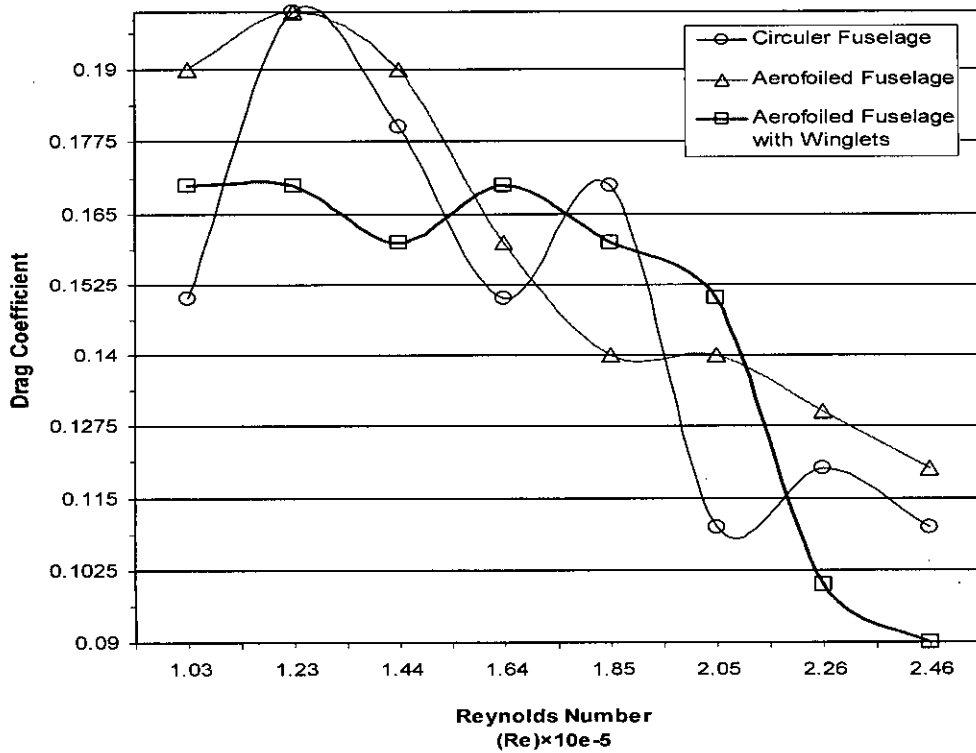
Figure 6.2.3. (a) (ii).: Drag Coefficient vs. Reynolds No. curves for $\theta f = 8°$, $\theta w = 2°$

56
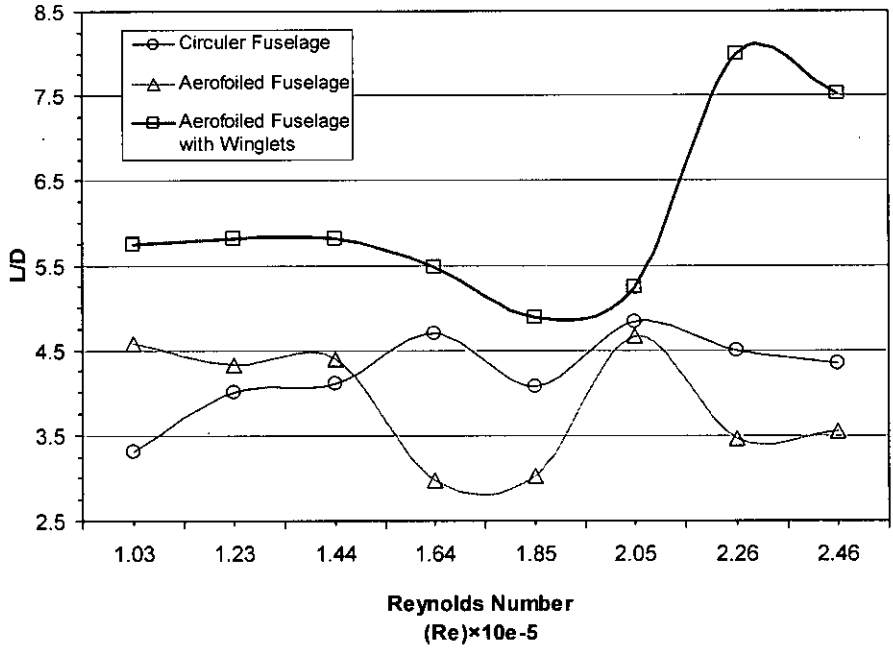
Figure 6.2.3. (a) (iii).: L/D vs. Reynolds No. curves for θf = 8°, θw = 2°
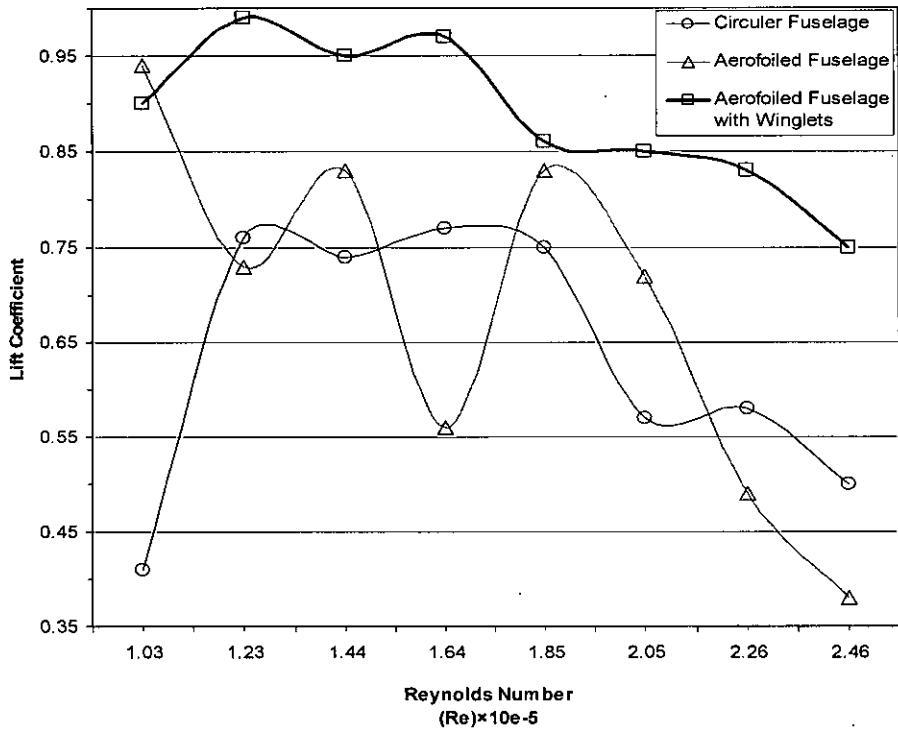
Figure 6.2.3. (b) (i).: Lift Coefficient vs. Reynolds No. curves for θf = 8°, θw = 4°

57
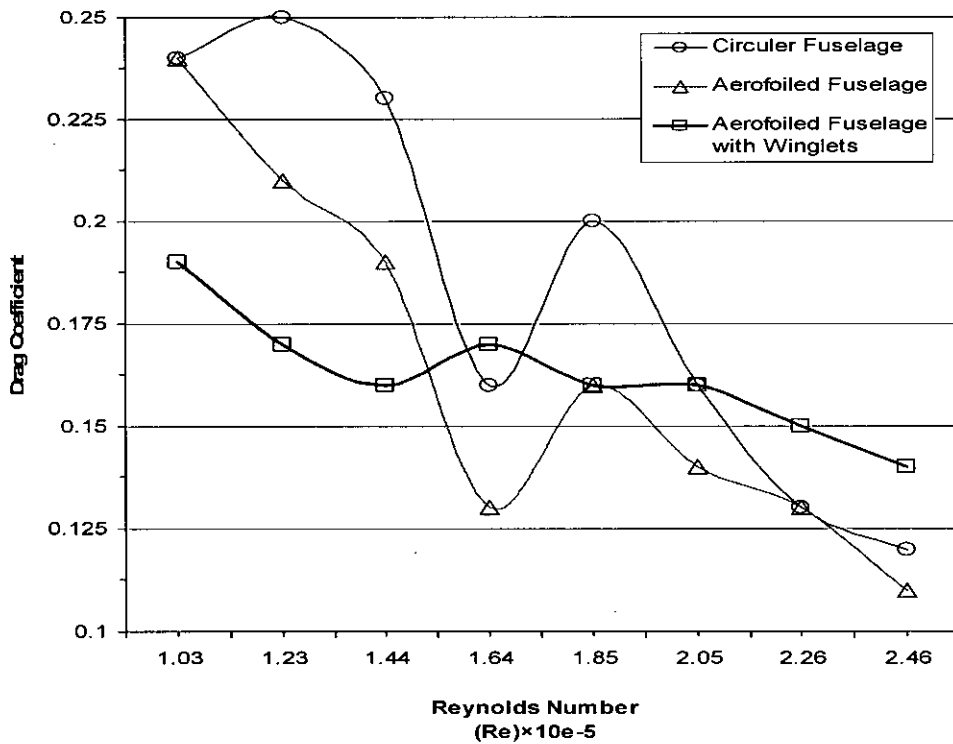
Figure 6.2.3. (b) (ii).: Drag Coefficient vs. Reynolds No. curves for $\theta f = 8°$, $\theta w = 4°$
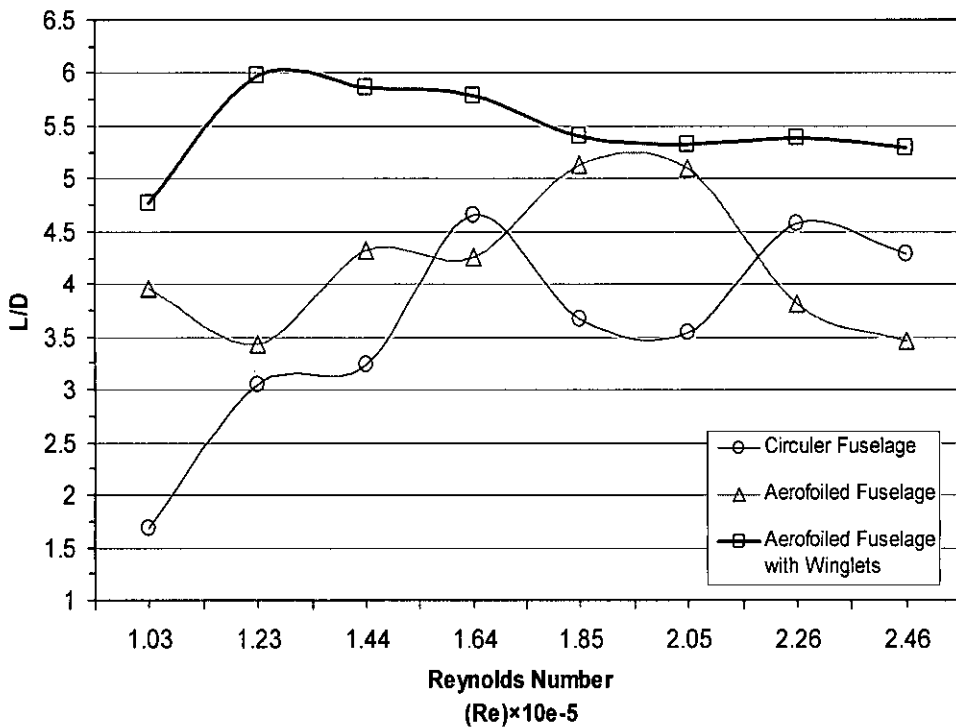
Figure 6.2.3. (b) (iii).: L/D vs. Reynolds No. curves for $\theta f = 8°$, $\theta w = 4°$

58
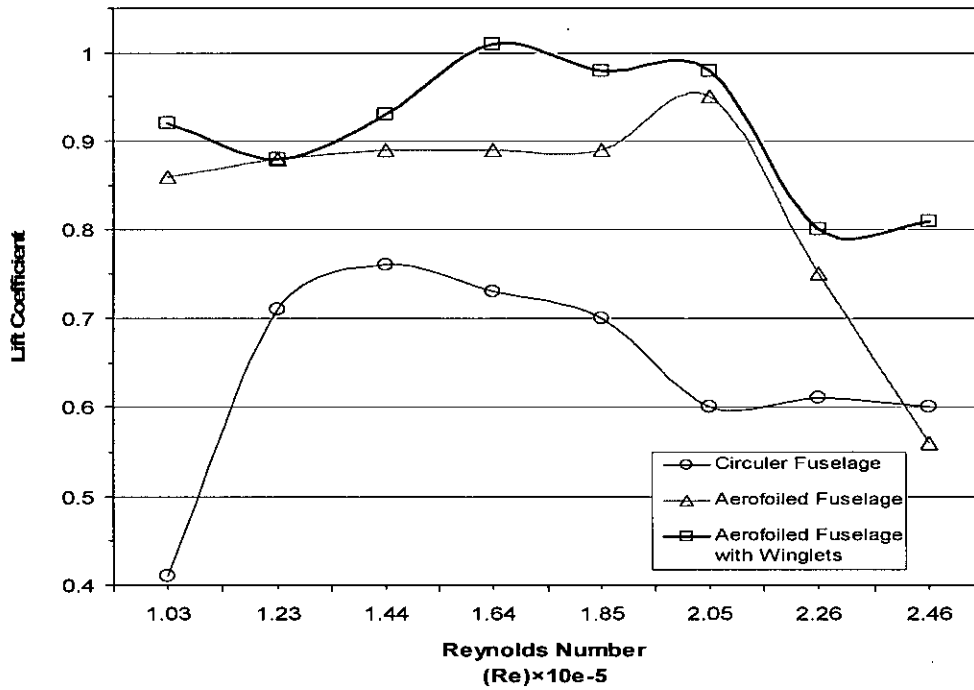
Figure 6.2.3. (c) (i).: Lift Coefficient vs. Reynolds No. curves for θf = 8°, θw = 6°
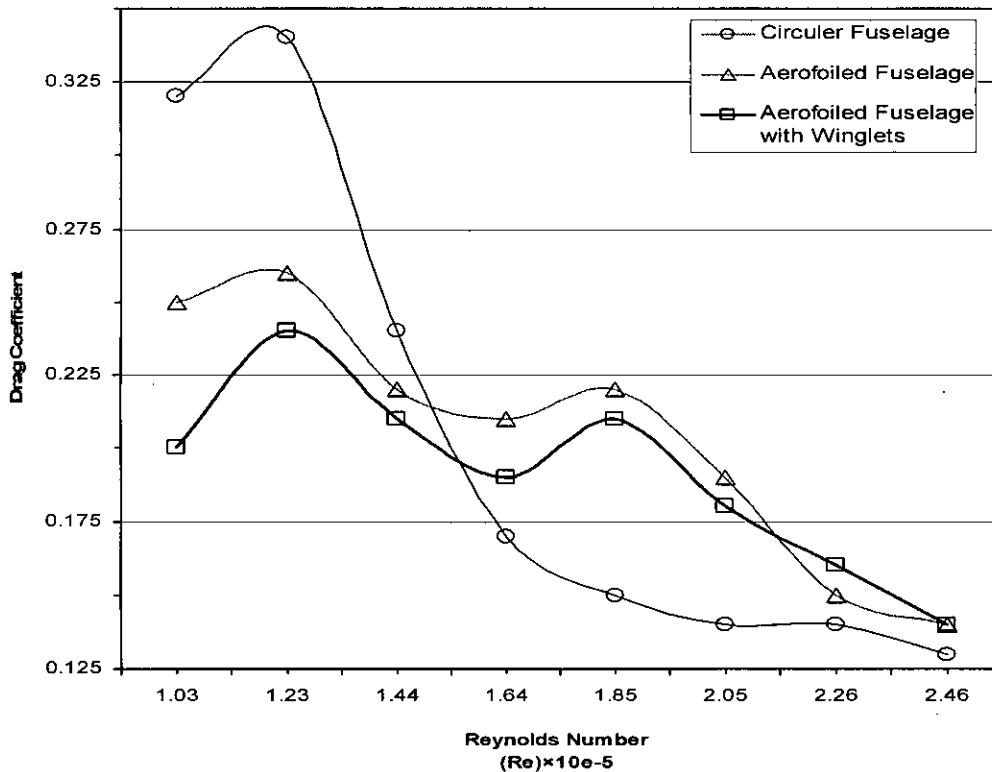
Figure 6.2.3. (c) (ii).: Drag Coefficient vs. Reynolds No. curves for θf = 8°, θw = 6°
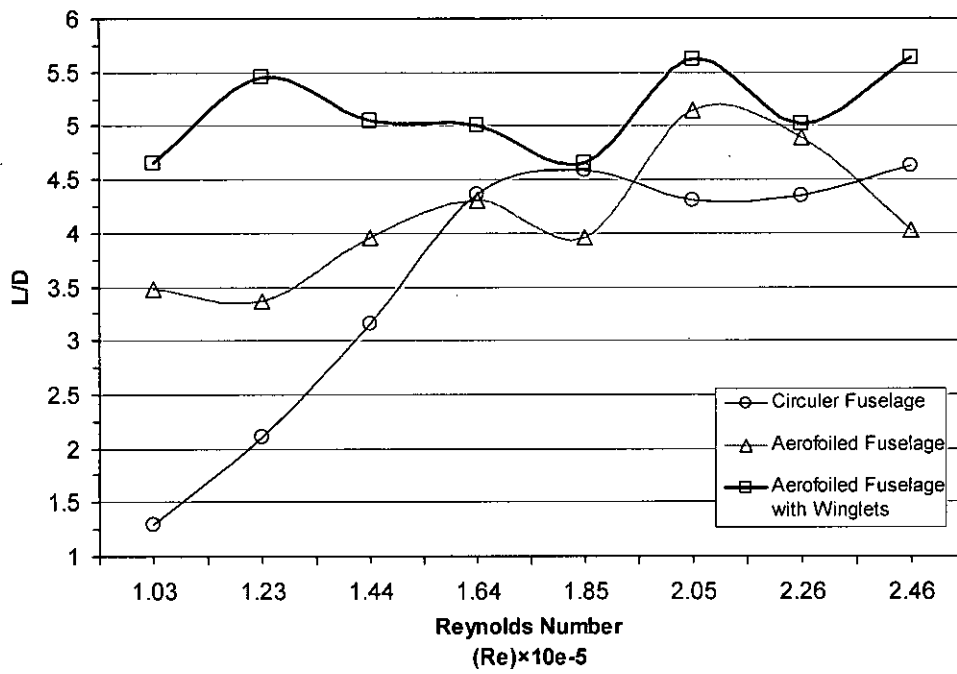
Figure 6.2.3. (c) (iii).: L/D vs. Reynolds No. curves for θf = 8°, θw = 6°
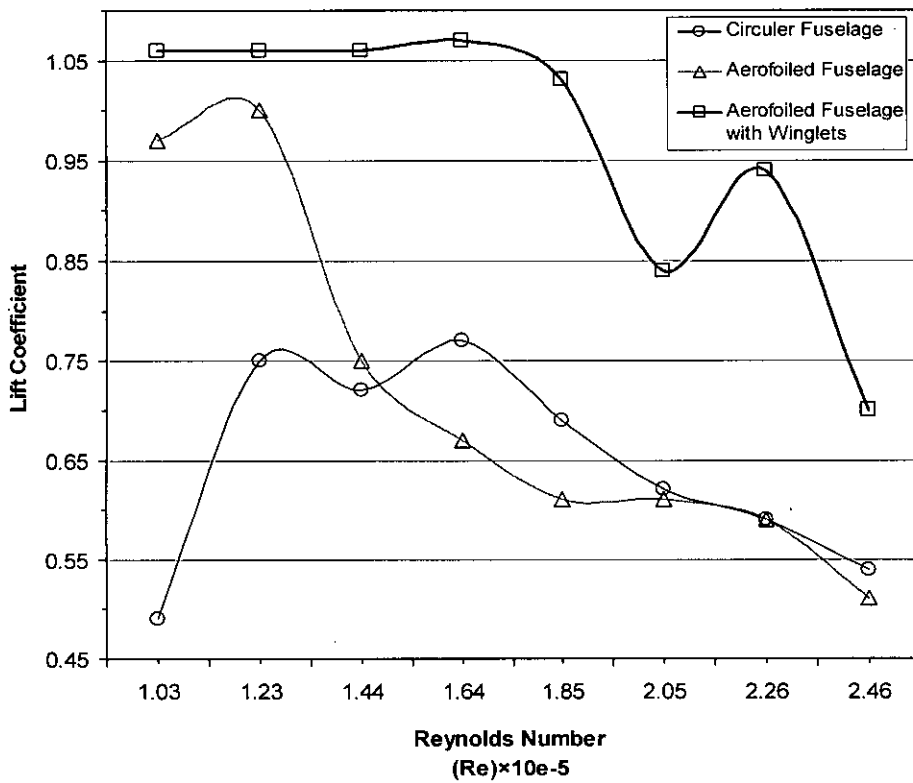
Figure 6.2.4. (a) (i).: Lift Coefficient vs. Reynolds No. curves for θf = 12°, θw = 2°
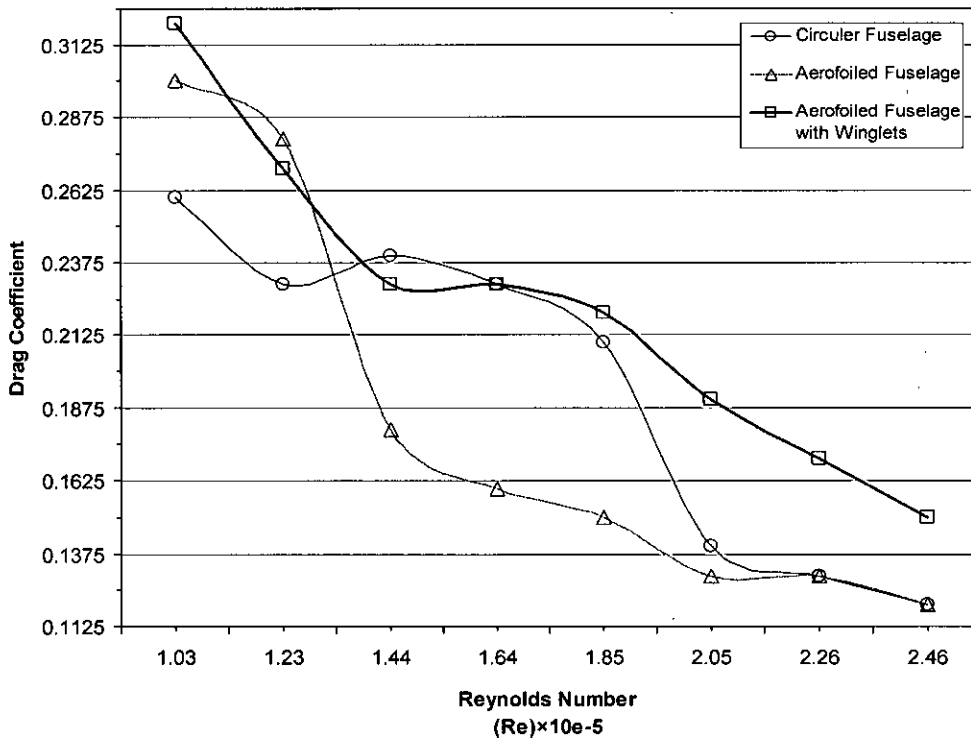
Figure 6.2.4. (a) (ii).: Drag Coefficient vs. Reynolds No. curves for θf = 12°, θw = 2°
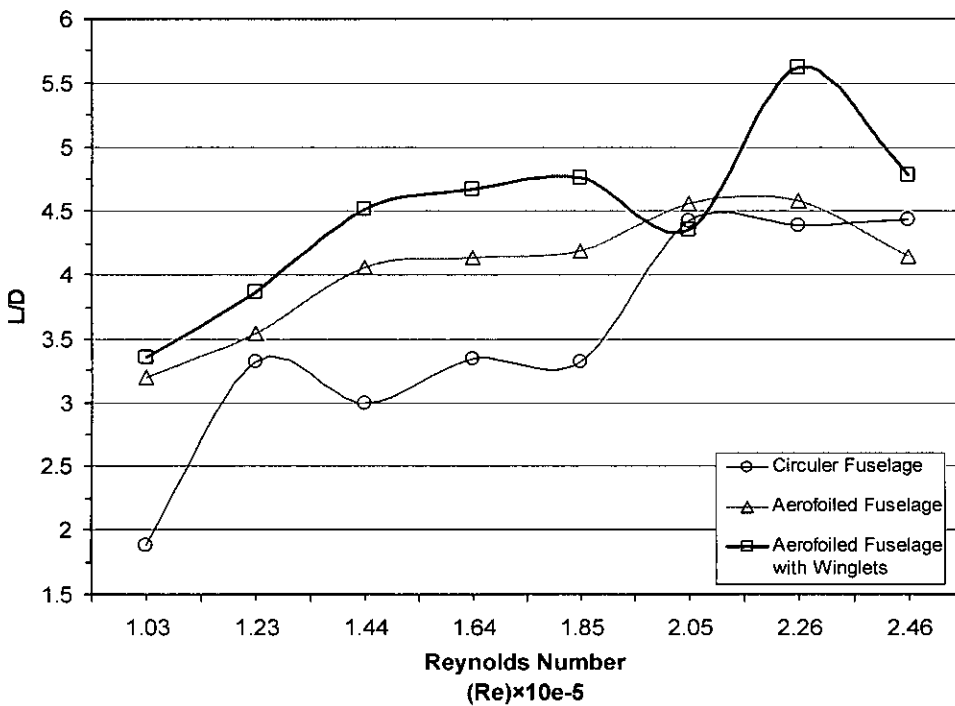
Figure 6.2.4. (a) (iii).: L/D vs. Reynolds No. curves for θf = 12°, θw = 2°
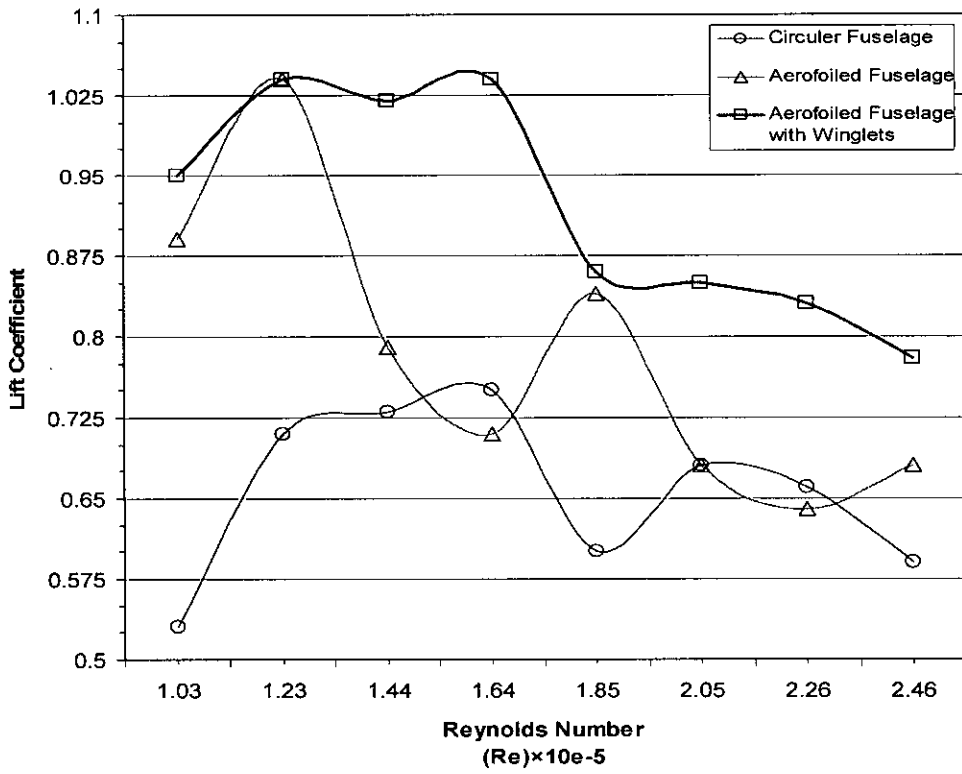
Figure 6.2.4. (b) (i).: Lift Coefficient vs. Reynolds No. curves for θf = 12°, θw = 4°
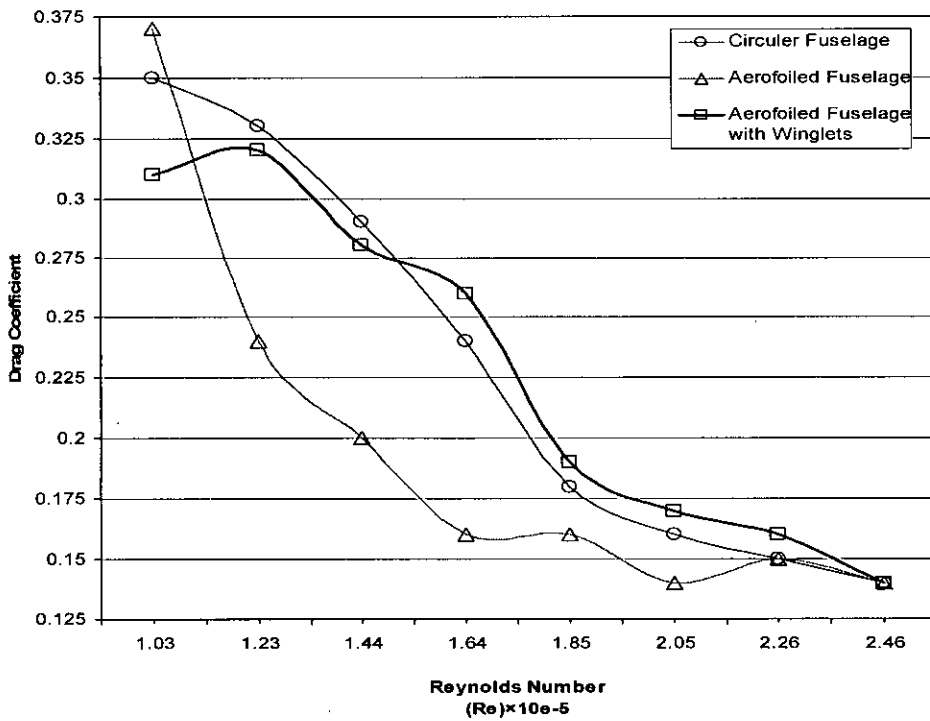
Figure 6.2.4. (b) (ii).: Drag Coefficient vs. Reynolds No. curves for θf = 12°, θw = 4°
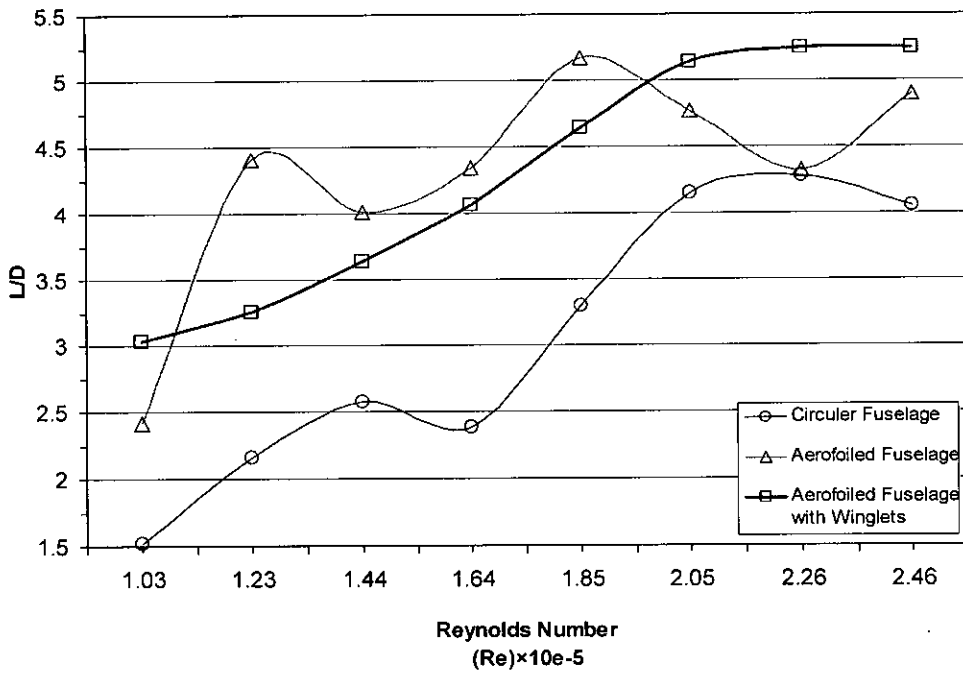
Figure 6.2.4. (b) (iii).: L/D vs. Reynolds No. curves for θf = 12°, θw = 4°
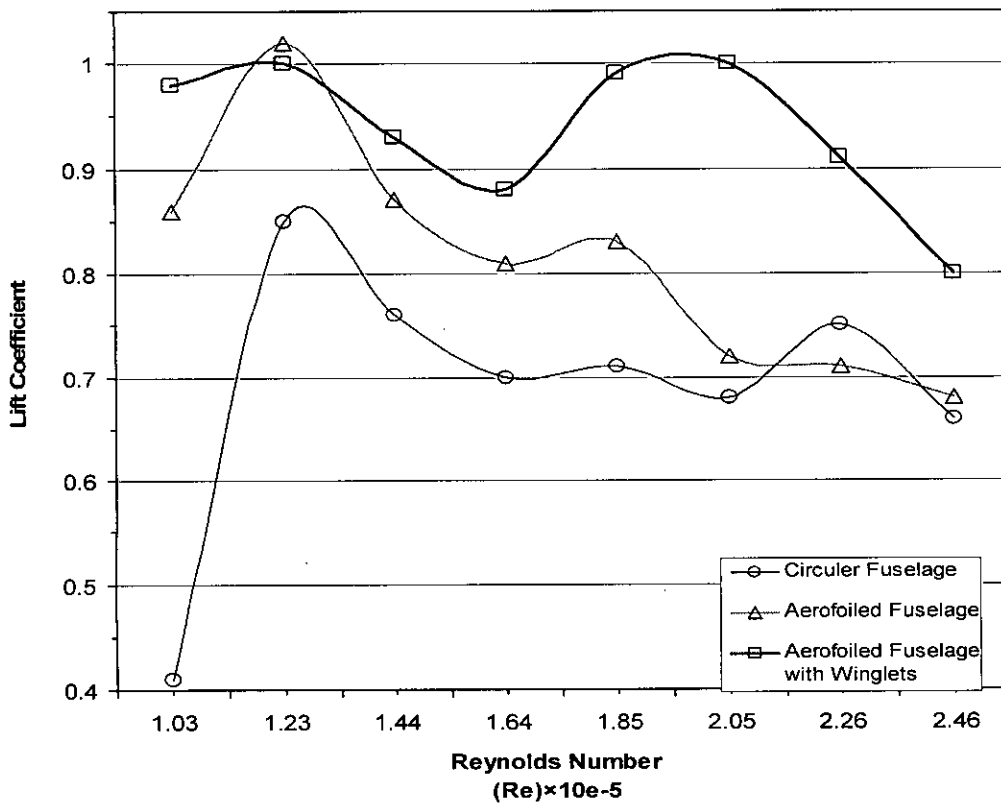
Figure 6.2.4. (c) (i).: Lift Coefficient vs. Reynolds No. curves for θf = 12°, θw = 6°
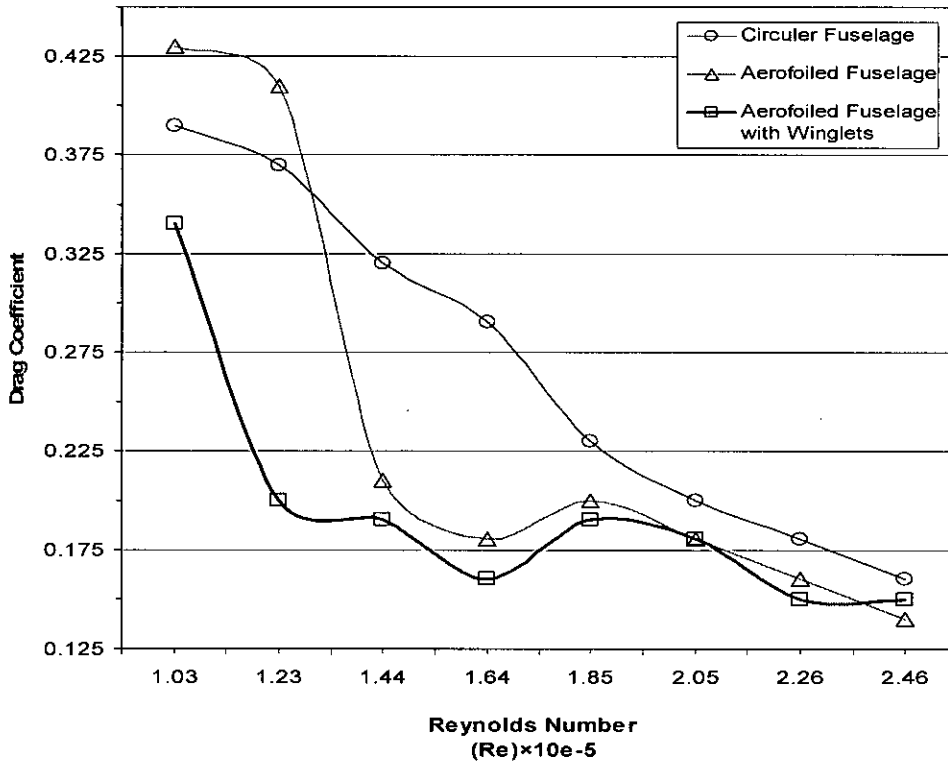
Figure 6.2.4. (c) (ii).: Drag Coefficient vs. Reynolds No. curves for $\theta f = 12°$, $\theta w = 6°$
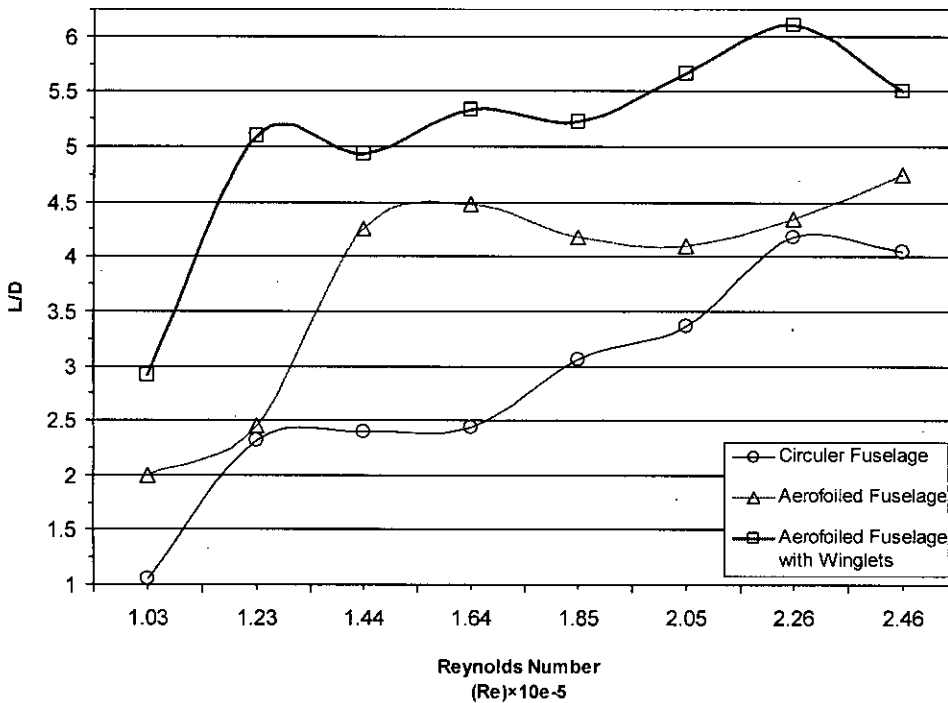
Figure 6.2.4. (c) (iii).: L/D vs. Reynolds No. curves for $\theta f = 12°$, $\theta w = 6°$

64
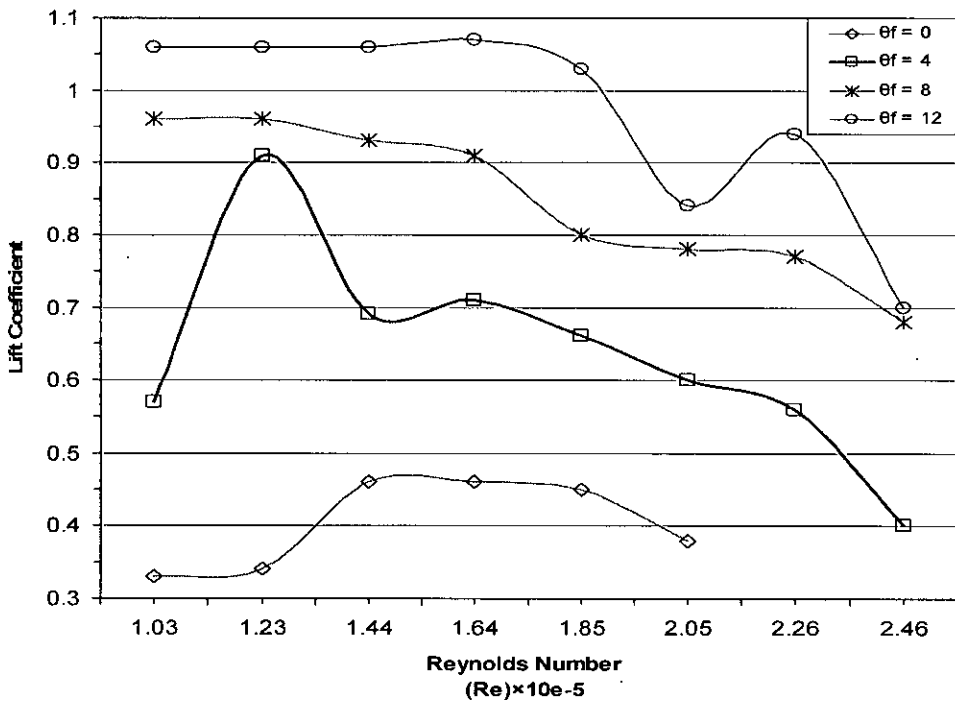
Figure 6.2.5. (a) (i): Lift Coefficient vs. Reynolds No. curves for $\theta w = 2°$
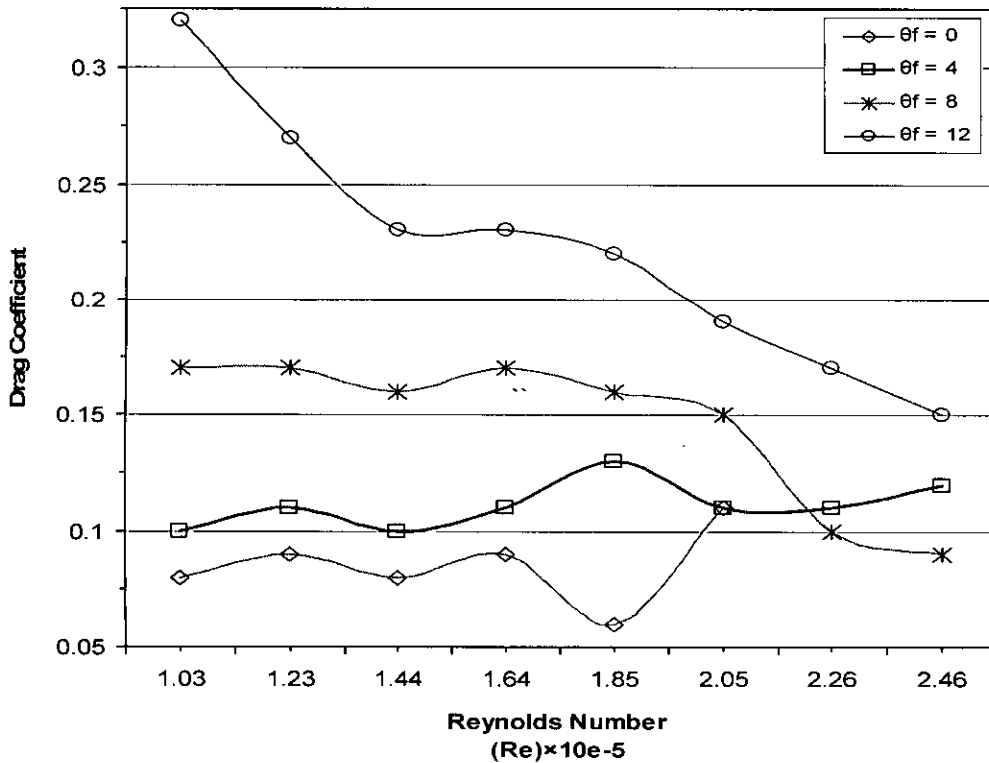
Figure 6.2.5. (a) (ii): Drag Coefficient vs. Reynolds No. curves for $\theta w = 2°$
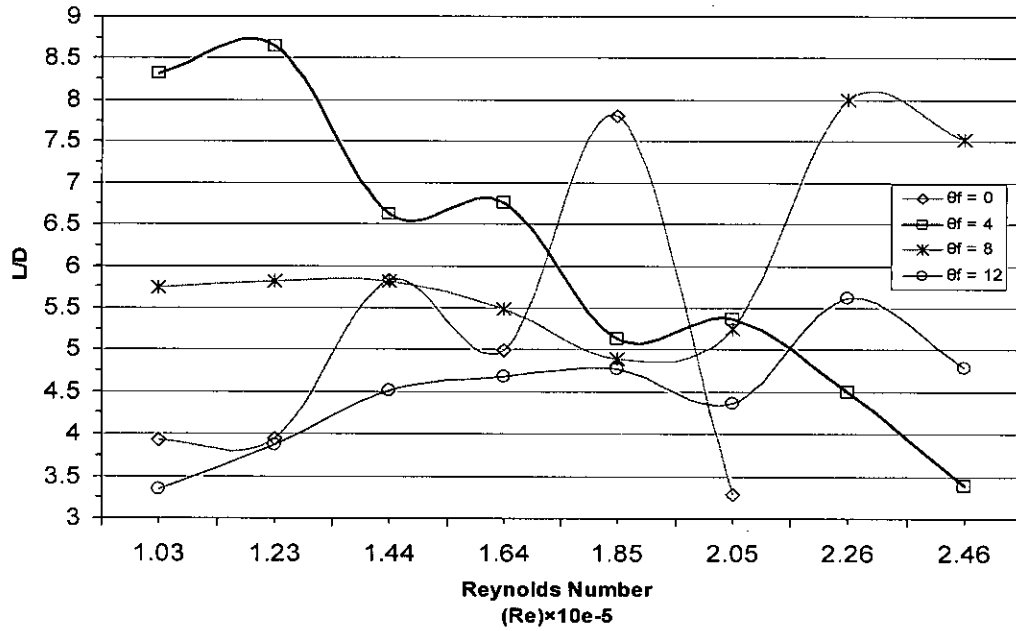
Figure 6.2.5. (a) (iii): L/D vs. Reynolds No. curves for θw = 2°
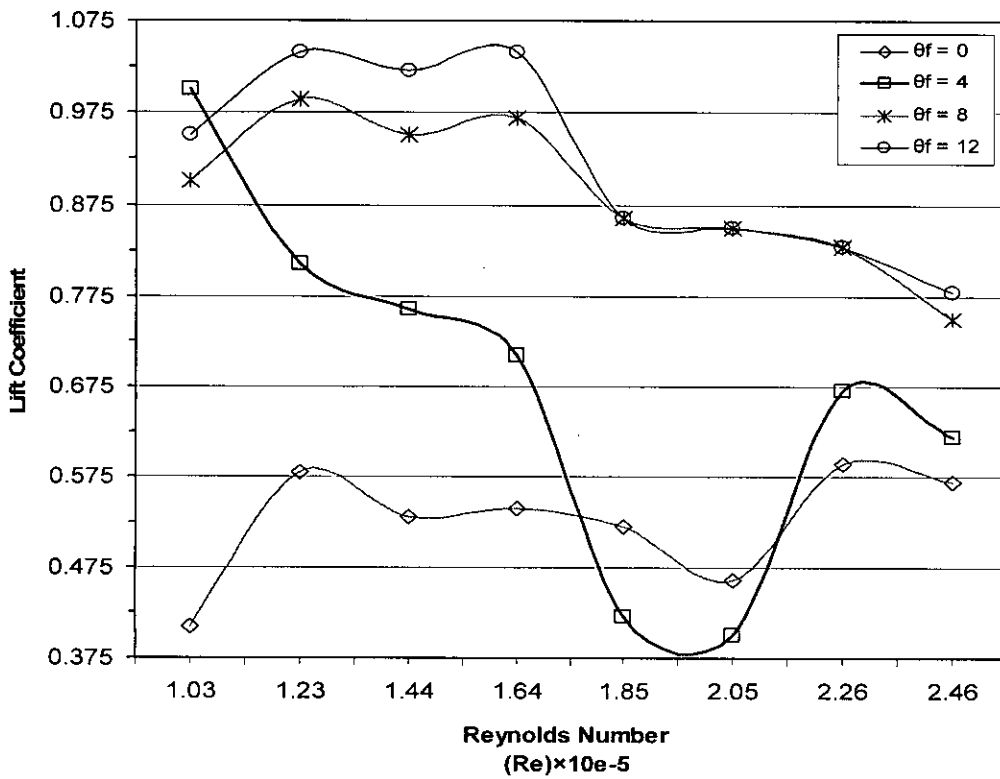
Figure 6.2.5. (b) (i): Lift Coefficient vs. Reynolds No. curves for θw = 4°
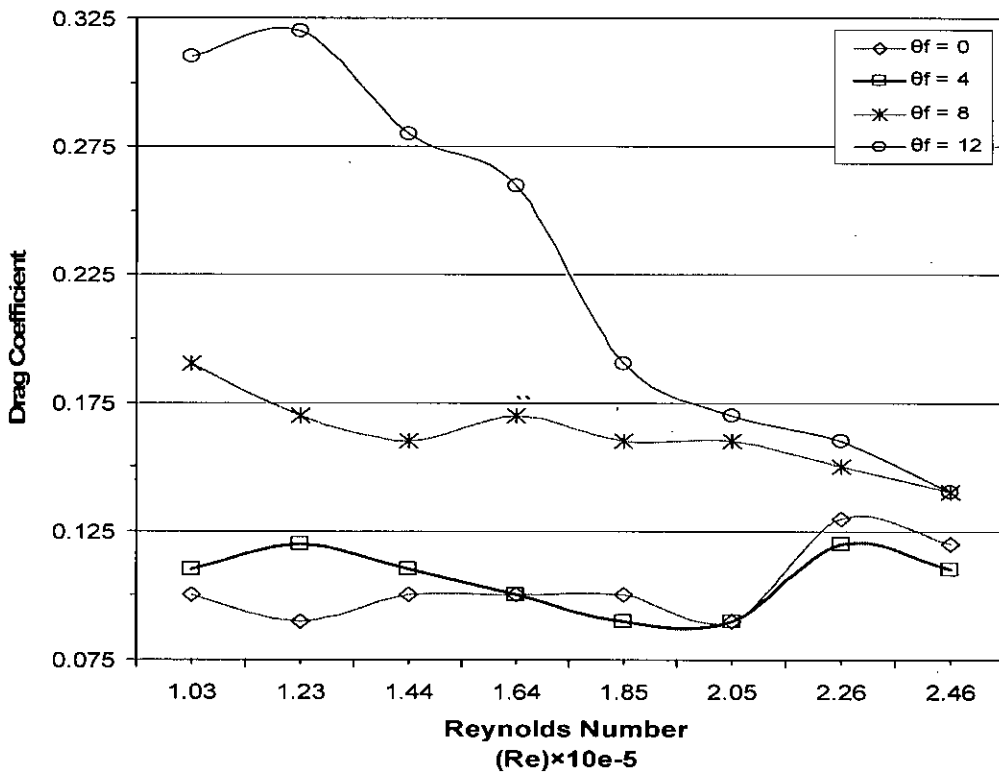
Figure 6.2.5. (b) (ii): Drag Coefficient vs. Reynolds No. curves for θw = 4°
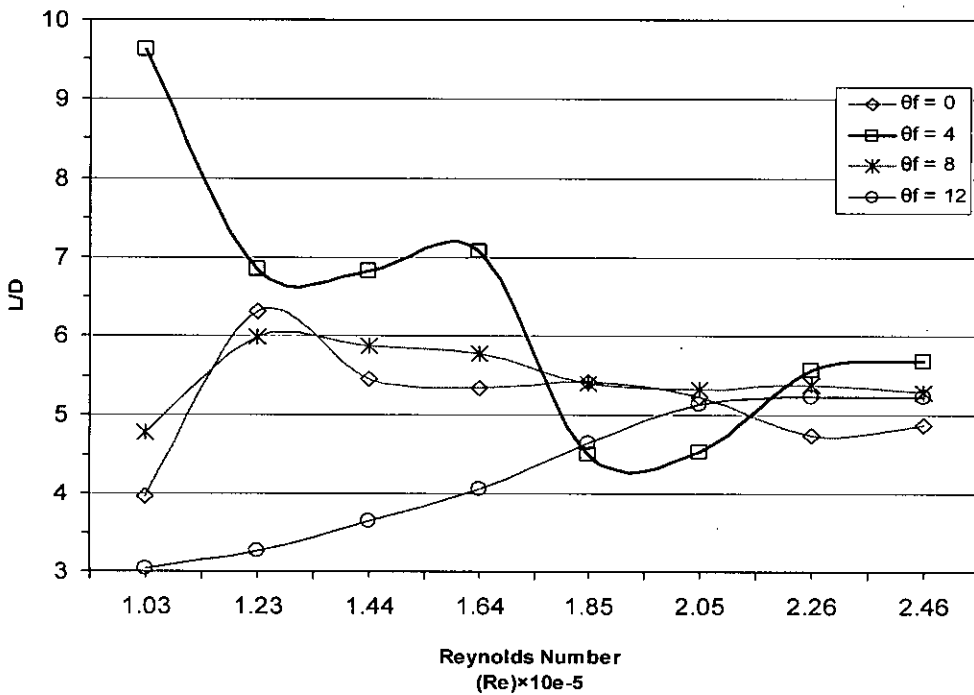
Figure 6.2.5. (b) (iii): L/D vs. Reynolds No. curves for θw = 4°

67
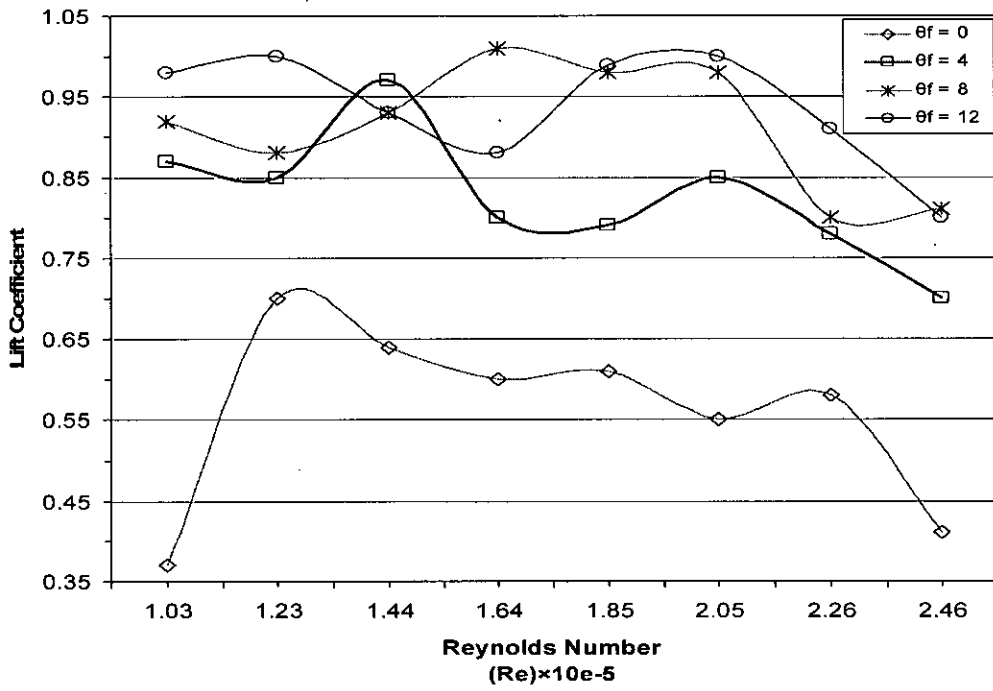
Figure 6.2.5. (c) (i): Lift Coefficient vs. Reynolds No. curves for $\theta w = 6°$
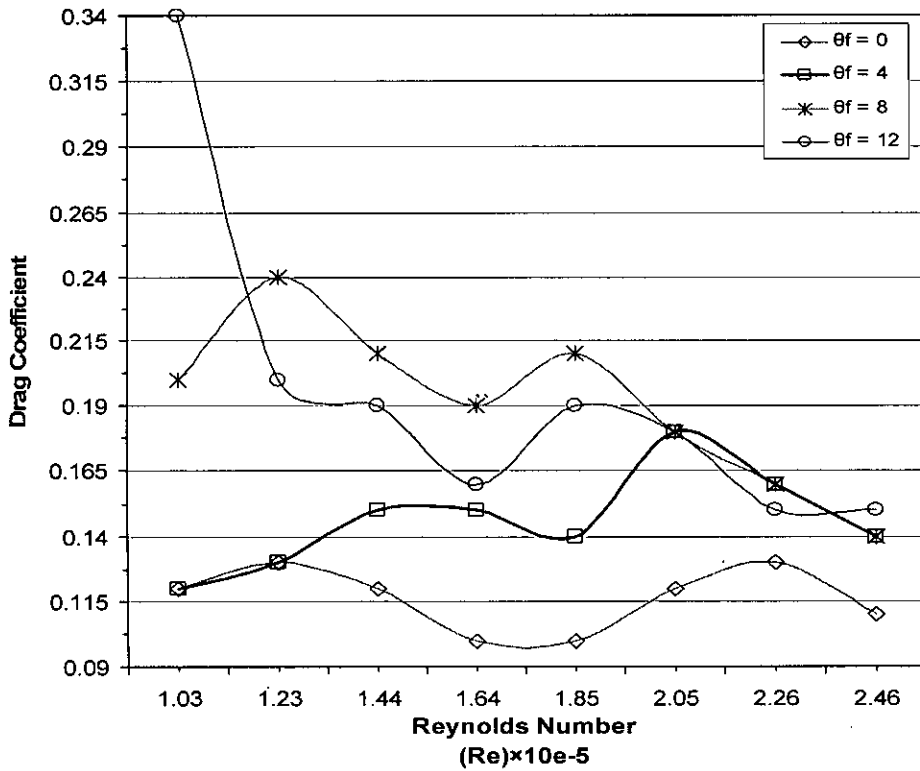
Figure 6.2.5. (c) (ii): Drag Coefficient vs. Reynolds No. curves for $\theta w = 6°$

68
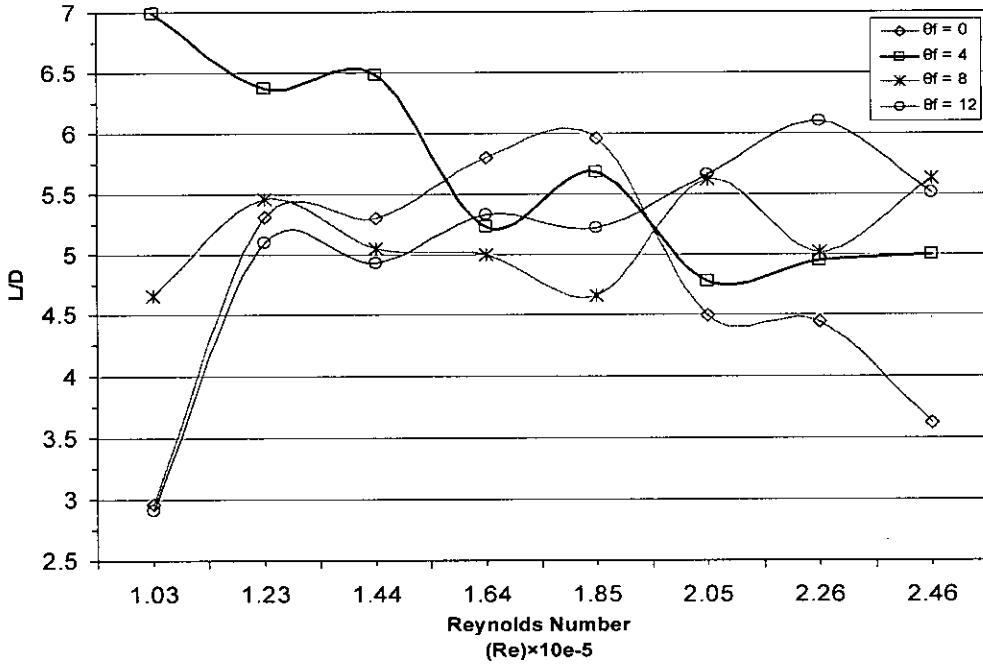
Figure 6.2.5. (c) (iii): L/D vs. Reynolds No. curves for θw = 6°
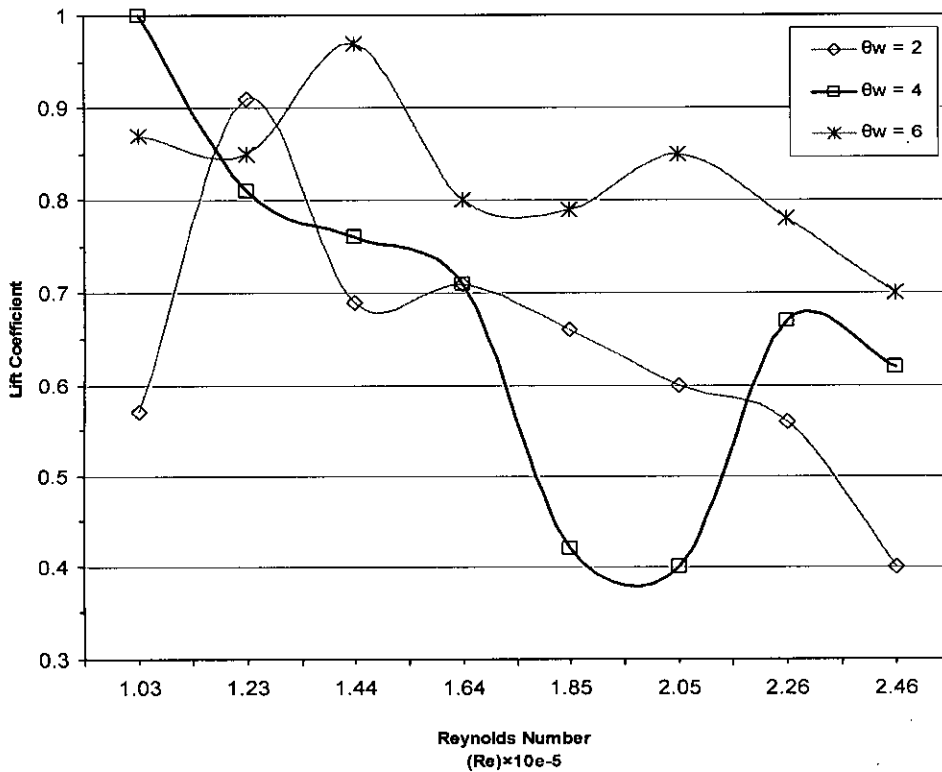
Figure 6.2.6 (i): Lift Coefficient vs. Reynolds No. curves for θf = 4°
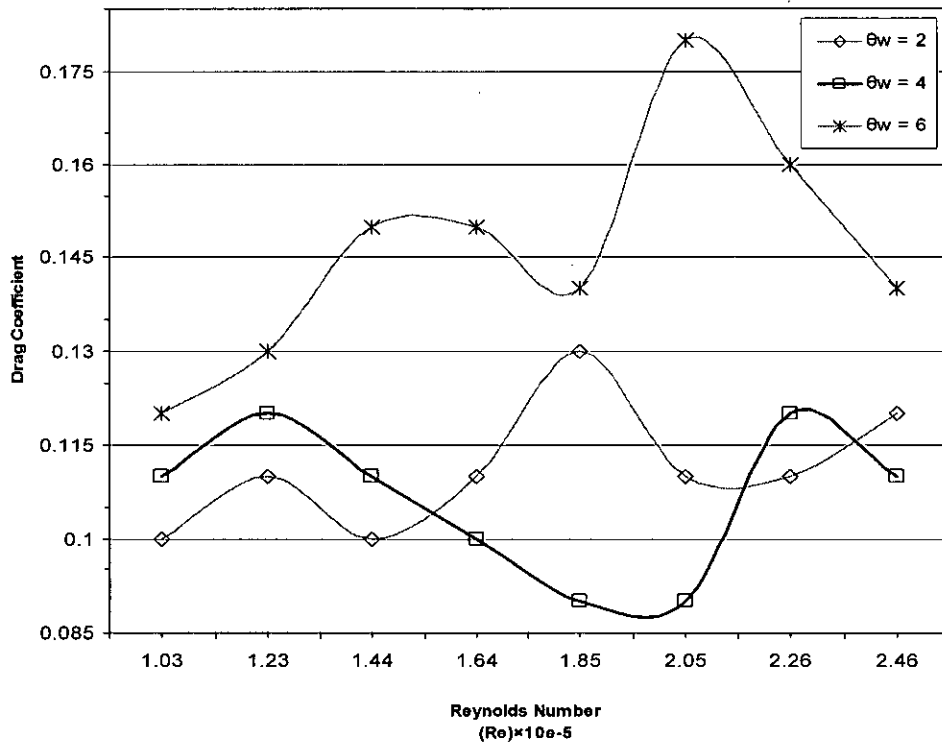
Figure 6.2.6 (ii) : Drag Coefficient vs. Reynolds No. curves for θf = 4°
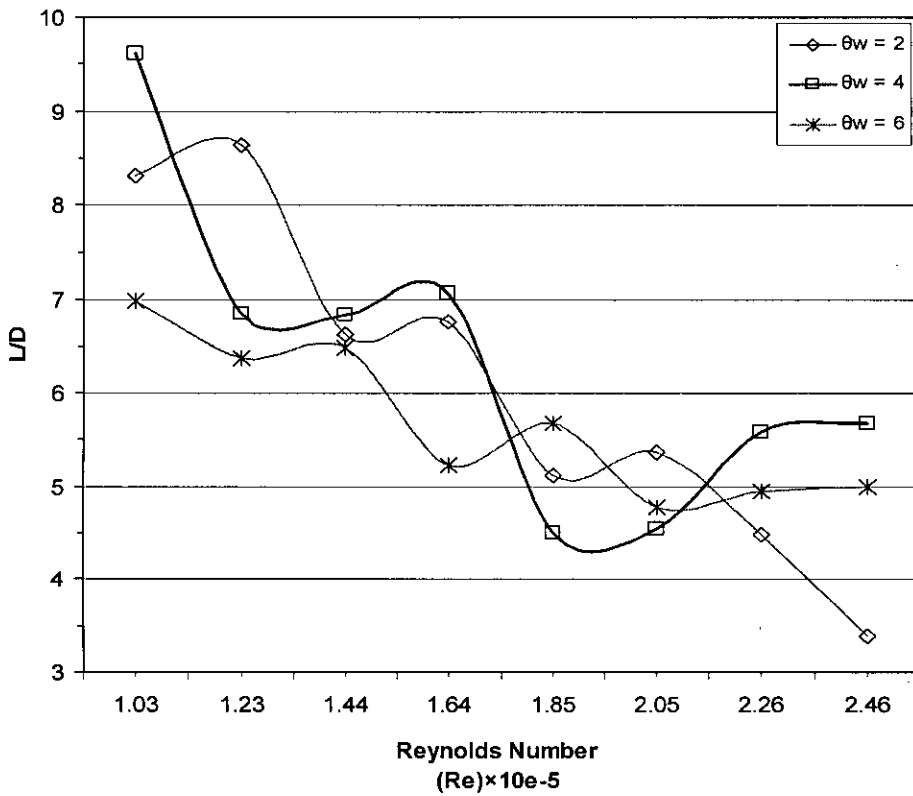
Figure 6.2.6 (iii): L/D vs. Reynolds No. curves for θf = 4°
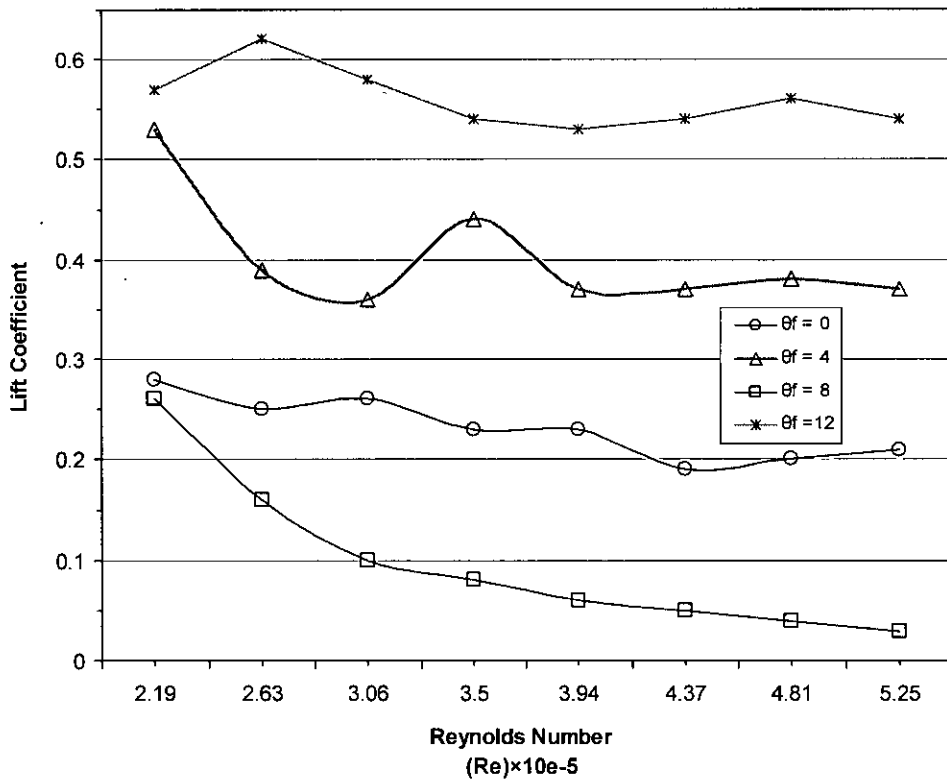
Figure 6.3 (i): From pressure tapping Lift Coefficient vs. Reynolds No. curves for θw = 4°
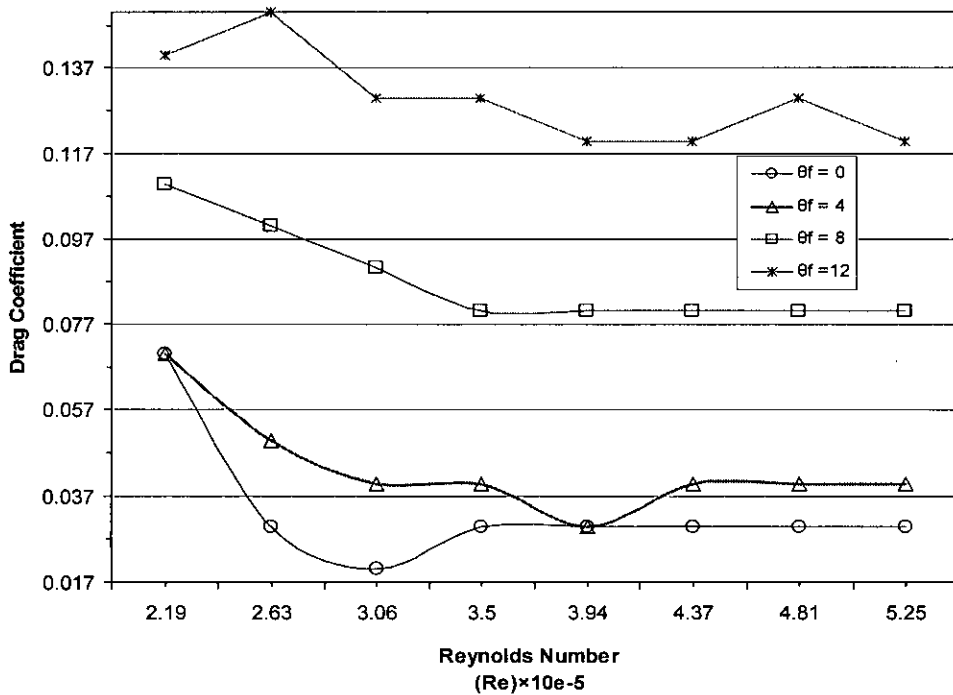
Figure 6.3 (ii): From pressure tapping Drag Coefficient vs. Reynolds No. curves for θw = 4°

71
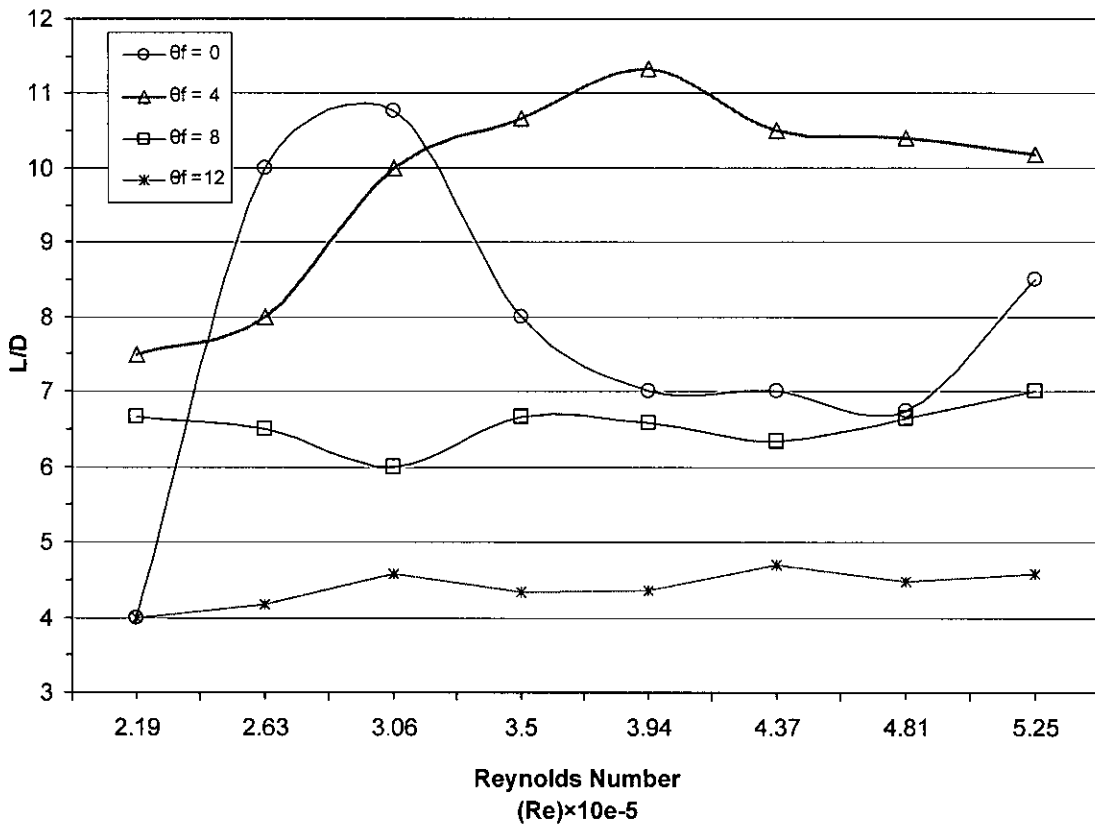
Figure 6.3 (iii): From pressure tapping **L/D** vs. Reynolds No. curves for θw = 4 °

Chapter 7

CONCLUSIONS AND RECOMENDATIONS

7.1. Conclusions:

1. From the analysis of lift to drag ratio curves it can be concluded that the minimum speed required to take off is decreased from circular fuselage model to aerofoiled fuselage model and least for wingleted aerofoiled fuselage model.

2. From most of the drag coefficient vs. Reynolds No. curves it is seen that the drag crisis is quite visible in the velocity range from 80 km/hr (Re = 1.64×10^{-5}) to 100 km/hr (Re = 2.05×10^{-5}) for wingleted fuselage model over the other models.

3. For wingleted fuselage if the angle of attack for fuselage is zero ($\theta_f = 0^\circ$), then it should be maintain a minimum wing angle (i.e. $\theta_w > 2^\circ$) at higher cruising speed (beyond 100km/hr), otherwise the plane become unstable and could not maintain level flight at higher speed. To avoid this instability it is better to maintain some fuselage angle of attack during high cruising speed. Again, during take-off, a higher angle of attack of the fuselage reduced the take-off speed; thereby it will require a shorter runway and less take-off time at operating condition.

4. Although aerofoiled fuselages provide a greater lift over circular fuselage but overall lift to drag ratio is reduced due to induced drag in aerofoil fuselages.

5. If the induced drag is checked by using winglets in the aerofoiled fuselage then a greater improvement of the overall lift to drag ratio is achieved.

6. Wing angle with fuselage $\theta_w = 4^\circ$ provide the maximum lift corresponding to a drag when this airplane fly with fuselage angle of attack, $\theta_f = 4^\circ$.

7.2. Recommendations

1. This research work did not consider the moment forces on the models which have a greater influence on the stability of an airplane. So the whole investigation can be done by considering the moment forces on the models.

2. Flaps and ailerons improve the controlling and maneuvering capability of an airplane. So flaps can be introduced in the aerofoiled fuselage to show their effect on the overall stability of the model plane.

3. Conventional winglets are used in this research work. By using computer software (e.g., FLUENT) one can redesigned the aerodynamic winglets to provide a better reduction of the induced drags.

4. Blended Wing Body (BWB) concepts are frequently being considered in modern aircraft designs. In this research the birds body shapes are considered as aerofoiled shapes but their body shapes are also an example of BWB. So a comparison between Circular fuselage, Aerofoiled fuselage and Blended Wing Body fuselage will be more practical.

5. The flow characteristics and pressure distribution around the airplane should be measured to know the behavior of flow separation, wake formation and circulation around it as these greatly influence its lift and drag characteristics.

REFERENCES

1) Levy, H. and Riding, R.: "Burnelli's Lifting Fuselages." Aeroplane Monthly, Vol. 8, No.7, July 1980, pp. 348-350.

2) Levy, H.: "Burnelli Lifting Fuselage Projects." Aeroplane Monthly, Vol. 8, No. 10, Oct. 1980, pp.516-517. 6. Wood, R. M. and Bauer, S. X. S.: Flying Wings/Flying Fuselages. AIAA 2001-0311, Jan. 8-11, 2001.

3) Cantilli, E.: "Saga of the Lifting Body/Flying Wing." Flight, pp. 56-61, Fall 1996.

4) Mitchell, K. A.: "Burnelli and His Lifting-Body Transports." American Aviation Historical Society Journal, pp. 2-19, Spring 1997.

5) Riding, R.: "Burnelli's Lifting Fuselages." Aeroplane Monthly, Vol. 8, No. 6, June 1980, pp. 329-331.

6) Wood R. M., "The Contributions of Vincent Justus Burnelli" AIAA 2003-0292, Jun. 2003.

7) Wertenson, I. F., "Investigation of the Burnelli Type Airplane" Jan. 1931.

8) Wertenson, I. F., "Investigation into the Development of the Burnelli Type Airplane" Aero Digest, March 1931.

9) Wertenson, F., "The Economical Cruising Speed of the Burnelli All-Wing Monoplane Flight" Aug. 24, 1933, pp. 854-856.

10) Klemin, A., "All-Wing Lifting Fuselage, Scientific America" April 1935.

11) Burnelli Model UB-14 14-Passenger Transport Aero Digest, August 1935.

12) Watter, M. "The Burnelli Airfoil Body. Flight" The Aircraft Engineer, Sept 26, 1935.

13) Wood, R. M. and Bauer, S. X. S. "Flying Wings/Flying Fuselages" AIAA 2001-0311, Jan. 8-11, 2001.

14) http://www1.msfc.nasa.gov/Newsroom/news/releases/2002/02-182.html, November 2002.

15) Jenkins D. R., Landis T., and Miller J., "American X-Vehicles, An Inventory— X-1 to X-50, Centennial of Flight Edition, Monographs in Aerospace" History No. 31, SP-2003-4531, June 2003.

16) Hansen J. R., Kinney J., "Taylor D. B., Prickett M., and Lee J. L., The Wind and Beyond, A Documentary Journey into the History of Aerodynamics in America" Volume II: Reinventing the Airplane June 2000.

17) Tucker V. A., "Gliding Birds: Reduction of Induced Drag by Wing Tip Slots Between the Primary Feathers" Department of Zoology, Duke University, Durham, NC 27706, USA, Accepted 5 March 1993.

18) Hummel, D. (1980), "The aerodynamic characteristics of slotted wing-tips in soaring birds." In Acta XVII Congressus Internationalis Ornithologici (ed. R. Nöhring), pp. 391–396.

19) Munk, M. M. (1921), "The minimum induced drag of airfoils." National Advisory Committee for Aeronautics Tech. Rept121.

20) Tucker, V. A. (1987), "Gliding birds: the effect of variable wing span." J. exp. Biol, 133, 33–58.

21) Tucker, V. A.(1990), "Measuring aerodynamic interference drag between a bird body and the mounting strut of a drag balance." J. exp. Biol. 154, 439–461.

22) Tucker, V. A. (1992), "Pitching equilibrium, wing span and tail span in a gliding Harris' hawk, Parabuteo unicinctus." J. exp. Biol. 165, 21–41.

23) Tucker, V. A. and Heine, C. (1990), "Aerodynamics of gliding flight in a Harris' hawk, Parabuteo unicinctus." J. exp. Biol. 149, 469–489.

24) Tucker, V. A. and Parrott, G. C. (1970), "Aerodynamics of gliding flight in a falcon and other birds." J. exp. Biol. 52, 345–367.

25) Eastman N. Jacobs and Albert Sherman, "Wing-Fuselage interference comparison of conventional and aerofoil type fuselage combination." March 1937.

26) I. Kroo Stanford University, U.S.A. "Nonplanar wing concepts for increased aircraft efficiency" VKI lecture series on Innovative Configurations and Advanced Concepts for Future Civil Aircraft, June 6-10, 2005

27) J. Reneaux, Onera, Applied Aerodynamics Department "Overview on drag reduction technologies for civil transport aircraft" European Congress on Computational Methods in Applied Sciences and Engineering (ECCOMAS) 2004.

28) Levy, H. and Riding, R.: "Burnelli's Lifting Fuselages." Aeroplane Monthly, Vol. 8, No. 3, March 1980, pp. 144-152.

29) Levy, H. and Riding, R.: "Burnelli's Lifting Fuselages." Aeroplane Monthly, Vol. 8, No. 5, April 1980, pp. 172-176.

30) Levy, H. and Riding, R.: "Burnelli's Lifting Fuselages." Aeroplane Monthly, Vol. 8, No. 6, May 1980, pp. 234-238.

31) Levy, H. and Riding, R.: "Burnelli's Lifting Fuselages." Aeroplane Monthly, Vol. 8, No. 7, July 1980, pp. 348-350.

32) Levy, H.: "Burnelli Lifting Fuselage Projects." Aeroplane Monthly, Vol. 8, No. 10, Oct. 1980, pp.516-517.

33) Wood, R. M. and Bauer, S. X. S.: "Flying Wings/Flying Fuselages." AIAA 2001-0311, Jan. 8-11, 2001.

34) Cantilli, E.: "Saga of the Lifting Body/Flying Wing." Flight, pp. 56-61, Fall 1996.

35) Mitchell, K. A.: "Burnelli and His Lifting-Body Transports." American Aviation Historical Society Journal, pp. 2-19, Spring 1997.

36) Katz, J. and Byrne, S.: "Stall Resistance Features of Lifting-Body Airplane Configurations." AIAA 1998

37) Burnelli Monoplane. Aero Digest, Feb. 1929, pp. 94-96.

38) ttp://www.burnelli.com , November 2008

39) http: // www1.msfc.nasa.gov /Newsroom / news / releases / 2002/02-182.html, November 2002.

40) http://www.naa-usa.org/website/, November 2008

41) http://www.aerofiles.com, November 2008

42) Bushnell DM, Moore KJ. 1991. "Drag reduction in nature." Annu. Rev. Fluid Mech. 23:65- 79.

43) Yates JE, Donaldson CD. 1986. "A fundamental study of drag and an assessment of conventional drag-due-to-lift reduction devices." NASA CR 4004.

44) Spalart PR. 1998. "Airplane trailing vortices." Annu. Rev. Fluid Mech. 30:107-38.

45) Rokhsaz K. 1993. "A brief survey of wing tip devices for drag reduction." SAE 932574.

46) Munk M. 1981. "My early aerodynamic research – thoughts and memories." Annu. Rev. Fluid Mech. 13:1-7.

47) Kroo IM, Smith SC. 1990. "Computation of induced drag with nonplanar and deformed wakes." SAE 901933.

48) Whitcomb RT. 1994. "Research on methods for reducing the aerodynamic drag at transonic speeds." The Inaugural Eastman Jacobs Lecture, NASA Langley Research Center.

49) Lowson MV. 1990. "Minimum induced drag for wings with spanwise camber." AIAA J. Aircraft 27.\

50) Butler GF. 1982. "Effect of downwash of the induced drag of canard-wing combinations." AIAA J. Aircraft 19:410.

51) McGeer T, Kroo IM, 1983. "A fundamental comparison of canard and conventional configurations." AIAA J. of Aircraft.

52) Hackett JE. 1980. "Vortex drags reduction by aft-mounted diffusing vanes." ICAS Paper 80-13.4.

53) Rubbert PE. 1992. "Aircraft wingtip vorticity redistribution apparatus." United States Patent 5100085.

54) Patterson JC. 1985. "Wingtip vortex propeller." United States Patent 4533101.

55) La Roche U, Palffy S. 1996. "Wing-grid, a novel device for reduction of induced drag 20th wings." 20 ICAS Congress. Naples Italy. pg. 2303-9.

56) Hall KC, Hall SR. 1996. "Minimum induced power requirements for flapping flight." J. Fluid Mech. 323:285-315

57) De Young, J., "Induced Drag Ideal-Efficiency Factor of Arbitrary Lateral-Vertical Wing Forms," NASA CR-3357, Dec. 1980.

58) Smith, S.C., "A Computational and Experimental Study of Nonlinear Aspects of Induced Drag," Ph.D. Thesis, Stanford University, June 1995.

59) Van Dam, C.P., "Induced Drag Characteristics of Crescent-Moon-Shaped Wings," J. of Aircraft, Vol. 24, No.2, 1987.

APPENDIX
(Data Tables)

Table 6.2.1. (a).

Air Velocity km/hr	Reynolds No. (Re)×10e-5	Circular Fuselage					Aerofoil Fuselage					Aerofoil Fuselage with winglet				
		L (kg)	C_L	D (kg)	C_D	L/D	L (kg)	C_L	D (kg)	C_D	L/D	L (kg)	C_L	D (kg)	C_D	L/D
50	1.03	0.162	0.25	0.049	0.07	3.31	0.162	0.25	0.07	0.11	2.31	0.216	0.33	0.055	0.08	3.93
60	1.23	0.216	0.23	0.063	0.07	3.43	0.27	0.28	0.112	0.12	2.41	0.324	0.34	0.082	0.09	3.95
70	1.44	0.27	0.21	0.112	0.09	2.41	0.477	0.37	0.14	0.11	3.41	0.601	0.46	0.103	0.08	5.83
80	1.64	0.553	0.33	0.12	0.07	4.61	0.641	0.38	0.193	0.11	3.32	0.773	0.46	0.155	0.09	4.99
90	1.85	0.671	0.31	0.165	0.08	4.07	0.768	0.36	0.232	0.11	3.31	0.96	0.45	0.123	0.06	7.81
100	2.05	0.725	0.27	0.173	0.07	4.19	1.064	0.4	0.287	0.11	3.71	0.997	0.38	0.303	0.11	3.29
110	2.26	0.825	0.26	0.248	0.08	3.33	1.046	0.33	0.343	0.11	3.05	Unstable				
120	2.46	0.934	0.25	0.37	0.1	2.52	0.846	0.22	0.349	0.09	2.42	Unstable				

θf = 0°, θw = 2°

Table 6.2.1. (b).

Air Velocity (km/hr)	Reynolds No. (Re)×10e-5	Circular Fuselage					Aerofoiled Fuselage					Aerofoiled Fuselage with winglet				
		L (kg)	C_L	D (kg)	C_D	L/D	L (kg)	C_L	D (kg)	C_D	L/D	L (kg)	C_L	D (kg)	C_D	L/D
50	1.03	0.189	0.29	0.077	0.12	2.45	0.216	0.33	0.07	0.11	3.09	0.27	0.41	0.068	0.1	3.97
60	1.23	0.216	0.23	0.111	0.12	1.95	0.46	0.48	0.119	0.13	3.86	0.555	0.58	0.088	0.09	6.31
70	1.44	0.571	0.44	0.149	0.11	3.83	0.568	0.44	0.156	0.12	3.64	0.682	0.53	0.125	0.1	5.46
80	1.64	0.716	0.42	0.166	0.1	4.13	0.713	0.42	0.195	0.12	3.66	0.918	0.54	0.172	0.1	5.34
90	1.85	0.907	0.42	0.199	0.09	4.56	0.732	0.34	0.246	0.11	2.97	1.118	0.52	0.206	0.1	5.43
100	2.05	1.225	0.46	0.246	0.09	4.98	1.091	0.41	0.266	0.1	4.1	1.209	0.46	0.231	0.09	5.23
110	2.26	1.279	0.4	0.309	0.1	4.14	1.064	0.33	0.387	0.12	2.75	1.897	0.59	0.4	0.13	4.74
120	2.46	1.007	0.26	0.523	0.14	1.92	0.9	0.24	0.422	0.11	2.13	2.17	0.57	0.445	0.12	4.88

θf = 0°, θw = 4°

Table 6.2.1. (c).

		Circular Fuselage					Aerofoil Fuselage					Aerofoil Fuselage with winglet				
Air Velocity km/hr	Reynolds No. (Re)×10e-5	L (kg)	C_L	D (kg)	C_D	L/D	L (kg)	C_L	D (kg)	C_D	L/D	L (kg)	C_L	D (kg)	C_D	L/D
50	1.03	0.243	0.37	0.07	0.11	3.47	0.324	0.49	0.112	0.17	2.17	0.243	0.37	0.082	0.12	2.96
60	1.23	0.562	0.59	0.113	0.12	4.97	0.586	0.62	0.128	0.13	4.58	0.664	0.7	0.125	0.13	5.31
70	1.44	0.653	0.5	0.157	0.12	4.16	0.931	0.72	0.178	0.14	5.23	0.825	0.64	0.156	0.12	5.3
80	1.64	0.716	0.42	0.18	0.11	3.98	0.931	0.55	0.222	0.13	4.19	1.009	0.6	0.174	0.1	5.8
90	1.85	1.152	0.54	0.213	0.1	5.41	1.194	0.56	0.292	0.14	4.09	1.3	0.61	0.218	0.1	5.96
100	2.05	1.324	0.5	0.257	0.1	5.15	1.427	0.54	0.3	0.11	4.76	1.445	0.55	0.322	0.12	4.49
110	2.26	1.606	0.5	0.315	0.1	5.1	1.59	0.5	0.368	0.12	4.32	1.846	0.58	0.416	0.13	4.44
120	2.46	1.787	0.47	0.348	0.09	5.11	1.337	0.35	0.376	0.1	3.02	1.555	0.41	0.429	0.11	3.62

θf = 0°, θw = 6°

Table 6.2.2. (a).

		Circular Fuselage					Aerofoil Fuselage					Aerofoil Fuselage with winglet				
Air Velocity km/hr	Reynolds No. (Re)×10e-5	L (kg)	C_L	D (kg)	C_D	L/D	L (kg)	C_L	D (kg)	C_D	L/D	L (kg)	C_L	D (kg)	C_D	L/D
50	1.03	0.27	0.41	0.084	0.13	3.21	0.27	0.41	0.084	0.13	3.21	0.374	0.57	0.069	0.1	8.31
60	1.23	0.662	0.7	0.1	0.11	6.62	0.623	0.65	0.128	0.13	4.86	0.864	0.91	0.1	0.11	8.64
70	1.44	0.843	0.65	0.132	0.1	6.39	0.786	0.61	0.175	0.14	4.49	0.9	0.69	0.136	0.1	6.62
80	1.64	1.079	0.64	0.173	0.1	6.24	1.04	0.61	0.256	0.15	4.06	1.209	0.71	0.179	0.11	6.75
90	1.85	1.297	0.61	0.209	0.1	6.21	0.882	0.41	0.259	0.12	3.41	1.408	0.66	0.275	0.13	5.12
100	2.05	1.442	0.55	0.245	0.09	5.89	1.5	0.57	0.333	0.13	4.5	1.596	0.6	0.297	0.11	5.37
110	2.26	1.611	0.5	0.353	0.11	4.56	1.046	0.33	0.343	0.11	3.05	1.807	0.56	0.366	0.11	4.49
120	2.46	1.629	0.43	0.399	0.1	4.08	1.055	0.28	0.387	0.1	2.73	1.537	0.4	0.453	0.12	3.39

θf = 4°, θw = 2°

Table 6.2.2. (b).

Air Velocity km/hr	Reynolds No. (Re)×10e-5	Circular Fuselage					Aerofoil Fuselage					Aerofoil Fuselage with winglet				
		L (kg)	C_L	D (kg)	C_D	L/D	L (kg)	C_L	D (kg)	C_D	L/D	L (kg)	C_L	D (kg)	C_D	L/D
50	1.03	0.324	0.49	0.098	0.15	3.31	0.477	0.72	0.077	0.12	6.2	0.664	1	0.0695	0.11	9.62
60	1.23	0.753	0.79	0.145	0.15	5.19	0.658	0.69	0.143	0.15	4.61	0.773	0.81	0.113	0.12	6.84
70	1.44	0.952	0.73	0.178	0.14	5.35	0.859	0.66	0.198	0.15	4.34	0.991	0.76	0.145	0.11	6.83
80	1.64	1.206	0.71	0.222	0.13	5.43	1.076	0.64	0.234	0.14	4.6	1.209	0.71	0.171	0.1	7.07
90	1.85	1.46	0.68	0.285	0.13	5.12	0.822	0.38	0.278	0.13	2.96	0.9	0.42	0.2	0.09	4.5
100	2.05	1.606	0.61	0.332	0.13	4.84	1.662	0.63	0.34	0.13	4.89	1.063	0.4	0.234	0.09	4.54
110	2.26	1.787	0.56	0.398	0.12	4.49	1.137	0.36	0.347	0.11	3.27	2.147	0.67	0.385	0.12	5.58
120	2.46	2.319	0.61	0.439	0.12	5.28	1.064	0.28	0.387	0.1	2.75	2.358	0.62	0.415	0.11	5.68

θf = 4°, θw = 4°

Table 6.2.2. (c).

Air Velocity km/hr	Reynolds No. (Re)×10e-5	Circular Fuselage					Aerofoil Fuselage					Aerofoil Fuselage with winglet				
		L (kg)	C_L	D (kg)	C_D	L/D	L (kg)	C_L	D (kg)	C_D	L/D	L (kg)	C_L	D (kg)	C_D	L/D
50	1.03	0.351	0.53	0.119	0.18	2.95	0.541	0.82	0.127	0.19	4.26	0.574	0.87	0.082	0.12	6.99
60	1.23	0.725	0.76	0.151	0.16	4.8	0.777	0.82	0.204	0.21	3.81	0.809	0.85	0.127	0.13	6.37
70	1.44	0.952	0.73	0.256	0.2	3.72	0.967	0.75	0.216	0.17	4.48	1.263	0.97	0.195	0.15	6.48
80	1.64	1.261	0.75	0.286	0.17	4.41	1.095	0.65	0.265	0.16	4.13	1.36	0.8	0.259	0.15	5.23
90	1.85	1.497	0.7	0.311	0.15	4.81	1.59	0.74	0.353	0.16	4.5	1.694	0.79	0.298	0.14	5.68
100	2.05	1.503	0.57	0.348	0.13	4.32	1.754	0.66	0.392	0.15	4.47	2.245	0.85	0.47	0.18	4.78
110	2.26	1.629	0.51	0.384	0.12	4.24	1.663	0.52	0.41	0.13	4.06	2.492	0.78	0.503	0.16	4.95
120	2.46	1.738	0.46	0.421	0.11	4.13	1.7	0.45	0.451	0.12	3.77	2.655	0.7	0.531	0.14	5

θf = 4°, θw = 6°

Table 6.2.3. (a)

		Circular Fuselage					Aerofoil Fuselage					Aerofoil Fuselage with winglet				
Air Velocity km/hr	Reynolds No. (Re)×10e-5	L (kg)	C_L	D (kg)	C_D	L/D	L (kg)	C_L	D (kg)	C_D	L/D	L (kg)	C_L	D (kg)	C_D	L/D
50	1.03	0.324	0.49	0.098	0.15	3.31	0.586	0.89	0.128	0.19	4.58	0.637	0.96	0.111	0.17	5.74
60	1.23	0.753	0.79	0.188	0.2	4	0.822	0.86	0.19	0.2	4.33	0.918	0.96	0.158	0.17	5.81
70	1.44	0.943	0.73	0.23	0.18	4.1	1.058	0.82	0.241	0.19	4.39	1.209	0.93	0.208	0.16	5.81
80	1.64	1.224	0.72	0.261	0.15	4.69	0.804	0.48	0.27	0.16	2.98	1.535	0.91	0.28	0.17	5.48
90	1.85	1.497	0.7	0.367	0.17	4.08	0.895	0.42	0.295	0.14	3.03	1.717	0.8	0.351	0.16	4.89
100	2.05	1.448	0.55	0.3	0.11	4.83	1.754	0.66	0.376	0.14	4.66	2.061	0.78	0.393	0.15	5.24
110	2.26	1.666	0.52	0.371	0.12	4.49	1.463	0.46	0.422	0.13	3.47	2.474	0.77	0.309	0.1	8
120	2.46	1.811	0.48	0.417	0.11	4.34	1.572	0.41	0.443	0.12	3.55	2.601	0.68	0.346	0.09	7.52

θf = 8°, θw = 2°

Table 6.2.3. (b).

		Circular Fuselage					Aerofoil Fuselage					Aerofoil Fuselage with winglet				
Air Velocity km/hr	Reynolds No. (Re)×10e-5	L (kg)	C_L	D (kg)	C_D	L/D	L (kg)	C_L	D (kg)	C_D	L/D	L (kg)	C_L	D (kg)	C_D	L/D
50	1.03	0.27	0.41	0.161	0.24	1.68	0.623	0.94	0.157	0.24	3.96	0.592	0.9	0.124	0.19	4.77
60	1.23	0.725	0.76	0.238	0.25	3.05	0.695	0.73	0.202	0.21	3.44	0.945	0.99	0.158	0.17	5.98
70	1.44	0.961	0.74	0.297	0.23	3.24	1.076	0.83	0.249	0.19	4.32	1.227	0.95	0.209	0.16	5.87
80	1.64	1.296	0.77	0.279	0.16	4.65	0.949	0.56	0.223	0.13	4.26	1.644	0.97	0.285	0.17	5.79
90	1.85	1.606	0.75	0.437	0.2	3.67	1.772	0.83	0.345	0.16	5.14	1.844	0.86	0.341	0.16	5.41
100	2.05	1.503	0.57	0.423	0.16	3.55	1.917	0.72	0.376	0.14	5.1	2.238	0.85	0.42	0.16	5.33
110	2.26	1.847	0.58	0.403	0.13	4.58	1.572	0.49	0.413	0.13	3.81	2.649	0.83	0.492	0.15	5.38
120	2.46	1.92	0.5	0.447	0.12	4.29	1.463	0.38	0.422	0.11	3.47	2.848	0.75	0.538	0.14	5.29

θf = 8°, θw = 4°

Table 6.2.3. (c)

Air Velocity km/hr	Reynolds No. (Re)×10e-5	Circular Fuselage					Aerofoil Fuselage					Aerofoil Fuselage with winglet				
		L (kg)	C_L	D (kg)	C_D	L/D	L (kg)	C_L	D (kg)	C_D	L/D	L (kg)	C_L	D (kg)	C_D	L/D
50	1.03	0.27	0.41	0.209	0.32	1.29	0.568	0.86	0.163	0.25	3.48	0.61	0.92	0.131	0.2	4.65
60	1.23	0.68	0.71	0.323	0.34	2.1	0.84	0.88	0.249	0.26	3.37	0.842	0.88	0.225	0.24	5.46
70	1.44	0.988	0.76	0.313	0.24	3.16	1.149	0.89	0.29	0.22	3.96	1.2	0.93	0.271	0.21	5.05
80	1.64	1.243	0.73	0.285	0.17	4.36	1.512	0.89	0.352	0.21	4.3	1.712	1.01	0.32	0.19	5
90	1.85	1.497	0.7	0.327	0.15	4.58	1.899	0.89	0.479	0.22	3.96	2.1	0.98	0.452	0.21	4.65
100	2.05	1.575	0.6	0.366	0.14	4.3	2.523	0.95	0.49	0.19	5.15	2.601	0.98	0.48	0.18	5.62
110	2.26	1.956	0.61	0.45	0.14	4.35	2.396	0.75	0.49	0.15	4.89	2.547	0.8	0.507	0.16	5.02
120	2.46	2.3	0.6	0.497	0.13	4.63	2.117	0.56	0.527	0.14	4.02	3.084	0.81	0.548	0.14	5.63

θf = 8°, θw = 6°

Table 6.2.4. (a)

Air Velocity km/hr	Reynolds No. (Re)×10e-5	Circular Fuselage L/D					Aerofoil Fuselage L/D					Aerofoil Fuselage with winglet L/D				
		L (kg)	C_L	D (kg)	C_D	L/D	L (kg)	C_L	D (kg)	C_D	L/D	L (kg)	C_L	D (kg)	C_D	L/D
50	1.03	0.324	0.49	0.172	0.26	1.88	0.641	0.97	0.2	0.3	3.2	0.701	1.06	0.209	0.32	3.35
60	1.23	0.716	0.75	0.216	0.23	3.32	0.949	1	0.268	0.28	3.54	1.009	1.06	0.261	0.27	3.87
70	1.44	0.934	0.72	0.311	0.24	3	0.967	0.75	0.238	0.18	4.06	1.372	1.06	0.304	0.23	4.51
80	1.64	1.297	0.77	0.388	0.23	3.34	1.131	0.67	0.274	0.16	4.13	1.808	1.07	0.387	0.23	4.67
90	1.85	1.479	0.69	0.445	0.21	3.32	1.303	0.61	0.311	0.15	4.19	2.206	1.03	0.463	0.22	4.76
100	2.05	1.63	0.62	0.369	0.14	4.42	1.608	0.61	0.353	0.13	4.56	2.224	0.84	0.51	0.19	4.36
110	2.26	1.884	0.59	0.429	0.13	4.39	1.899	0.59	0.415	0.13	4.58	2.994	0.94	0.533	0.17	5.62
120	2.46	2.065	0.54	0.465	0.12	4.44	1.935	0.51	0.466	0.12	4.15	2.649	0.7	0.554	0.15	4.78

θf = 12°, θw = 2°

Table 6.2.4. (b)

		θf = 12°, θw = 4°														
Air Velocity km/hr	Reynolds No. (Re)×10e-5	Circular Fuselage L/D					Aerofoil Fuselage L/D					Aerofoil Fuselage with winglet L/D				
		L (kg)	C_L	D (kg)	C_D	L/D	L (kg)	C_L	D (kg)	C_D	L/D	L (kg)	C_L	D (kg)	C_D	L/D
50	1.03	0.351	0.53	0.231	0.35	1.52	0.586	0.89	0.242	0.37	2.42	0.628	0.95	0.207	0.31	3.03
60	1.23	0.68	0.71	0.315	0.33	2.16	0.986	1.04	0.224	0.24	4.4	0.991	1.04	0.304	0.32	3.26
70	1.44	0.952	0.73	0.371	0.29	2.57	1.022	0.79	0.255	0.2	4.01	1.318	1.02	0.362	0.28	3.64
80	1.64	1.261	0.75	0.401	0.24	2.38	1.203	0.71	0.277	0.16	4.34	1.753	1.04	0.432	0.26	4.06
90	1.85	1.279	0.6	0.387	0.18	3.3	1.79	0.84	0.346	0.16	5.17	1.843	0.86	0.397	0.19	4.64
100	2.05	1.793	0.68	0.432	0.16	4.15	1.808	0.68	0.379	0.14	4.77	2.254	0.85	0.438	0.17	5.14
110	2.26	2.102	0.66	0.491	0.15	4.28	2.044	0.64	0.473	0.15	4.32	2.667	0.83	0.509	0.16	5.24
120	2.46	2.228	0.59	0.55	0.14	4.05	2.578	0.68	0.527	0.14	4.89	2.957	0.78	0.546	0.14	5.24

Table 6.2.4. (c)

		θf = 12°, θw = 6°														
Air Velocity km/hr	Reynolds No. (Re)×10e-5	Circular Fuselage L/D					Aerofoiled Fuselage L/D					Aerofoiled Fuselage with winglet L/D				
		L (kg)	C_L	D (kg)	C_D	L/D	L (kg)	C_L	D (kg)	C_D	L/D	L (kg)	C_L	D (kg)	C_D	L/D
50	1.03	0.27	0.41	0.258	0.39	1.05	0.568	0.86	0.284	0.43	2	0.646	0.98	0.222	0.34	2.91
60	1.23	0.807	0.85	0.349	0.37	2.31	0.968	1.02	0.395	0.41	2.45	0.955	1	0.187	0.2	5.1
70	1.44	0.979	0.76	0.409	0.32	2.39	1.131	0.87	0.266	0.21	4.25	1.209	0.93	0.245	0.19	4.93
80	1.64	1.188	0.7	0.489	0.29	2.43	1.376	0.81	0.307	0.18	4.48	1.481	0.88	0.278	0.16	5.33
90	1.85	1.515	0.71	0.495	0.23	3.06	1.783	0.83	0.428	0.2	4.17	2.111	0.99	0.404	0.19	5.22
100	2.05	1.802	0.68	0.535	0.2	3.37	1.91	0.72	0.466	0.18	4.1	2.637	1	0.466	0.18	5.66
110	2.26	2.385	0.75	0.571	0.18	4.18	2.273	0.71	0.523	0.16	4.35	2.921	0.91	0.479	0.15	6.1
120	2.46	2.53	0.66	0.625	0.16	4.05	2.578	0.68	0.543	0.14	4.75	3.048	0.8	0.553	0.15	5.51

Table 6.2.5 (a).

Air Velocity km/hr	Reynolds No. (Re)×10e-5	$\theta f = 0°$			$\theta f = 4°$			$\theta f = 8°$			$\theta f = 12°$		
		C_L	C_D	L/D	C_L	C_D	L/D	C_L	C_D	L/D	C_L	C_D	L/D
50	1.03	0.33	0.08	3.93	0.57	0.1	8.31	0.96	0.17	5.74	1.06	0.32	3.35
60	1.23	0.34	0.09	3.95	0.91	0.11	8.64	0.96	0.17	5.81	1.06	0.27	3.87
70	1.44	0.46	0.08	5.83	0.69	0.1	6.62	0.93	0.16	5.81	1.06	0.23	4.51
80	1.64	0.46	0.09	4.99	0.71	0.11	6.75	0.91	0.17	5.48	1.07	0.23	4.67
90	1.85	0.45	0.06	7.81	0.66	0.13	5.12	0.8	0.16	4.89	1.03	0.22	4.76
100	2.05	0.38	0.11	3.29	0.6	0.11	5.37	0.78	0.15	5.24	0.84	0.19	4.36
110	2.26	Unstable			0.56	0.11	4.49	0.77	0.1	8	0.94	0.17	5.62
120	2.46	Unstable			0.4	0.12	3.39	0.68	0.09	7.52	0.7	0.15	4.78

Table 6.2.5 (b).

Air Velocity km/hr	Reynolds No. (Re)×10e-5	$\theta f = 0°$			$\theta f = 4°$			$\theta f = 8°$			$\theta f = 12°$		
		C_L	C_D	L/D	C_L	C_D	L/D	C_L	C_D	L/D	C_L	C_D	L/D
50	1.03	0.41	0.1	3.97	1	0.11	9.62	0.9	0.19	4.77	0.95	0.31	3.03
60	1.23	0.58	0.09	6.31	0.81	0.12	6.84	0.99	0.17	5.98	1.04	0.32	3.26
70	1.44	0.53	0.1	5.46	0.76	0.11	6.83	0.95	0.16	5.87	1.02	0.28	3.64
80	1.64	0.54	0.1	5.34	0.71	0.1	7.07	0.97	0.17	5.79	1.04	0.26	4.06
90	1.85	0.52	0.1	5.43	0.42	0.09	4.5	0.86	0.16	5.41	0.86	0.19	4.64
100	2.05	0.46	0.09	5.23	0.4	0.09	4.54	0.85	0.16	5.33	0.85	0.17	5.14
110	2.26	0.59	0.13	4.74	0.67	0.12	5.58	0.83	0.15	5.38	0.83	0.16	5.24
120	2.46	0.57	0.12	4.88	0.62	0.11	5.68	0.75	0.14	5.29	0.78	0.14	5.24

The aerofoiled fuselage with winglet is at $\theta w = 2°$ (Table a) and $\theta w = 4°$ (Table b).

Table 6.2.5. (c)

Air Velocity km/hr	Reynolds No. (Re)×10e-5	$\theta f = 0°$			$\theta f = 4°$			$\theta f = 8°$			$\theta f = 12°$		
		C_L	C_D	L/D	C_L	C_D	L/D	C_L	C_D	L/D	C_L	C_{D}	L/D
								Aerofoiled Fuselage with winglet, $\theta w = 6°$					
50	1.03	0.37	0.12	2.96	0.87	0.12	6.99	0.92	0.2	4.65	0.98	0.34	2.91
60	1.23	0.7	0.13	5.31	0.85	0.13	6.37	0.88	0.24	5.46	1	0.2	5.1
70	1.44	0.64	0.12	5.3	0.97	0.15	6.48	0.93	0.21	5.05	0.93	0.19	4.93
80	1.64	0.6	0.1	5.8	0.8	0.15	5.23	1.01	0.19	5	0.88	0.16	5.33
90	1.85	0.61	0.1	5.96	0.79	0.14	5.68	0.98	0.21	4.65	0.99	0.19	5.22
100	2.05	0.55	0.12	4.49	0.85	0.18	4.78	0.98	0.18	5.62	1	0.18	5.66
110	2.26	0.58	0.13	4.44	0.78	0.16	4.95	0.8	0.16	5.02	0.91	0.15	6.1
120	2.46	0.41	0.11	3.62	0.7	0.14	5	0.81	0.14	5.63	0.8	0.15	5.51

Table 6.2.6.

Air Velocity km/hr	Reynolds No. (Re)×10e-5	$\theta w = 2°$					$\theta w = 4°$					$\theta w = 6°$				
		L (kg)	C_L	D (kg)	C_D	L/D	L (kg)	C_L	D (kg)	C_D	L/D	L (kg)	C_L	D (kg)	C_D	L/D
							Aerofoiled Fuselage with winglet, $\theta f = 4°$									
50	1.03	0.374	0.57	0.069	0.1	8.31	0.664	1	0.0695	0.11	9.62	0.574	0.87	0.082	0.12	6.99
60	1.23	0.864	0.91	0.1	0.11	8.64	0.773	0.81	0.113	0.12	6.84	0.809	0.85	0.127	0.13	6.37
70	1.44	0.9	0.69	0.136	0.1	6.62	0.991	0.76	0.145	0.11	6.83	1.263	0.97	0.195	0.15	6.48
80	1.64	1.209	0.71	0.179	0.11	6.75	1.209	0.71	0.171	0.1	7.07	1.36	0.8	0.259	0.15	5.23
90	1.85	1.408	0.66	0.275	0.13	5.12	0.9	0.42	0.2	0.09	4.5	1.694	0.79	0.298	0.14	5.68
100	2.05	1.596	0.6	0.297	0.11	5.37	1.063	0.4	0.234	0.09	4.54	2.245	0.85	0.47	0.18	4.78
110	2.26	1.807	0.56	0.366	0.11	4.49	2.147	0.67	0.385	0.12	5.58	2.492	0.78	0.503	0.16	4.95
120	2.46	1.537	0.4	0.453	0.12	3.39	2.358	0.62	0.415	0.11	5.68	2.655	0.7	0.531	0.14	5

Table 6.3 (a):

Air Velocity (km/hr)	Aerofoiled fuselage for θf = 0°																
	Pressure taps																
	Top surface										Bottom surface							
	T1	T2	T3	T4	T5	T6	T7	T8	T9	T10	B1	B2	B3	B4	B5	B6	B7	B8
50	7	-1	-5.8	-5	-4.8	-3.5	-6	-5.5	-6.5	-4.8	-4	-5.5	-4.5	-4.5	-3	-2	-1	-1
60	3	-3	-6	-6.5	-6.8	-4	-7	-5.5	-5.8	-3.5	-2.7	-5.9	-5	-3.6	-2.5	-1	-0.3	-0.1
70	2.6	-1.5	-6	-7.5	-10	-8.8	-8.4	-6.4	-8.5	-4	-4	-7.8	-6.2	-5.5	-5	-2	1.9	1.2
80	8.5	-2.5	-10	-9	-13	-8	-11	-9	-10.5	-6	-4.5	-10.5	-8.2	-7.6	-6.6	-2.8	0.7	0.9
90	11.2	-4.2	-13.4	-15	-16	-11.8	-15.8	-12.6	-14.4	-8.4	-5	-15	-10	-9.8	-7.8	-3.8	-1	0.2
100	7	-7	-14.5	-16	-17	-12.5	-18.8	-13.5	-14.5	-9	-5	-15	-12	-11	-7	-5	-2	-1.8
110	3.3	-6.8	-18	-19	-19.5	-17	-21	-19	-19	-12	-9	-18	-13.5	-13.8	-11.5	-5	-2.5	-3
120	2.3	-7.5	-23	-22.5	-23	-23	-22	-20	-19.8	-10.5	-9	-23	-16	-15.5	-9	-2.5	-1	1

Table 6.3 (b):

Air Velocity (km/hr)	Pressure taps																	
	Top surface										Bottom surface							
	T1	T2	T3	T4	T5	T6	T7	T8	T9	T10	B1	B2	B3	B4	B5	B6	B7	B8
50	8.2	-8	-8.2	-8.2	-7.9	-5	-7	-5.8	-5.7	-3	3.5	0.2	-0.2	-0.1	1	1	0.4	0.9
60	-0.7	-7	-8.5	-8.2	-8.2	-5.2	-7.8	-6	-6.5	-3.1	5.5	-0.5	-0.65	-0.8	-0.5	0.4	0.6	0.7
70	-0.3	-9	-13	-12.8	-12.5	-8.5	-11.5	-9	-9	-5	5.5	-2.5	-3	-3	-2	-1	0.3	0.4
80	-15	-15.5	-17	-16.5	-15.5	-11	-15	-11	-12	-7	10	2	-1	-1.6	-0.5	0.9	1.6	1.2
90	-13.5	-19	-20.5	-20	-19.5	-14.5	-18.5	-14.5	-14.5	-8.5	10	-3	-3	-3	-1.5	-0.5	-1	-1
100	-20	-20	-24.5	-23.5	-23	-17	-22	-17	-17	-10	11	-3	-3	-3.5	-3	-0.1	2	0
110	-19	-27	-33	-28	-28.5	-23	-27	-21.5	-21	-12.5	18.5	-1.5	-3	-5	-3	0	1	-1
120	-30.5	-31	-37.5	-36	-34	-27	-31	-23.5	-25	-15.5	22.5	1.4	0.8	-2.8	-1	-0.2	0	-2.5

Aerofoiled fuselage for $\theta f = 4°$

Table 6.3 (c):

Air Velocity (km/hr)	Aerofoiled fuselage for θf = 8°																	
	Pressure taps																	
	Top surface										Bottom surface							
	T1	T2	T3	T4	T5	T6	T7	T8	T9	T10	B1	B2	B3	B4	B5	B6	B7	B8
50	-13	-14	-12	-12	-12	-8.5	-9	-7	-6.5	-2.7	6.5	1.5	1	-1	-0.5	1	1.5	1.1
60	-14	-13.5	-13	-11.5	-11	-7	-9.5	-8	-7	-4.5	11	3.5	2.5	1.3	1.4	2.2	2.8	2.4
70	-13.5	-17	-18	-15	-10	-13	-9.5	-9	-9	-6	13	2.5	1.8	0.4	2	2.7	3	2.2
80	-23	-24	-21	-19.5	-19	-13	-17	-11.5	-12	-8	17	6	4.2	2.6	2.4	3	2.4	2.3
90	-22	-28	-28	-25	-25	-17	-21	-15	-14.5	-8.5	23.5	6.5	4	2	2.5	2.5	2	0.2
100	-35	-36	-33.5	-31	-28	-20	-25	-18	-18	-11	27	9	5.5	3	3	3.5	3	0.2
110	-34.5	-48	-46	-40	-38	-27	-32	-23	-22.5	-12	36	13	8.5	6	5	4	3	1.5
120	-53.5	-55	-52	-47	-43	-31	-37	-26	-26	-14	42	15	9.5	5.5	5.5	5	4	1

Table 6.3 (d):

Air Velocity (km/hr)	Pressure taps																	
	Top surface										Bottom surface							
	T1	T2	T3	T4	T5	T6	T7	T8	T9	T10	B1	B2	B3	B4	B5	B6	B7	B8
50	-5.2	-4	-10.5	-10	-9	-5	-7	-5	-5	-3	8	3	2	1.8	1.5	1.2	1	0.5
60	-15.5	-16.5	-15	-13.5	-13	-9	-11	-7.5	-9	-5	11	2.5	2.2	1	0	1.5	1	0.3
70	-16	-20	-20	-18	-17	-10.5	-14.5	-10	-9.5	-6	14.5	5.5	3	2	1.8	2.5	1.2	0.8
80	-25.5	-26	-25	-22	-20	-14.5	-18	-12	-11.5	-7	21	7.5	5	2	2	1.3	1.8	1
90	-29	-31.5	-30	-27	-26	-17	-21	-15	-15	-8.5	24	8.5	7.5	4	4.5	2.5	1	1
100	-37	-39	-36	-32.5	-29.5	-22.5	-25	-18	-20	-9	30	12	8.5	3.8	4.5	4.5	4	2.5
110	-35.5	-52	-47	-39	-38	-27.5	-33	-24	-23	-13	38	14	10	7	6.2	5	4.5	1.2
120	-54	-58	-53	-46	-43	-31	-37	-25	-25	-15.5	44.5	17.5	11	8	7.5	7	5	2

Aerofoiled fuselage for θf = 12°

92

Table 6.3 (e): Values of β*i* and *li*

Pressure taps	Top surface										Bottom surface							
	T1	T2	T3	T4	T5	T6	T7	T8	T9	T10	B1	B2	B3	B4	B5	B6	B7	B8
β*i* (Degree)	132	114	108	100	98.5	97	90	83	78.3	78	60	79	82	85	86	88	92	92
li (mm)	9	8.5	8	8	9.5	11	44	46	48	64	10	10	10	14	20	46	53	80

Table 6.3 (f): Calculated Lifts & Drags of wingleted aerofoiled fuselage by pressure tapping.

Air Velocity km/hr	Reynolds No. (Re)×10e-5	θf = 0°					θf = 4°					θf = 8°					θf =12°				
		L (kg)	C_L	D (kg)	C_D	L/D	L (kg)	C_L	D (kg)	C_D	L/D	L (kg)	C_L	D (kg)	C_D	L/D	L (kg)	C_L	D (kg)	C_D	L/D
50	2.19	0.08	0.28	0.02	0.07	4	0.15	0.53	0.02	0.07	7.5	0.2	0.26	0.03	0.11	6.67	0.16	0.57	0.04	0.14	4
60	2.63	0.1	0.25	0.01	0.03	10	0.16	0.39	0.02	0.05	8	0.26	0.16	0.04	0.1	6.5	0.25	0.62	0.06	0.15	4.17
70	3.06	0.14	0.26	0.013	0.02	10.77	0.2	0.36	0.02	0.04	10	0.3	0.1	0.05	0.09	6	0.32	0.58	0.07	0.13	4.57
80	3.5	0.16	0.23	0.02	0.03	8	0.32	0.44	0.03	0.04	10.67	0.4	0.08	0.06	0.08	6.67	0.39	0.54	0.09	0.13	4.33
90	3.94	0.21	0.23	0.03	0.03	7	0.34	0.37	0.03	0.03	11.33	0.46	0.06	0.07	0.08	6.57	0.48	0.53	0.11	0.12	4.36
100	4.37	0.21	0.19	0.03	0.03	7	0.42	0.37	0.04	0.04	10.5	0.57	0.05	0.09	0.08	6.33	0.61	0.54	0.13	0.12	4.69
110	4.81	0.27	0.2	0.04	0.03	6.75	0.52	0.38	0.05	0.04	10.4	0.73	0.04	0.11	0.08	6.64	0.76	0.56	0.17	0.13	4.47
120	5.25	0.34	0.21	0.04	0.03	8.5	0.61	0.37	0.06	0.04	10.17	0.84	0.03	0.12	0.08	7	0.87	0.54	0.19	0.12	4.58

Reynolds Number (Re) Calculation:

As the fuselages of the models are volumetrically equivalent and same set of wings are used for all the models so the characteristic lengths for all the models are equal. Again the characteristic length for a model is the combination of individual characteristic length of the fuselage and the wings.

As **NACA-2412** cambered aerofoil sections are used for both of the fuselage and the wings so the characteristic length can be calculated in the following method:

The individual characteristics length of the fuselage i.e. the cord length of the fuselage is, $C_f = 238$ mm and the span of the fuselage, $b_f = 100$ mm.

The individual characteristics length of the wing i.e. the cord length of the wing is, $C_w = 80$ mm and the total span of the two wings, $b_w = 400$ mm.

So the characteristics length for the whole model is $(C_f \times b_f + C_w \times b_w)/ (b_f + b_w)$, and putting the values it can be found the characteristics length is 111.6 mm.

Now from the expression **Re = $\rho v l/\mu$**, Reynolds Number of the flow can be calculated for different air speed, where l is the characteristics length of the models.